UNIVERSITY OF OKLAHOMA

GRADUATE COLLEGE

# BACTERIOPHAGE NANOFIBERS ENABLED NANOSTRUCTURES AND TARGET-RECOGNITION FOR BIO-APPLICATIONS

A DISSERTATION

SUBMITTED TO THE GRADUATE FACULTY

in partial fulfillment of the requirements for the

Degree of

DOCTOR OF PHILOSOPHY

By

HONG XU
Norman, Oklahoma
2015

Downloaded from SHAREOK. Persistent Handle URL: https://hdl.handle.net/11244/23319

BACTERIOPHAGE NANOFIBERS ENABLED BIO-NANOSTRUCTURES AND BIO-APPLICATIONS

A DISSERTATION APPROVED FOR THE
DEPARTMENT OF CHEMISTRY AND BIOCHEMISTRY

BY

_____
Dr. Chuanbin Mao, Chair

_____
Dr. Lloyd Bumm

_____
Dr. Wai Tak Yip

_____
Dr. Shaorong Liu

_____
Dr. Zhibo Yang

© Copyright by HONG XU 2015
All Rights Reserved.

## Dedication

This dissertation is dedicated to my brilliant, loving, and supportive husband, Binrui, and our brave, sweet, and kind-hearted little boy, Brady, and to my always encouraging parents, Qingwei and Lina.

## Acknowledgements

Over the past seven years, I have received support from a great number of individuals. I would never have been able to finish my dissertation without the guidance of my committee members, help from colleagues and friends, and support from my family.

Dr. Chuanbin Mao has been a mentor, colleague, and friend. His guidance has made my Ph.D. pursuit to be a thoughtful and rewarding journey. I would like to thank him for his excellent guidance, caring, patience and providing me great supports for doing research. I would like to express my gratitude to my committee members, Dr. Wai Tak Yip, Dr. Shaorong Liu, Dr. Zhibo Yang, and Dr. Lloyd Bumm for their support over the past years. In addition, I would like to than Dr. Ashby and Dr. Cook who attended my qualification defense.

During data collection and writing, Dr. Chuanbin Mao and Dr. Binrui Cao spent hours proofreading and listening to my talk of research. Dr. Haibo Zhu and Dr. Kun Ma generously provided me collaboration to my research, as I could not finish the work without their help. I would also like to thank all the members in Dr. Mao's lab for their support and collaboration over the years.

Finally, I would like to thank my parents and my husband. They are always there supporting me and encouraging me through the good times and bad.

# Table of Contents

Acknowledgements ..... iv

List of Tables ..... xi

List of Figures ..... xii

Abstract ..... xvii

Chapter 1: Introduction ..... 1

1.1 Filamentous Bacteriophage Biology ..... 2

1.1.1 Phage structure as a biological nanorod ..... 2

1.1.2 Phage Life Cycle ..... 6

1.2 Phage display: displaying a peptide on the surface to change the surface chemistry ..... 7

1.2.1 Principles and different phage display modes ..... 7

1.3 Phage display: Screening random phage-displayed peptide library against biological systems - Biopanning ..... 10

1.3.1 The construction of a phage library ..... 10

1.3.2 Biopanning on live cells – Cell Panning ..... 11

1.3.3 The basic procedure of in vitro cell panning/in vivo panninng ..... 11

1.3.4 Identified peptide motifs using phage screening against mammalian cells and tissues ..... 14

1.4 Limitation on the peptides to be displayed ..... 18

1.5 Applications ..... 19

1.5.1 Phage as a template to synthesize and assemble nanoparticles ..... 19

1.5.2 Bone Regeneration ..... 20

1.5.3 Proteomic analysis (Ligand-receptor/Antibody-antigen interaction) ..... 22
1.5.4 Custom diagnostics and targeted therapy ..... 23
Chapter 2: Oriented Nucleation of Hydroxylapatite Crystals on Self-assembled Bacteriophage Bundles ..... 26
2.1 Introduction ..... 26
2.2 Materials and Methods ..... 30
2.2.1 Reagents. ..... 30
2.2.2 Molecular cloning of M13 bacteriophage PVIII display. ..... 30
2.2.3 The production, amplification, and purification of engineered phage. .. 31
2.2.4 The preparation of HAP supersaturated solution. ..... 32
2.2.5 Nucleation of phages in HAP supersaturated solution. ..... 32
2.2.6 Ultraviolet (UV) Absorption and Circular Dichroism (CD) spectroscopy. ..... 32
2.2.7 Transmission Electron Microscopy Characterization. ..... 33
2.3 Results and Discussions ..... 33
2.4 Conclusions ..... 44
Chapter 3: Bacteriophage-Gold Nanocomposites As a Model to Study Transmission Electron Microscopy of bioinorganic nanohybrids ..... 45
3.1 INTRODUCTION ..... 45
3.2 Materials and Methods ..... 48
3.2.1 Materials ..... 48
3.2.2 M13 Amplification ..... 49
3.2.3 Synthesis of Gold Nanoparticles ..... 50

3.2.4 Preparation of Phage-Gold Nanoparticle Hybrid ..... 50
3.2.5 Negative Staining ..... 50
3.2.6 Pre-fixation with 1% Glutaraldehyde (GA) ..... 51
3.3 Results ..... 51
3.3.1 Preparation of Gold Nanoparticles. ..... 51
3.3.2 Wild-Type M13 Bacteriophage. ..... 52
3.3.3 Gold Nanoparticle-Phage Hybrids. ..... 53
3.3.4 Best Negative Staining Conditions. ..... 53
3.3.5 Choice of Stains. ..... 57
3.3.6 Choice of the Concentrations of the Stain. ..... 58
3.3.7 Staining Time. ..... 61
3.3.8 pH of the Stain. ..... 61
3.3.9 Drying Method. ..... 62
3.3.10 Choice of Pre-fixation. ..... 63
3.4 Discussion ..... 63
3.4.1 Mechanism of Negative Staining with UA and PTA. ..... 63
3.4.2 Bio-Inorganic Nanohybrids and Negative Staining. ..... 64
3.4.3 Choice of Stain and Working pH Based on Specific Bio-Inorganic Nanohybrids. ..... 66
3.4.4 Choice of Stain Concentration Based on Specific Bio-Inorganic Nanohybrids. ..... 68
3.4.5 Choice of Fixation Based on Specific Bio-Inorganic Nanohybrids ..... 69
3.4.6 Why Rapid Drying is better ..... 69

3.5 Conclusion ..... 70

Chapter 4: A novel stem cell binding motif identified by phage display promotes non-viral gene delivery to stem cells ..... 71

4.1 Introduction ..... 71

4.2 Experimental Procedure ..... 74

4.2.1 Materials ..... 74

4.2.2 Primary rat mesenchymal stem cell isolation and culture ..... 74

4.2.3 Selection of rMSC-binding peptide from a phage-displayed random peptide library: Biopanning ..... 75

4.2.4 Phage titering, amplification and purification ..... 77

4.2.5 Statistical Analysis ..... 78

4.2.6 Fluorescence imaging using synthetic peptide ..... 78

4.2.7 The construction of Liposome/Protamine/DNA complex (LPD) ..... 79

4.2.8 Transfection Efficiency ..... 80

4.2.9 Cytotoxicity Assay ..... 80

4.3 Results ..... 81

4.3.1 Identification of peptides that can specifically bind with primary rMSCs by phage display ..... 81

4.3.2 Bioinformatics analysis suggests that CX3CL1-CX3CR1 axis may mediate binding between the identified peptide, HMGMTK, and rMSCs. ..... 88

4.3.3 Synthetic peptide HMGMTK showed higher binding affinity to primary rMSCs compared to scrambled peptide as control and its affinity binding

could be competitively inhibited by engineered phages displaying HMGMTK peptide ..... 92
4.3.4 Integrating MSC-binding peptide HMGMTK and NLS peptide into Liposome/Protamine/DNA (LPD) nanocomplex showed increased transfection Efficiency but remain low cytotoxicity ..... 93
4.4 Discussion ..... 97
4.4.1 Peptide HMGMTK may serve as CX3CL1-like ligand and bind to CX3CR1 which may narrow the putative binding site region of CX3CL1 ..... 101
4.4.2 MSC binding peptide HMGMTK may serve as a binding motif and agonist of CX3CR1 for facilitating the systemic delivery of gene or drug to MSCs via receptor mediated endocytosis and improving the use of MSCs in the field of cell therapy and regenerative medicine ..... 103
4.5 Conclusion ..... 105
Chapter 5: Summary of Results and Future Directions ..... 106
5.1 Summary of results ..... 106
5.2 Outlook and future directions ..... 108
5.2.1 Tissue engineering for bone regeneration ..... 108
5.2.2 Proteomic analysis (Ligand-receptor/Antibody-antigen interaction) ... 109
5.2.3 Customized diagnosis and targeted therapy ..... 110
Chapter 6: References ..... 112
[Appendix A: Permissions and Copyrights] ..... 130

[Appendix B: Copy of Approval from Institutional Animal Care and Use Committee (IACUC)]..... 143

# List of Tables

Table 1-1 The coat proteins on one M13 bacteriophage and their functions ..... 4

Table 1-2 Identified peptide motifs using phage screening against mammalian cells and tissues. ..... 17

Table 3-1 A summary of conditions interrupting the association of Au-NPs and phage with justification. ..... 66

Table 4-1 Peptide sequences identified by phage display. Homological motifs were underlined and the most frequent one (A/H)MG(M/L)(T/L/S/R)(K/T/S) were also highlighted in bold. ..... 87

Table 4-2 The cell surface molecular profile of mesenchymal stem cells ..... 89

# List of Figures

Figure 1-1 Schematic structure of the filamentous bacteriophage ..... 3

Figure 1-2 3D structure of one M13 phage (PDB:1ifd) and its top view and bottom view. Crystal structure of pVIII which can be divided into four portions: a mobile segment colored in dark blue, an amphipatic helix in bright blue, and a highly hydrophobic helix in yellow, and another amphipatic helix in pink but with four positively charged amino acids in red which are responsible for binding negatively charged DNA phosphate backbone. ..... 6

Figure 1-3 A sketch of Phage life cycle ..... 7

Figure 1-4 Different types of phage display based on different types of coat proteins.[9] ..... 8

Figure 1-5 Basic procedure of phage library screening on biological systems. A) In vitro cell panning; B) In vivo panning against live animals. ..... 13

Figure 1-6 Bone formation in natural bone ..... 21

Figure 1-7 Scheme of phage display applied in the fabrication of bone materials ..... 22

Figure 2-1 Phage display technique. a) TEM images of wild type M13 phages. b) Display of a foreign peptide on the side wall of M13 phage by fusing the peptide to the N-terminus of pVIII. c) 3D model of M13 phage pVIII protein coat (PDB id: 1ifd). ... 30

Figure 2-2. TEM images of engineered phages. a) E phages; b) Q phage bundles; c) mixed EQ phage bundles. d) Circular dichroism spectra of wildtype, E, Q and EQ phages. ..... 35

Figure 2-3 TEM images of nucleation of HAP on E and Q phages after incubation in supersaturated HAP solution for 10 days and 20 days. a) HAP nucleation on E phages

for 10 days. b) HAP nucleation on E phages for 20 days. c) HAP nucleation on Q phages for 10 days. d) HAP nucleation on Q phages for 20 days. ..... 37
Figure 2-4 TEM images of the HAP nucleation on EQ phage bundles after incubation for: a) 5 days, b) 10 days, c) 15 days and d) 20 days. ..... 39
Figure 2-5 The three dimensional simulation of possible HAP nucleation mechanism. a) 3D model of possible EQ phage bundles. b) The simulation of intermolecular beta sheet formed by two HAP nucleating peptides displayed on phage pVIII. This model includes the aspartic acid (D) which is the following amino acid right after the inserted foreign peptides in pVIII due to its possible contribution to the beta sheet formation. c) describes the possible mechanism of the HAP nucleation and growth along c-axis due to the specific match between the negatively charged amino acid in HAP nucleating peptides forming intermolecular beta sheet and the (001) plane of HAP crystals. d) shows the four calcium ions on HAP (001) plane that can perfectly match four negatively charged amino acids. e) is a closer look of electrostatic attraction between matched negatively charged amino acids and calcium ions. f) is the 3D model which schematically illustrates the possible mechanism of HAP crystal nucleation and oriented growth triggered by EQ phage bundles. ..... 43
Figure 3-1 a) M13 wild type phage particles composed of ~2700 copies of major coat proteins (pVIII) and 5 copies of each minor coat protein (including pIII, pVI, pVII, and pIX); b) Positively charged Au-NPs interacted with anionic phage particles into bundle structures..... 48

Figure 3-2 a) Synthesized gold nanoparticles and the electron diffraction pattern; b) wild type M13 phages stained with 1% UA; c) gold-nanoparticle-phage hybrids precipitation; d) TEM image of the hybrid precipitation from c. ..... 55

Figure 3-3 Comparison of Figure 3-2d and Figure 3-4b. Au-NPs in Figure 3-4b are highlighted by red circles. The density of Au-NPs on the hybrids after negative staining is almost the same as without staining. ..... 56

Figure 3-4 a) Au-NP-phage hybrids were stained with 0.5% UA solution (pH=4.5, 10 s of staining, rapid drying); b) high resolution image of a); c) Au-NP-phage hybrids were stained with 0.5% PTA solution (pH=7, 10s of staining, rapid drying); d) high resolution image of c). ..... 57

Figure 3-5 a) Au-NP-phage hybrids were stained with 2% UA solution (pH=4.5, 10s of staining, rapid drying); b) Au-NP-phage hybrids were stained with 0.5% UA solution (pH=4.5, 1 minute of staining, rapid drying); c) high resolution image of b); d) Au-NP-phage hybrids were stained with 0.5% UA solution (pH=3.5, 10s of staining, rapid drying); e) Au-NP-phage hybrids were stained with 0.5% UA solution (pH=4.5, 10s of staining, slow drying); f) Au-NP-phage hybrids were pre-fixed by 1% GA solution and stained with 0.5% UA solution (pH=3.5, 1 minute of staining, slow drying). ..... 60

Figure 4-1 Scheme of applying phage display and mesenchymal stem cells to customized therapy. ..... 73

Figure 4-2 Recovery of phages after affinity selection on primary rat MSCs (O/I ratio) ..... 82

Figure 4-3 Plot of the information content of peptide sequences calculated by RELIC-INFO program. RELIC-INFO program was used to measure the probability of a peptide

sequence by random selection or by affinity selection. In this program, the probability of any one peptide in the library is defined by a parameter called Information content= - ln (P) where P is the product of the probability of each amino acid at each position, a.k.a. $P = P_1P_2P_3 \bullet\bullet\bullet P_{12}$. The red curve with round dots is the information content of selected sequences from affinity selection on rMSC. The black curve with square dots is the information content of originally random Ph.D.-12 library sequences used as control. The dark blue dash line shows the cutoff indicating significant improvement of the reliability of selected sequences compared to random library sequences. ..... 85

Figure 4-4 The similarity score of reliable selected sequences and several known ligands that interact with both MSC positive and negative surface receptor. Stro-1, SB10, CX3CL1, SDF-1, CXCL16, ICAM-1, VCAM-1, fibronectin are the known ligands that could bind to the MSC expressed cell surface receptors (MSC+). LYN and CCL11 are two examples of known ligands binding the receptors that MSCs could not express (MSC-). A cutoff value 10 was set for indicating the significant similarity by arrows. ..... 91

Figure 4-5 Best match position in the full length CX3CL1 with reliable selected sequences aligned by RELIC-MATCH program. This match position in CX3CL1 is localized in its N-terminal chemokine domain (CX3CL1-CD) which may suggests the exact binding site of CX3CL1. ..... 91

Figure 4-6 The fluorescence imaging showing the higher affinity of peptide HMGMTK compared to scrambled peptide as control. A) rMSCs after interacted with FITC-HMGMTK peptide; B) rMSCs after interacted with FITC-scrambled control peptide; C) rMSCs after treated with phage displaying HMGMTK first and then interacted with

FITC-HMGMTK peptide; D) rMSCs after treated with phage displaying HMGMTK first and then interacted with FITC-scrambled peptide. E) fibroblasts incubated with FITC-HMGMTK peptide; F) MCF-7 cells incubated with FITC-scrambled peptide. Cell nucleus was stained by DAPI. Scale bars in A, B, C, and D are 50μm and in E and F are 100μm. ..... 93

Figure 4-7 TEM image of LPD particles. ..... 94

Figure 4-8 Transfection efficiency of LPD with peptide HMGMTK and NLS peptide in rMSC. GFP expression level in rMSCs due to the delivery of EGFP reporter gene by LPD only (a) and LPD+PA+NLS (b) was visualized by fluorescence imaging. Scale bar: 100 μm. ..... 95

Figure 4-9 MTT assay for evaluating cytotoxicity of LPD+PA+NLS at different liposome concentrations. Lipofectamine™ 2000 and LPD without peptide were used as a control. The cell viability of samples with LPD with PA and NLS above liposome concentrations 50mM was higher than 60%. Lipofectamine™ 2000 had obvious toxicity as concentrations over 20 mM. The data points represent the mean ±SD of three trials. ..... 96

Figure 4-10 The tertiary structure of chemokine domain of CX3CL1. It consists of a flexible N-terminal region three beta strands (in yellow), and a C-terminal helix (in red). The six amino acids showing highest similarity to peptide HMGMTK are marked in magenta. ..... 102

## Abstract

Nanostructure is an object system that has dimensions on the nanoscale, i.e. between 0.1 and 100 nanometers. It includes nanotextured surface, nanotube, nanorod, nanofilament, nanoparticle, etc. The field of nanostructure science and technology is an explosively growing area in the past decades. Its tremendous potential for innovating the material science (referred as nanotechnology) and promising applications in the conjugation with current medicine (referred as nanomedicine) to preserve and improve human health is already clear, though the understanding of nanostructure functionalities is just beginning to reveal. Nanostructures can be considered as novel rising objects in the scientific community. However, to biologists, nanostructures are familiar since even the simplest organism contains astoundingly sophisticated elements functionalizing at the nanoscale which are still difficult even under the most advanced technologies, such as protein folding, formation of protein aggregates, pairing of nucleotides, and precise assembly of microbes.

Filamentous bacteriophage, the subject of this dissertation, is a representative instance of naturally biological nanostructures. Using standard molecular cloning technique, foreign peptides can be fused into the phage protein on the surface, termed as Phage Display technique. Although phage display has primarily been used for studying protein-protein interactions, it has two main research directions in the area of nanotechnology by using two different aspects of phage. The filamentous shape of the phage in the nano range provides the bio-template function of phages used within nanotechnology and material science while phage display can also provide an easy way to discover new targeting motifs, drugs or epitopes for medical applications. Both

methods are becoming more popular, but the possibility of identifying targeting peptides against live cells and intact tissues including tumors greatly increases the potential application of using phage display in the biomedical field. My research followed the two main research directions of phage display in nanotechnology. I also focused on the uses and advances of phage display in the biomedical field.

Chapter 2 is the application of phage as a bio-template for bone regeneration: Oriented nucleation of hydroxylapatite crystals on self-assembled bacteriophage bundles. This work demonstrates the hydroxyapatite crystals can be nucleated on self-assembled bacteriophages in a preferred c-axis orientation. The resultant bacteriophage may serve as the building block to substitute collagen and form bone implant. It has a great potential in the field of tissue engineering. It also proved that the driving force of phage self-assembly is beta sheet secondary structure and beta sheet between phage bundles can induce the orientated nucleation of hydroxyapatite crystals. The beta sheet formation can be used as a general method to precisely control assemblies between engineerable biomaterials. In natural bone, HAP crystals are nucleated and grown with their c-axis preferentially parallel to collagen fibrils. In the work of Chapter 2, we also found that HAP crystals were also nucleated on EQ bundles with their c-axis preferentially parallel to phage bundles, which greatly mimicked the base level of hierarchical structure of natural bone. We further found that calcium ions were attracted to the glutamic acids and aspartic acids of peptide E and Q with a pattern matching with calcium ions on the (001) plane of HAP crystals. This specific matching then induced the HAP nucleation on the beta sheet and the growth along the c-axis. This work

provided the proof for a new way of fabricating bone biomaterials by biomimicking and bioinspiration.

Chapter 3 is the phage as a bio-template for the synthesis of phage-gold nanocomposites. Bacteriophage-gold nanocomposite was constructed in the work of Chapter 3 to use as a model to study the optimum condition for best TEM imaging of bioinorganic nanohybrids. In this work, wild type M13 phage was combined with gold nanoparticles to form phage-gold nanocomposite. Most Au-NPs were aligned into large belts, forming a net-like structure. TEM imaging of negatively stained bioinorganic nanohybrids is a simple way to characterize these nanostructures that may have biomedical functions. By studying the effects of different factors on the negative staining of phage-gold nanocomposites, we found that the optimum staining conditions for these bioinorganic nanohybrids are using 0.5% UA solution with pH 4.5, staining for 10 seconds, and rapidly drying the stains. This work demonstrates that each staining factor has an influence to the final appearance of stained specimens and optimum staining condition needs to be customized to the individual type of bioinorganic nanohybrids. The effects of each staining factor and a general guideline for selecting staining condition were provided in this work. Therefore, this research provides useful information for the characterization of bioinorganic nanomaterials by TEM imaging. It will help the research in the field of nanomaterials and bionanotechnology.

Chapter 4 is discovering a novel targeting motif to mesenchymal stem cells by phage display to improve the efficiency and specificity of gene or drug delivery. In this work, we did cell panning on primary mesenchymal stem cells and identified peptide HMGMTK as MSC binding peptide. Further bioinformatics analysis suggests that

peptide HMGMTK has high similarity to the signaling regions of chemokine CX3CL1. This may suggest a possible mechanism that could explain the MSC homing effect of the selected peptide. We then constructed a novel and effective mesenchymal stem cell gene delivery vector by liposome/protamine/DNA complex incorporating with identified MSC-targeting motif and Nuclear localized signal (NLS) motif. Through several evaluations, we proved that this resultant complex is multifunctional, effective, but low-cytotoxic MSC gene delivery vector. The transfection mediated by the resultant complex LPD+PA+NLS showed higher efficiency and specificity compared to those achieved by LPD only, LPD with control peptide, or LPD with PA only. Meanwhile, MTT results supported the low cytotoxicity of LPD+PA+NLS complex. Based on all the results, we can conclude that a novel rMSC binding peptide HMGMTK was identified and could be used to build up a promising gene carrier for facilitating liposome-mediated MSC gene delivery.

# Chapter 1: Introduction

2010 is the 25th anniversary of phage display since George Smith first introduced it in 1985 [1]. Phage display is a term defining fusion of exogenous peptide sequences onto the capsid proteins of filamentous bacteriophages. The subject of phage display is filamentous bacteriophage (simply phage) including M13, Fd phage, etc.[2]. Phage is a linear-shaped type of virus that specifically infects gram-negative bacteria, such as Escherichia coli (E. coli) TG1, XL-1 Blue, ER2738. In phage display, different foreign peptide sequence variants (up to 1010 diversity) could be expressed or displayed on the surface of the phage concurrently by designing randomized primers during genetic engineering rather than having to express and purify peptide sequence one after another in the traditional recombinant protein expression. The resultant phage display product displaying various peptide sequences is visually termed as "phage library". Coupled with affinity selection process (known as panning), phage library renders the feasibility of rapid and efficient identification of acting or signalling regions of proteins or peptides with high affinity and specificity to most targets, including molecules in vitro, living cells, human or animal tissues and even human tumor patients. This is the most valuable aspect of phage technology since no pre-attentive knowledge about the interaction is necessary.

In this chapter, I will provide the basics of bacteriophage: the biology and structure of bacteriophage. I will explain the principles of phage display technique. A detailed explanation will be given to the phage display-based peptide screening against cells *in vitro* and tissues *in vivo*. I will then introduce the applications of phage display in nanotechnology and biomedical science. Further attention will be on the application

of the identified cell/tissue-targeting peptides for improving biomedical research and in the novel design of a therapeutic strategy to overcome barriers in traditional drugs or clinical treatments.

## 1.1 Filamentous Bacteriophage Biology

### *1.1.1 Phage structure as a biological nanorod*

Filamentous bacteriophage is a rod-shaped type of viruses that usually infects Gram-negative bacteria and its main type is Ff phages. The Ff class of filamentous bacteriophages includes M13, fd, f1, and lke phages possessing 98% identical DNA sequences, though M13 is the most studied type [2].

Till now, there are two main research directions in which filamentous bacteriophages are investigated by utilizing different properties of phages. First, Ff phages are nonlytic and parasitic viruses, which means that infection and production of Ff phages will give rise to progeny virus extruded out of the bacterial membranes without causing host death, but rather leaving the infected cells continuing to grow and proliferate. This parasitic nature of Ff phage becomes one of the reasons that made the filamentous bacteriophage, especially M13 phage, become an efficacious workshop for expressing protein or peptide of interest; while little limitation of inserted DNA and the superbly high viral productivity are the other two reasons. Second, the Ff phages are in nanometric dimensions, about 1 μm in length and 6 nm in width, which could fit into the definition of nanostructures and thus can be adapted into the exploitation of nano-bio-technological use, together with other biological molecules, such as DNA, actin filament or amyloid fibrils (Figure 1-1). As biological nanorods, filamentous

bacteriophages can provide the scientists a natural biotemplate for nanomaterial synthesis.

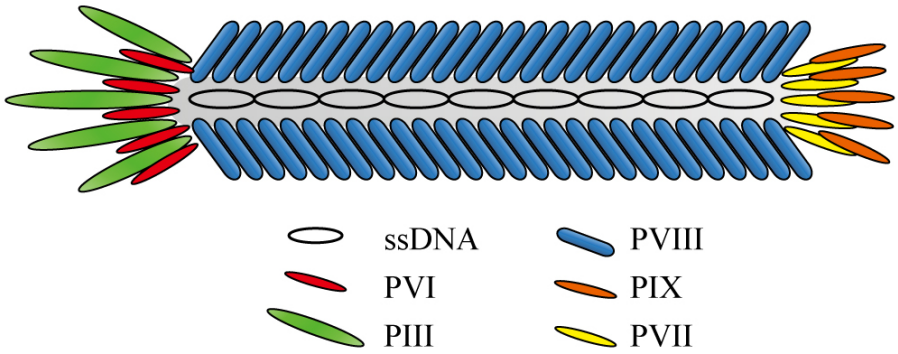



**Figure 1-1 Schematic structure of the filamentous bacteriophage**

Wild type M13 phages consist of a circular single-stranded DNA (ssDNA) with 6407 bases surrounded by 2700 copies of the major coat protein pVIII. Five copies of four different types of minor coat protein are on both of the ends: pIII and pVI cap one end, while pVII and pIX cap on the other one. These five types of coat protein together are categorized as structural protein since they are expressed on the surface of phages to form the final intact phage structure, while the other six types of protein are only involved in the infection and replication process of phages as non-structural proteins (Table 1-1). Among five structural proteins, pVIII occupies the majority of phage in mass, about 85%. The high amount of pVIII present on one phage particle makes it become a productive candidate for foreign protein expression on phages, though pIII is the first coat protein that studied for this purpose.

| Categories | Protein name | # of amino acids | M.W. | Copies | Function |
|---|---|---|---|---|---|
| Structural | pIII | 406 | 42,522 | 5 | Host infection |
| | pVI | 112 | 12,342 | 5 | Minor coat protein |
| | pVIII | 50 | 5,235 | 2700 | Major coat protein |
| | pVII | 33 | 3,599 | 5 | Minor coat protein |
| | pIX | 32 | 3650 | 5 | Minor coat protein |
| Non-structural | pI | 348 | 39,502 | | Assembly |
| | pII | 410 | 46,137 | | DNA replication |
| | pIV | 405 | 43,476 | | Viral assembly |
| | pV | 87 | 9,682 | | Binding ssDNA |
| | pX | 111 | 12,672 | | DNA replication |
| | pXI | 108 | 12,424 | | Viral assembly |

**Table 1-1 The coat proteins on one M13 bacteriophage and their functions**

pIII is the largest and most complex protein among all the phage proteins. It is responsible for recognizing the host cell surface via F-pilus and therefore infecting the host. Details will be introduced in the next section: phage life cycle. It has three domains, N1, N2 and N3; the two N-terminal segments N1 and N2 are believed to be somewhat flexible at the end of phage to do host infection, while the C-terminal N3 domain is interacted with pVIII and thus associated into the phage particle. The association is first formed by the N-terminal domains N1 and N2 of pIII with F-pili of male *E. coli* hosts; during the infection it is shifted to the complex of N1 and the C-terminal domain of Tol-A protein as a co-receptor in the Tol-QRA complex within the inner membrane of bacterial cells while N2 is still associated with F-pili [3]. This is

responsible for recognizing the host cell surface via attaching F-pilus of male *E. coli* to initiate the infection process.

The major coat proteins pVIII are arranged in a right-handed helical pattern with a fivefold rotational axis and a twofold screw axis with a pitch of about 3.2 nm to form a 1.5-2 nm thick protein coating around single-stranded DNA. Each of pVIII is alpha helical and can be divided into four portions from N-terimus to C-terminus: a mobile segment having 4 or 5 amino acids, an amphipathic helix portion, a highly hydrophobic helix portion, and another amphipathic helix portion with four positively charged amino acids for interacting with negatively charged phosphate backbone of ssDNA (Figure 1-2).

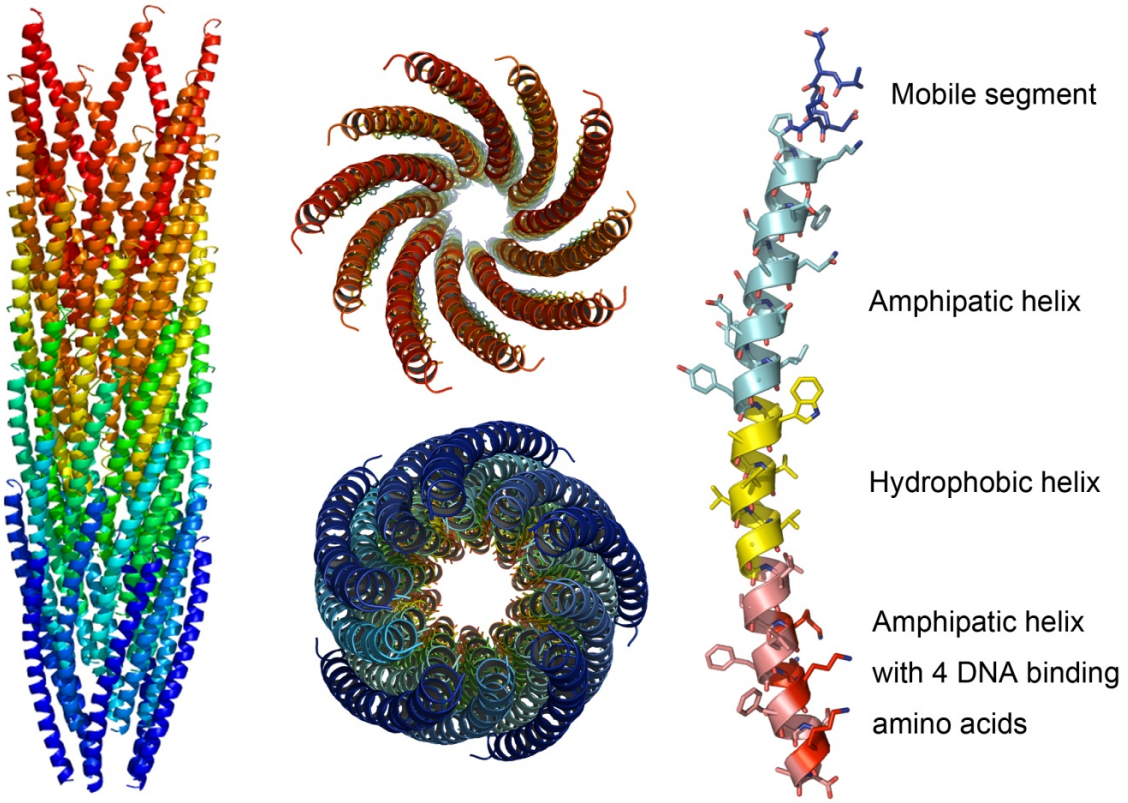



**Figure 1-2 3D structure of one M13 phage (PDB:1ifd) and its top view and bottom view. Crystal structure of pVIII which can be divided into four portions: a mobile segment colored in dark blue, an amphipatic helix in bright blue, and a highly hydrophobic helix in yellow, and another amphipatic helix in pink but with four positively charged amino acids in red which are responsible for binding negatively charged DNA phosphate backbone.**

### *1.1.2 Phage Life Cycle*

The life cycle of filamentous bacteriophage can be divided into three stages: infection, replication, and assembly (Figure 1-3). During filamentous phage infection, the virus first binds to its primary receptor – the tip of the F-pilus inserted on bacterial cell surface, followed by the phage coat protein integrating into the bacterial cell membrane, so that the viral ssDNA injected into host cell cytoplasm to enter the replication stage. pII and pX, two of non-structural proteins, are crucial for the

replication. pII has both endonuclease and topoisomerase activities required during the DNA replication phase of infection.

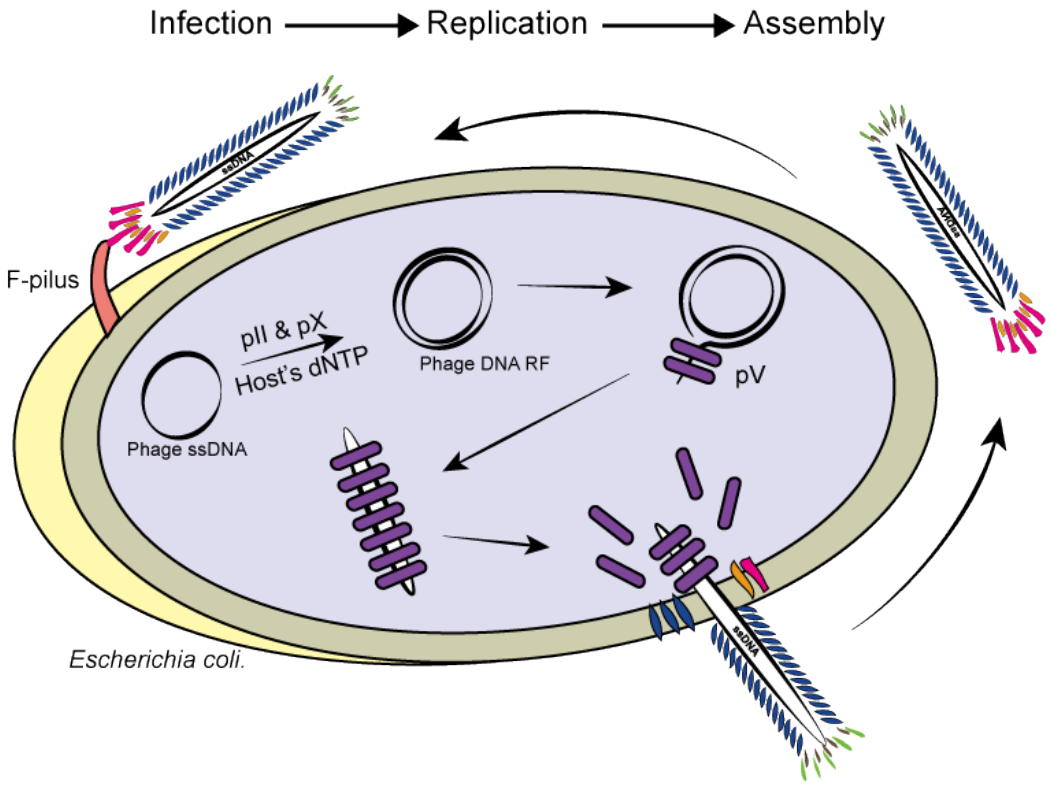



**Figure 1-3 A sketch of Phage life cycle**

## 1.2 Phage display: displaying a peptide on the surface to change the surface chemistry

### *1.2.1 Principles and different phage display modes*

The main theme of phage display is to incorporate foreign peptides into the coat protein of filamentous bacteriophages. Yet the various types of phage coat protein and the necessity of ensuring engineered coat protein still functional as well as the biological bottlenecks during phage replication course question the phage display and the construction of phage library, making the following three queries: (1) Which types

of coat protein are used in phage display? (2) What is the strategy for phage display? (3) What is the strategy for constructing phage library? (4) Which foreign protein or peptide we could display on phages? Is there any limit for them?

Years of experiments have led to the successful peptide and protein fusions into all the five types of structural coat protein of phage (Figure 1-4): to the N-terminus of display on pIII, pVII, pVIII and pIX and on the C-terminus of pVI [4-8]. pIII is the first phage coat protein used for fusing foreign peptide. pIII and pVIII display is the most common approach so far mainly by reason of their prominent merits which are wider tolerance range and stronger productivity, respectively. Wider tolerance range means that the larger peptides or proteins could be displayed more easily on pIII and stronger productivity describes that displayed peptide or proteins will have greater yield on pVIII than other types of protein. Both of them have highly significant value in consideration of the essence of phage display that bring pIII and pVIII display into fashion.

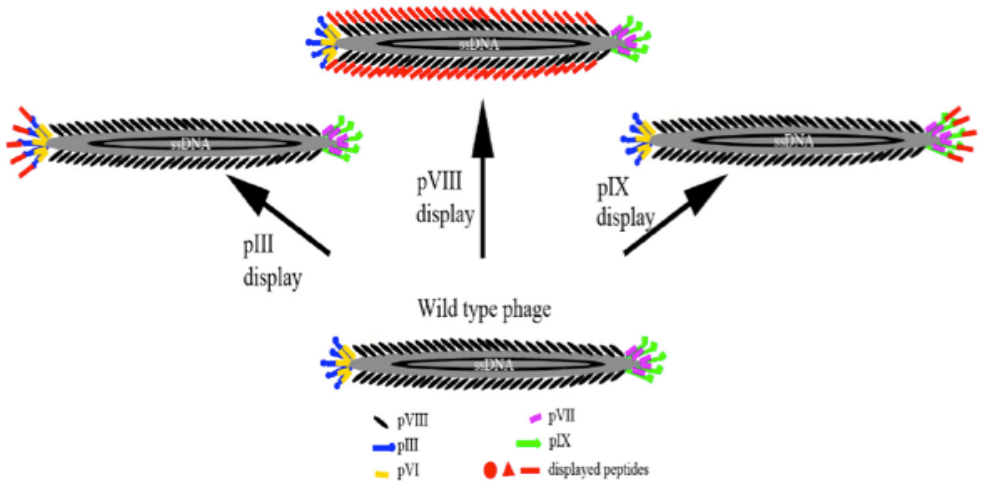



**Figure 1-4 Different types of phage display based on different types of coat proteins.[9]**

Regardless of the different structural protein types in phage display, the strategies for achieving phage display is mainly three types: phage, hybrid and phagemid systems termed by Kehoe *et al*, or type *n*, *nn*, and *n*+*n* named by Smith *et al* (*n* represents the type of coat protein used in phage display. For example, *n* is 3 for pIII and 8 for pVIII.) [10, 11]. The different modes of phage display on pVIII are taken for instance in order to minimize the possible confusion. The phage system or type 8 is that the exogenous protein or peptide to be displayed is fully expressed on each copy of coat protein by incorporating the coding gene of displayed peptide into the single stranded phage genome. Till now phage system is only obtained positively on pIII and pVIII that make types 3 and 8. In hybrid system or type 88, the phage genome is harboring two gVIII (coding gene for pVIII): one is the wild type gVIII and the other one is recombinant gVIII fused with displayed peptide or protein coding gene; rather than having just only recombinant gVIII in the genome as the phage (type 8) system. The consequence is that the capsid of phage virions is hybrid which is a mixture of wild type and recombinant pVIII. Speaking of phagemid system, it is necessary to explain the definition of phagemid. A phagemid is a hybrid of the phage and plasmid which is also packaged as ssDNA inside the phage virions. It has both the plasmid origin of replication (*ori.*) which allows its replication in *E. coli* host and the phage *ori.* which is functional only after the infection by wild type phages termed as helper phage in type *n*+*n* phage display since the non-structural proteins coded in helper phage genome are required for phage replication. Similar to hybrid system (type 88), the capsid of the resultant phage virion in phagemid system (type 8+8) is a mixture of wildtype and recombinant pVIII.

## 1.3 Phage display: Screening random phage-displayed peptide library against biological systems - Biopanning

Since invented in 1985, phage display was further developed and improved by many scientists such as John McCafferty [12-14]. Analogous to natural evolutionary selection, large libraries of proteins in the phage library could be screened and amplified in an affinity selection called phage panning or biopanning. Custom phage libraries could be constructed though the commercial phage libraries are already enough for identifying a targeting motif to a certain biological target.

### *1.3.1 The construction of a phage library*

Besides the different phage display strategy, the genetic engineering method for phage display is also diversified, especially for the construction of phage displayed libraries. While other methods are also available, such as random mutagenesis including *in vitro* chemical mutagenesis and error-prone PCR, combinatorial infection and recombination, and DNA shuffling [15-20], the most commonly used method for this purpose is oligonucleotide-directed mutagenesis based on degenerate codons and PCR. Degenerate codons can be represented by NNK in which N = A/T/G/C and K = G/T. By means of designing the inserted gene of displayed peptide sequence in the format of degenerate codon $(NNK)_n$ (n is the number of amino acids in the displayed peptide sequence.), one will create the DNA source for random displayed peptide library. Since there are only 20 possible amino acids available, the DNA encoded peptide diversity is restricted to $20^n$ but not $32^n$ which is the coding DNA diversity. For instance, if the phage library is displaying 7 mer random peptides, then its theoretical diversity will be $1.28 \times 10^9$ ($20^7$) instead of $3.4 \times 10^{10}$ ($32^7$). After synthesizing the designed mutagenic

oligonucleotides as a primer and doing PCR, one needs to incorporate it into an appropriate vector and produce the recombinant DNA by ligation. The recombinant DNA carrying random mutagenic oligonucleotides will be introduced into a bacterial host and eventually produce a phage library displayed random peptides encoded by the mutagenic oligonucleotides.

### *1.3.2 Biopanning on live cells – Cell Panning*

Originally, phage display was used to screen against the immobilized molecules on a plate or matrix by cross-linking. The most common linking reagent is biotin which endows the name "biopanning" to this type of phage screening. But the invention of direct panning against live cells or tissues or organs [21] broadens the application range of phage display, which refers to 'cell panning' and '*in vivo* panning' respectively in this dissertation.

### *1.3.3 The basic procedure of in vitro cell panning/in vivo panninng*

In general, the panning procedure for this purpose should be adjusted by adding the clearing step and depletion to minimize any nonspecific binding prior to panning against the target. The selection against live cells can be done on either adherent or suspended cells. Different from cell panning, originally in *in vivo* panning the library is introduced into a living animal through injection, ventilation, or gavage and the bound phage is collected from homogenized tissue biopsies.

The basic procedure of cell panning and *in vivo* panning can be represented by Figure 1-5 involving steps [22-27]:

(1) Prepare the initial phage library or amplified library from previous panning rounds

(2) Pre-clear the surface receptors of cells or tissues by incubating with serum-free medium

(3) Deplete the initial library by exposing onto the blank substrate (plastic plate) or multiple cell lines (such as cells co-existing with target cells in the tissue).

(4) Expose the depleted library to the pre-cleared target cell or tissue

(5) Remove any non-specific bound phages by washing

(6) Elute out the bound phage and amplify them by infecting bacterial hosts.

(7) Repeat steps 1-6 above several times.

(8) Identify target motifs by sequencing the output of the final panning round.

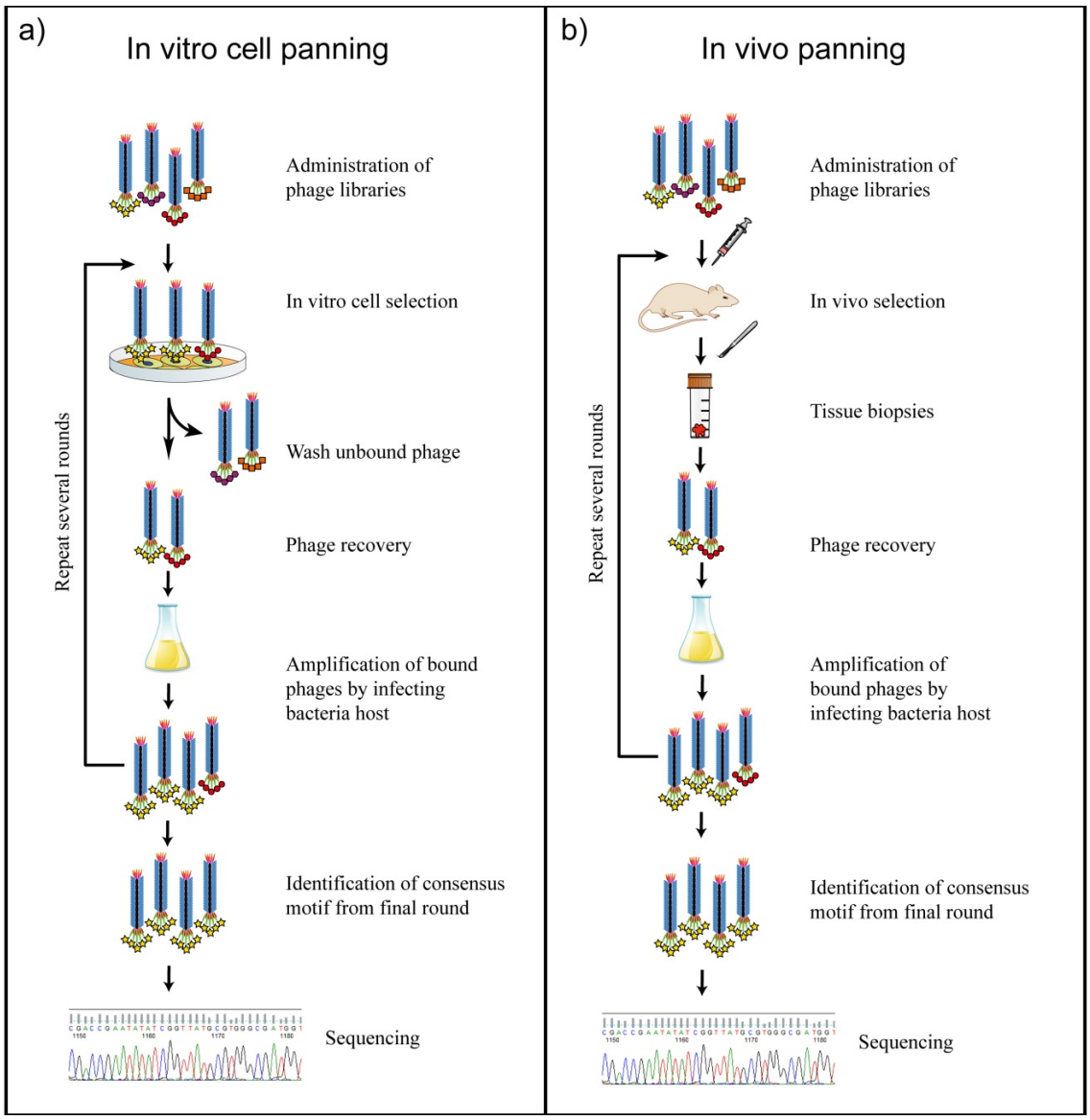



**Figure 1-5 Basic procedure of phage library screening on biological systems. A) In vitro cell panning; B) In vivo panning against live animals.**

### *1.3.4 Identified peptide motifs using phage screening against mammalian cells and tissues*

Recent technical advances allow sufficient data collection from affinity selection against multiple tissues and organs, which further ease the phage screening against complex biological systems. For instance, the use of phage libraries for identifying tumor-targeting peptides has been reviewed in ref. [28-31]. The first clinical trial of phage panning on human patients is constructed by Krag *et al.* [32]. Identifying targeting peptides to stem cells has also proved feasible [33]. Table 1-2 lists the targeting peptides that have been identified by cell panning and *in vivo* panning with a random peptide-displayed phage library, and those using the scFv and combinatorial antibodies libraries are not listed.

| Targets | Sequence | Reference |
|---|---|---|
| ***Cell panning*** | | |
| *Cancer cells* | | |
| Human hepatic carcinoma cell ExTie2 | NSLSNASEFRAPY | [34] |
| Human breast cancer cells SKBR3 | LTVXPWX,VSSTQDFP,DGSIPWST | [35, 36] |
| Breast cancer cells MCF-7 | DMPGTVLP | [37] |
| Human neuroblastoma WAC-2 | HLQIQPWYPQIS | [38] |
| Human head and neck squamous cancer cells | TSPLNIHNGQKL | [39] |
| Melanoma cell B16F10-Nex2 | SSRTMHH | [40] |
| Murine B lymphoma A20. | pA20-6 | [41] |
| Pancreatic ductal adenocarcinoma (PDAC) cells | KTLLPTP | [42] |
| Esophageal adenocarcinoma cells OE33 | CSNFYMPLC | [43] |
| Prostate carcinoma cells P3 | DTDSHVNL,DTPYDLTG,DVVYALSDD | [44] |
| Non-small cell lung cancer cells | QQMHLMSYAPGP;TDSILRSYDWTY | [45, 46] |
| Human glioma cells | LLADTTHHRPWT | [47] |
| U87MG glioblastoma cell | VTWTPQAWFQWV | [48] |
| Human medullary thyroid carcinoma-derived TT cells | HTFEPGV | [49] |
| Nasopharyngeal carcinoma (NPC) cells | RLLDTNRPLLPY | [50] |
| *Epithelial cells* | | |
| Human gastric cancer vascular cells | CGNSNPKSC | [51] |
| Human airway epithelial cells | THALWHT | [52] |
| Human airway epithelial cell line | LQHKSMP | [53] |
| Endothelial cells ECV304 | SPL(W/F)(R/K)(N/H)S(V/H)L | [54, 55] |
| | YCPRYVRRKLENELLVL | |
| Lung endothelial cells | CGSPGWVRC | [56] |
| Human blood outgrowth endothelial cells (HBOEC) | SPTPS(P/L)PPSAGG | [57] |
| Human Vascular Endothelial Cells | SIGYPLP | [58] |
| Vascular smooth muscle cells (VSMC) | CESLWGGLMWTIGLSDC | [59] |
| | CNIWGVVlSWIGVFPEC | |
| Vascular Smooth Muscle Cells | EYHHYNK | [60] |
| | GETRAPL | |
| Murine myofibers | ASSLNIA | [61] |

| | | |
|---|---|---|
| Primary cardiomyocytes | WLSEAGPVVTVRALRGTGSW | [62] |
| Cardiac vasculature cells | DDTRHWG | [63] |
| TNF-α activated bovine aortic endothelial cells | CLWTVGGGC | [64] |
| *Stem cells* | | |
| Mouse neural stem cells C17.2 | CGLPYSSVC | [33] |
| Monkey neural stem cells | HGE*VPRFHAV*H | [65] |
| Mouse embryonic stem cells | KHMHWHPPALNT | [66] |
| Rhesus monkey embryonic stem cells RS366.4 | APWHLSSQYSRT | [67] |
| *Other types of cells* | | |
| Dendritic cells (DC) | YTYQGKL | [68] |
| Human dendritic cells | FYPSYHSTPQRP,AYYKTASLAPAE,SLSLLTMPGNAS | [69] |
| Rat malignant rat glial cells | D(T/S/L)TK motif | [70] |
| Murine microglial cells EOC20 | (S/T)F(T/X)YWS | [71] |
| Mouse PEA10 fibroblasts | KTLTLEAALRNAWLREVGLK | [72] |
| S100A4 knockout embryonic fibroblasts | F/YCC motif | [73] |
| Human colorectal cells WiDr | HEWSYLAPYPWF | [74] |
| M cell | SFHQLPARSPLP<br>GSTQAWMSPPLA<br>LLADTTHHRPWT<br>CSKSSDYQC<br>CTGKSC, PAVLG, LRVG | [75-77] |
| Plasmodium falciparum-infected red blood cells | LVDAAAL | [78] |
| Skin langerhans cells (LCs) | GPEDTSRAPENQQKTFHRRW | [79] |
| Human papilloma viruses (HPVs) transformed cells | C(R/Q)(L/R)T(G/N)XXG(A/V)GC | [80] |
| Human Sperm | XLWLLXXG | [81] |
| Human umbilical cords | KPSGLTY | [82] |
| Human and rabbit synovial cells | SFHQFARATLAS | [83] |
| Hyaluronan on cell surfaces | GAHWQFNALTVR | [84] |

## *In vivo panning*

| | | |
|---|---|---|
| Human medullary thyroid carcinoma | SRESPHP | [85] |
| Mouse mammary tumor | RLQLKL,RTRYED,RIPLEM,QFDEPR,TSAVRT | [86] |

| | | |
|---|---|---|
| Sprague-Dawley rat islets | LSGTPERSGQAVKVKLKAIP | [87] |
| PPC-1 human prostate carcinoma xenograft tumors | R/KXXR/K | [88] |
| Rat transient middle cerebral artery occlusion model | CLEVSRKNC | [89] |
| Mice oral cancer xenografts | SNPFSKPYGLTV, YPHYSLPGSSTL | [90] |
| Rat islet tumors | CRGRRST, CKAAKNK, CRSRKG | [91] |
| Rat glioblastoma | NIPYNPY,YLGDTIEEL,VLASPLN,NL GLETS, GNSLSFP,IRTPSTV,RRPVNCI, ELVKIFS,VAVTDSR,AISPRLSS,NISY NAY,DATRLSS,THVHMLS,HPTKWPL ,SLPPKTT,AHEHTYA,VGNNNYP, DHLHSSR,TCLQYLGRVV | [92] |
| Mouse lung | CGFECVRQCPERC | [93] |
| Mouse skin | CVALCREACGEGC | [93] |
| Mouse retina | CSCFRDVCC | [93] |
| Mouse pancreas | SWCEPGWCR | [93] |
| Mouse brain | CSSRLDAC | [21] |
| Mouse kidney | CLPVASC | [21] |
| Mouse placenta | TPKTSVT | [94] |
| Mouse fat | CKGGRAKDC | [94] |
| Abdominal skin of BALB/cA nude mice | ACSSSPSKHCG | [95] |
| Rat kidney | HTTHREP, HITSLLS | [96] |
| Gastrointestinal mucosal barrier | YPRLLTP, CSKSSDYQC | [97, 98] |
| Atherosclerotic Plaque-associated endothelium | VHPKQHR | [99] |
| Synovium | CKSTHDRLC | [100] |
| Atherosclerotic Lesion Surfaces | CAPGPSKSC | [101] |
| Murine pancreas langerhan islet | CVSNPRWKC, CHVLWSTRC | [102] |

**Table 1-2 Identified peptide motifs using phage screening against mammalian cells and tissues.**

### 1.4 Limitation on the peptides to be displayed

All the three paragraphs above answer three questions out of four in the beginning of this part, one per question. Subsequently in the last but not the least, the limitation in the displayed foreign peptides of phage display will be given an account of to the researchers dealing with phage work. Pondering over the protein synthesis and secretion process in the phage replication cycle, one would not be surprised that the main restriction of displayed peptides in phage display is imposed by the peptide size and amino acid preference during the protein insertion in the host bacterial inner membrane and protein processing for phage assembly. It is well established that excess basic amino acids in the displayed sequence harm its transport and insertion in the cell membrane due to the proton motive force (pmf) induced by extra positive charges [103-106]. Besides, cysteine residue of displayed peptide in odd number may facilitate the dimerization by intermolecular disulfide bonds formed between unpaired cysteine residues in displayed peptide and native pIII cysteine residue or between two displayed peptides on pVIII when they are inserting in the cell inner membrane [106, 107]. This spontaneous dimerization may interfere the infection by pIII or hinder the pVIII secretion and assembly as the ssDNA extruded out to form phage progeny. The study found that the cyclic disulfide rings have strong preference for the recombinant phage clones [107]. In addition, Rodi *et al.* also observed an overall under-abundance of arginine and glycine besides cysteine and an over-abundance of proline, threonine and histidine residues as well as three position-dependent amino acid bias on +1, +3, +12 downstream from the signal peptidase cleavage site in the 12-mer library [106]. Therefore, we can conclude that the actual peptide diversity of libraries (functional

diversity) is much lower than the theoretical one (technical diversity). Rodi *et al.* have also defined the functional diversity in the equation: $\text{diversity} = \text{d} = 1/(20^N \sum_k {p_k}^2)$, where N is the number of amino acids in the random peptide sequence, $p_k$ is the probability of $k$th sequence selected from the random peptide library.

## 1.5 Applications

### *1.5.1 Phage as a template to synthesize and assemble nanoparticles*

The assembly of nanomaterials into ordered hierarchical structures is a very important step towards the fabrication of supramolecular structures and nanodevices. A promising strategy is to employ well-defined nano-scale structures as templates to direct the assembly of nanomaterials. Till now, a wide variety of self-ordered nanostructures as templates has been studied. One important branch of these templates is refined biomolecules that are naturally occurred, including nucleic acids, proteins, viruses [108-111]. These natural biomolecules all have sophisticated hierarchical nanostructures with precise molecular recognition. Guiding the formation of functional inorganic nanomaterials with these biomolecules has led to many nanostructures with controlled size, shape, alignment, and orientation.

Filamentous bacteriophages, the subject of this research, have well-defined nanostructures, the genetically programmable surface chemistry, and excellent stability. All these properties are attractive to material scientists for using as template to fabricate nanomaterials.

### *1.5.2 Bone Regeneration*

Numerous reasons can cause bone loss and thus require bone repair, including traumatic injury, bone cancer, birth defects. The traditional treatment is to implant natural bone graft from the patients into the injured area. However, due to its limited supply and patient pain, in recent years scientists are turning to seek a substitute for bone implants by mimicking natural bone structure.

In natural bone, collagen molecules are first self-assembled into collagen fibrils and then served as template to nucleate HAP by absorbing calcium, phosphate, and hydroxide ions from our body fluid (Figure 1-6). The growth of HAP on collagen fibrils has an orientation preference. It will grow along its c-axis, a.k.a. <001>, parallel to the collagen fibrils. Although collagen is the dominant protein in bone, it has been proved that they are not greatly involved in the crystallographic control over HAP nucleation and growth. It is the non-collagenous proteins such as dentin matrix protein-1 (DMP-1) that manipulate HAP nucleation and oriented growth. After this, osteoblast, also called bone-forming cells, will attach and grow on these mineralized collagen fibrils and finally assemble into intact bone. Osteoblast is derived from mesenchymal stem cells found in bone marrows.

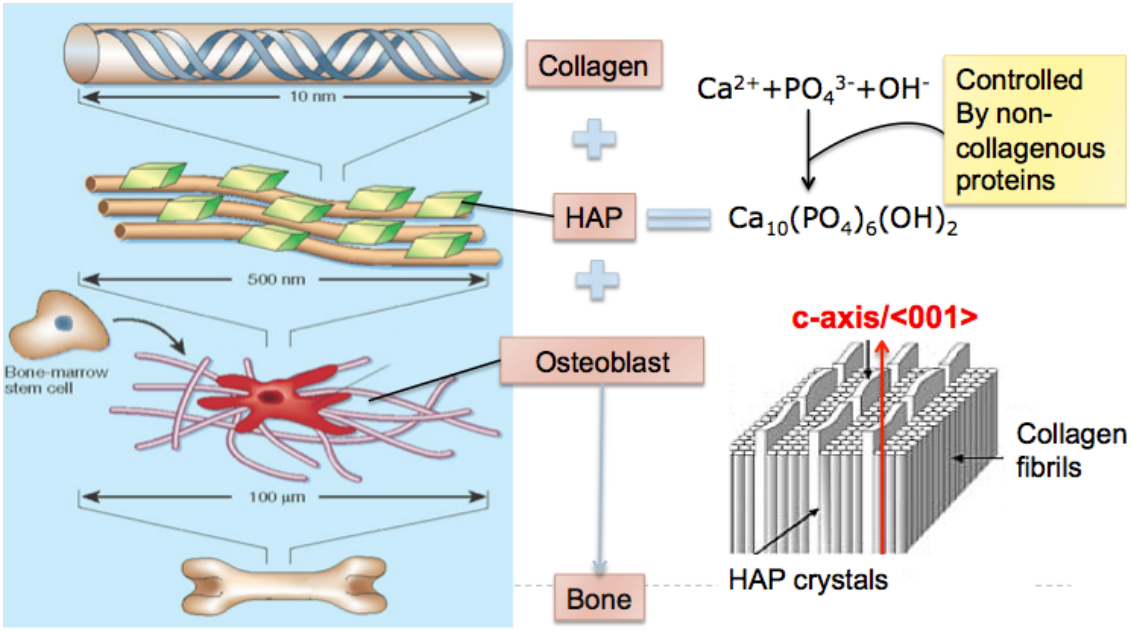



**Figure 1-6 Bone formation in natural bone**

There are three characteristics inherent to natural bone: osteoconductivity, osteogenicity, and osteoinductivity. An ideal bone material should be similar to natural bone and have all three properties (Figure 1-7). Osteoconductivity means the materials should have the ability to serve as a scaffold to support new bone formation and growth. Osteogenicity indicates the presence of osteoblasts or mesenchymal stem cells which can differentiate into osteoblasts. Osteoinducitivity means the material can promote new bone formation and growth with the presence of non-collagenous proteins that induce HAP nucleation.

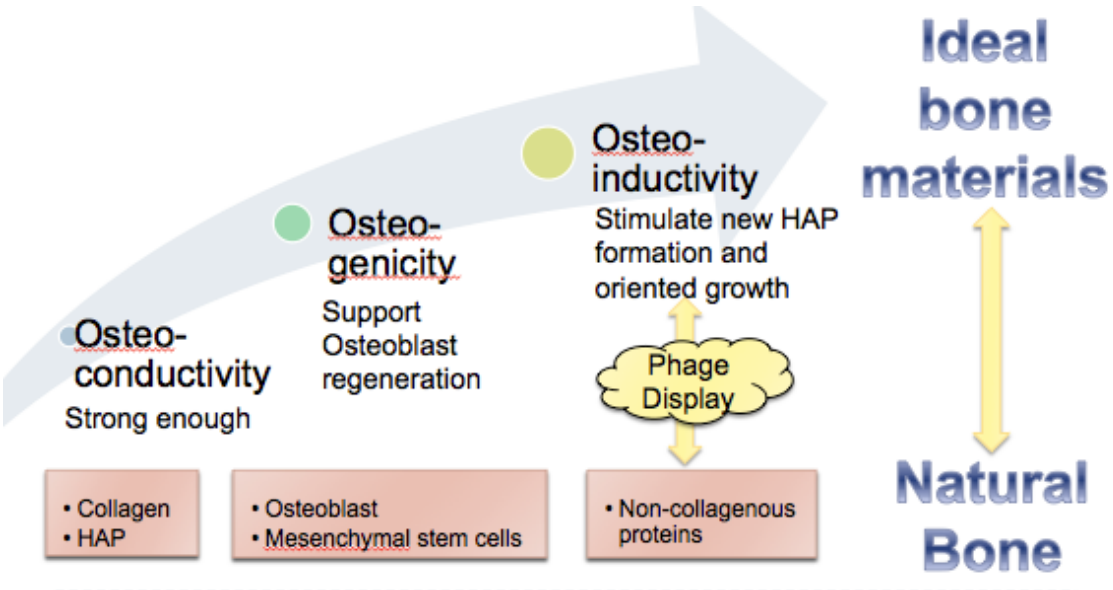



**Figure 1-7 Scheme of phage display applied in the fabrication of bone materials**

### *1.5.3 Proteomic analysis (Ligand-receptor/Antibody-antigen interaction)*

Proteomics is the study of proteins in the aspects of their structures and functions. It is an analog to genomics, the study of genes. Scientists are more interested in proteomics than genomics because genomics itself could not provide understanding of biological functions of all proteins as good as proteomics does. The genomic study may be limited by the level of transcription, post-translational modification, alternative splicing and conformational requirement. Therefore proteomics made researchers be able to study gene expression profiles at the protein level by complementing genomics. However, proteomics requires analyzing techniques, such as phage display technique, that could study small or specific populations of proteins in naïve or diseased conditions so that it could accurately reveal the protein characteristics [112, 113]. By using phage display as a screening system, receptors can be screened in their native conformation

which allows the unbiased identification of ligand-like peptides and the proteome mapping by combining the phage screening with the bioinformatics and further assays.

One of the advantages of applying phage library is that the antibodies or ligands could be selected and amplified by a process similar to natural selection occurring in living organism. Moreover, membrane proteins are one of the challenges in proteomics analysis because of their low abundance and poor solubility, though they are major drug targets. Panning on intact cells provides a direct and trustable path to identify antibodies binding to cell surface proteins in a natural manner. In addition, antibodies with conformational specificity could also be identified by using subtractive cell panning strategy in which target cells are selected by phage library with previous subtraction on equivalent non-target cells.

### *1.5.4 Custom diagnostics and targeted therapy*

Over the years, cellular labeling, cell tracking, and diagnostic imaging are hot areas of biomedical research. Utilizing designed nanoparticles to facilitate biological or medical research, termed bionanotechnology is a scientific breakthrough that has tremendously influenced and continues to influence current research. The applications include building nanoparticles for cellular labeling and imaging, and engineering nanodevices or nanostructures with biological or therapeutic function. These novel applications would make early disease diagnose and cell tracking become possible. Various types of nanoparticles can be exploited and modified for this purpose, such as quantum dots, liposomes, certain inorganic particles, etc.

In human diseases, protein expression often exhibits subject specificity which means that individual patients have different protein profiles even they have the same disease. This summons the need of identifying specific disease markers or targeting motif for personalized treatment. Phage display technique is widespreadly used for this purpose since it can provide polypeptide libraries as a source of targeting ligands and enable the rapid identification of target-specific binders. The inclusion of targeting peptides would improve the cell uptake of imaging or tracking particles [114, 115]. The general method to improve the targeting ability of nanoparticles is to involve targeting agents such as antibodies and specific peptides in which phage display can play a role [115-117].

The target specificity is also imperative for drug delivery. Many drugs tend to distribute to the whole human body through the bloodstream instead of heading into desired target organs or areas. In result, the curative effects of many drugs are decreased due to the degradation of drug by other parts of body before it reaches the desired target tissue. The distribution or digestion of drugs by other parts of body may also cause severe side effects or cytotoxicity. Moreover, the existence of physiological barriers of some organs also restricts the drug delivery to certain areas, for example, the human brain. Therefore, it is believed that the drugs conjugating with targeting ligands would be more effective and less toxic than normal drugs. Widespread researches are being conducted to build smart drug delivery systems that can deploy medication specifically to the target and/or release sustainably. There is also popular belief that nanoparticles or nanosystems would have several advantages for drug delivery: (1) nanoparticles can be modified to be targetable to increase therapeutic effects and reduce potential side effects

of drugs; (2) nanoparticles can be fabricated to protect drugs inside from possible digestion by stomach or livers; (3) nanoparticles could be sustainable to continuously release drugs. There are various types of nanoparticles used as drug carriers, such as biodegradable nanoparticles, polymeric micelles, liposomes, dendrimers, etc.

This identification of targeting motifs may support the investigation of targeted therapies and personalized diagnostic or imaging.

# Chapter 2: Oriented Nucleation of Hydroxylapatite Crystals on Self-assembled Bacteriophage Bundles

## 2.1 Introduction

This work has been published as reference [118, 119]. In recent decades, biomimetism/bioinspiration has been a promising direction for the innovative design of biological materials and systems. The fabrication of novel biomaterials for bone regeneration by mimicking the composition of natural bones is a hot area in the bioengineering field. Natural bone is a hierarchically structured composite material assembled under organism's fine control. It is mainly composed of organic collagen fibrils, non-collagenous proteins and inorganic carbonated hydroxylapatite (HAP). Collagen molecules self-assemble into triple helical polypeptides and then further assemble into fibrils which facilitate the nucleation and oriented growth of HAP crystals on them. Within these fibrils, non-collagenous proteins play a role in the preferential growth of oriented HAPs with c-axis parallel to the collagen fibrils, although other studies also show that the negatively charged noncollagenous proteins may simply inhibit extrafibrillar mineralization and the organization of the mineral inside the fibrils is controlled by collagen molecules [120]. Mimicking the natural method of HAP biomineralization on collagen fibrils is not only the key to but also a challenge for bone regeneration by biomimicry. To achieve this, several materials such as collagen,[121-123] polymers, and spider silks have been employed to demonstrate different levels of control over mineralization and the resultant mineralized structures showed good mechanical support and/or biocompatibility as the artificial bone materials.

M13 phage is a type of virus that specifically infects bacteria. It is a flexible biopolymer fiber with ~7 nm in width and ~1 $\mu$m in length which resembles the morphology of collagen fibrils. It has a single stranded genome DNA packed into an outer protein coat composed of 2700 copies of helically aligned major coat proteins (pVIII) on the side walls and 5 copies of various minor coat proteins (including pIII, pVI, pVII, and pIX) at the two distal tips. The N-terminal end of the coat protein is exposed to the external environment and can be genetically engineered to display foreign peptides on the phage surface, termed as phage display technique (Figure 2-1). Its main application is to study protein-protein interaction since invented in 1985. However, more importantly, M13 phage has also become a good candidate of biomaterials since it would not induce obvious toxicity and immune response in human beings as reported in previous literatures. This human friendly property indicates the safety of applying phage-inorganic composites into human bodies.

Earlier we have found that electrostatic interaction between the $Ca^{2+}$ ions and phage with a negatively charged surface (e.g., M13 phage genetically displaying a negatively charged $E_8$ peptide sequence on the side wall or fd phage with more negatively charged amino acids on the side wall) can drive the assembly of the filamentous phages into bundles.[124, 125] In this work, we report our recent findings that when two peptides, which can form beta-structure and promote HAP nucleation and growth in their free forms, can still form beta-structures once genetically fused to the major coat protein on the side wall of M13 phage, which can further drive the self-assembly of the phage into bundles and favor the nucleation and growth of HAP within the bundles. The N-terminus of pVIII in the filamentous phages, which consists of the

outer surface of filamentous phages, is negatively charged to some degree. But our previous results showed that the negative charge in the outer surface of wild-type M13 phage is not sufficient to induce phage self-assembly by interacting with calcium ions. [124, 125] On the other hand, the driving force of phage self-assembly and mineral nucleation in this work is the formation of beta sheet structure instead of electrostatic interaction which is easily affected by environments, such as pH value and solvents. This work is the first attempt to employ beta sheet structure for achieving phage self-assembly. The beta sheet structure formed in this work can easily form in water, and no additional inducting agent (e.g. $Ca^{2+}$ ions) is needed. This finding may introduce a novel way for molecular self-assembly and it is an improvement of our previous works.

The beta-structure-forming and HAP-nucleating peptides to be displayed on M13 phages are derived from a reported HAP-nucleating domain of dentin matrix protein 1 (DMP-1), one of the non-collagenous proteins that can promote HAP nucleation. [126] DMP-1 can be found in mineralized matrix of bone and dentin.[127] It is an acidic protein and processed into a 57kDa C-terminal domain and a 37kDa N-terminal domain. The C-terminus contains both HAP-nucleating domains and collagen-binding domains.[126] Two HAP-nucleating sites $_{386}$ESQES$_{390}$ (named pE) and $_{415}$QESQSEQDS$_{422}$ (named pQ) have been identified from the C-terminal fragment of DMP1.[126] In the presence of calcium ions, these two HAP-nucleating domains can form an intermolecular beta-sheet structure in their free forms and further self-assemble into a microfibril endowing its ability to precisely control the nucleation of HAP crystals.[126] By utilizing the phage display technique, these two HAP-nucleating peptides from DMP-1 (pE and pQ) were separately fused into the N terminal of pVIII

coat protein of M13 phage so that these two peptides were displayed on the surface of M13 phages. The engineered phage displaying pE peptide (ESQES) was termed as E phage and the one displaying pQ peptide (QESQSEQDS) was termed as Q phage. With the help of displayed HAP-nucleating peptides, E and Q phages are expected to have the ability to nucleate HAP crystals on them. In addition, due to the helically chiral surface of bacteriophage with periodically and precisely aligned HAP-nucleating peptides, the nucleation sitess are expected to be orderly aligned on the bacteriophage surface. This fine control allows us to organize HAP crystals along phage bundles with a preferred orientation.

Our strategy is to create a phage-HAP composite for mimicking the basic structure of natural bone. The methodology includes three main steps: first, two beta-structure-forming and HAP-nucleating peptides derived from DMP-1 are genetically displayed onto the surface of M13 phages separately; the intermolecular beta-structure formation between the peptides displayed on the neighbouring phages drives the self-assembly of phages into bundles to simulate collagen fibrils in nature bone; finally, HAP crystals are precisely nucleated from HAP supersaturated solution onto the HAP-nucleating beta structures on the formed engineered phage bundles with c-axis preferred orientation.

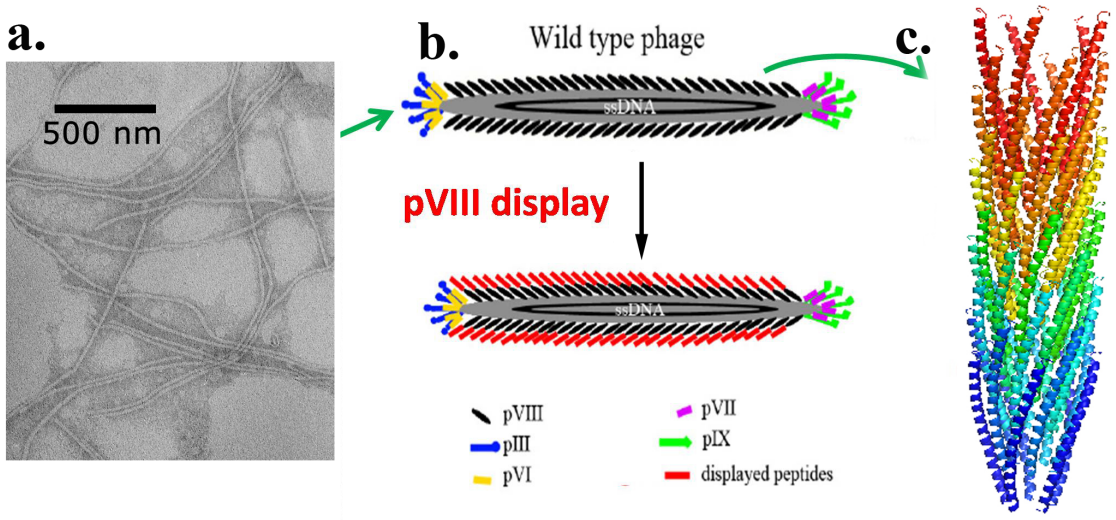



**Figure 2-1 Phage display technique. a) TEM images of wild type M13 phages. b) Display of a foreign peptide on the side wall of M13 phage by fusing the peptide to the N-terminus of pVIII. c) 3D model of M13 phage pVIII protein coat (PDB id: 1ifd).**

## 2.2 Materials and Methods

### *2.2.1 Reagents.*

Luria broth (LB) medium, tetracycline, chloramphenicol, and polyethylene glycol (PEG) were purchased from Sigma Co. Tris was obtained from Fisher. Kanamycin was obtained from Fluka and sodium chloride was purchased from EMD.

### *2.2.2 Molecular cloning of M13 bacteriophage PVIII display.*

Phage display technique was used to introduce two DMP-1 derived peptides (pE: $_{386}$ESQES$_{390}$ and pQ: $_{415}$QESQSEQDS$_{422}$) into the N-terminus of M13 phages' major coat protein (PVIII) respectively. Three primers were designed and synthesized by Invitrogen to introduce the desired peptides.

pE primer:

5'-ATCC*ATGGCG***GAATCTCAGGAATCT**GATCCCG CAAAAGC-3';

pQ primer:

5'-

ATCC*ATGGCG***CAGGAATCTCAGTCTGAACAGGACTCT**GATCCCGCAAAAG

CG-3';

Reverse primers: 5'-GC*AAGCTT*TTATCAGCTTGCTTTCGAG-3'.

Then M13KO7 phage replicative form (RF) DNA was used as template with pE or pQ primer and reverse primer to do PCR amplification. The purified PCR product was digested with appropriate restriction endonucleases (NcoI and HindIII) and fused into linearlized phagemid. The recombinant phagemids were confirmed by DNA sequencing (McLab Inc., CA).

### *2.2.3 The production, amplification, and purification of engineered phage.*

The recombinant phage virions (engineered phage) displaying two DMP-1 derived peptides were obtained by incubating one tube (5 ml) of recombinant phagemids-transfected *Escherichia coli* TG-1 strain with helper phage, wild type M13KO7 virions, for one hour at 37°C. LB-agar plates, antibiotics, LB broth, and chloramphenicol antibiotics were used during this process. The 5 ml recombinant phage virions were then transferred to 1L LB medium containing chloramphenicol on a shaking incubator at 37°C. Kanamycin and IPTG were added to make final concentration of 70 μg/ml and 0.1 mM, respectively. After obtaining enough engineered phage, we did PEG double precipitation to purify it. The overnight culture was first centrifuged at 3000g for 15 min at 4°C with a Beckman Coulter high-performance centrifuge. The supernatant was collected and recentrifuged at 8200g for 15min at 4°C. The precipitate was suspended by 0.15 volume of 20% PEG/2.5M NaCl solution and

stored at refrigerator overnight. Phage precipitate was collected at 8200g for 1 hour at 4$^{o}$C, dissolved in Tris-Buffered Saline (TBS), and recentrifuged for 10 min to clear. The final phage precipitate was diluted by appropriate volume of double distilled water. The concentrations of both harvested engineered phages were determined via ultraviolet-visible absorption at 269 nm and the suspensions were diluted by dd$H_2O$ to have the same value of optical density ($OD_{269nm}$=1).

### *2.2.4 The preparation of HAP supersaturated solution.*

Supersaturated HAP solution was prepared from HAP powder (Sigma) as described in our previous publications.[124, 125] Briefly, a stock solution was prepared first by dissolving HAP powder (Sigma) with 100mM of hydrochloric acid to reach a concentration of 50 mM of calcium. Then the HAP stock solution was diluted by sodium chloride solution to achieve the final concentration of 200 mM sodium chloride and 4 mM of calcium. The pH value was carefully adjusted to 7.01 with 0.05 M potassium hydroxide.

### *2.2.5 Nucleation of phages in HAP supersaturated solution.*

20 µl of 0.2 mg/ml phage suspension was mixed with 1ml supersaturated HAP solution in vials. After 5, 10, 15, and 20 days, 10 ml solution was transferred onto a transmission electron microscopy (TEM) copper grid, rinsed to remove soluble salts and characterized by TEM.

### *2.2.6 Ultraviolet (UV) Absorption and Circular Dichroism (CD) spectroscopy.*

300 µl of engineered phages fused with pE or pQ, were measured under UV and CD. Mixed phages were made by mixing 150 µl E phages and 150 µl Q phages. UV

absorption spectra were measured using a spectrophotometer. CD spectra were obtained using a JASCO 750 circular dichrometer. CD spectra were measured using a spectral band width of 1 nm in 0.1 cm cells. Measured CD spectra of the phages were then smoothed and plotted as [θ] in units of deg$10^{-3}$cm$^2$ dmol$^{-1}$. Each spectrum was the average of five measurements. The phage concentration used for the analyzed CD measurements is 0.2 mg ml$^{-1}$. Concentrations of phage solutions were determined from absorbance measurements and published extinction coefficients in unit of mg$^{-1}$cm$^2$ of 3.84 at 269 nm for M13 phages.[128]

### *2.2.7 Transmission Electron Microscopy Characterization.*

The TEM images were obtained using a transmission electron microscope (JEOL2000, 200 kV). For pure phage samples, 10 µl of phage solutions was dried on the copper grids and washed by 10 µl dd$H_2O$. Then the samples were negatively stained by 1% uranyl acetate (UA). For nucleation samples, 10 µl mineralized phage solution from each nucleation test was put onto the copper grid and allowed to dry. Then the sample was washed by distilled water twice to remove any soluble salts. Since no staining was done on the nucleation samples, under TEM the filamentous structures could be seen only when the phage and minerals were associated together.

## 2.3 Results and Discussions

Both pE and pQ peptides were derived from DMP1 and could direct the deposition of HAP crystals by an intermolecular beta-sheet structure between them.[126] In order to test whether these two peptides displayed on separate phages still function as their free form in DMP1, purified E and Q phages were mixed together and incubated

for 1 day (For convenience, we termed mixed E and Q phages as EQ phages.). At the same time, E phages and Q phages were separately incubated for 1 day as control.

Only individual flexible phage fibers were observed in pure E phage sample (Figure 2-2a), indicating no interactions occurred between E phages. For Q phages, much to our surprise, they could form small bundles in water by themselves (Figure 2-2b). The bundles were flexible and randomly distributed, each of which was composed of 3-4 individual Q phages along the width direction. This fact suggests the presence of certain driving force that facilitates the assembly of Q phages into bundles. When mixed together, E and Q phages could self-assemble into larger bundles in which individual phages were arranged parallel in a side-by-side fashion (Figure 2-2c). These bundles were relatively rigid and longer than Q bundles. About 9-10 phages comprised one bundle of EQ phages along the width direction. These results show that E and Q phages are able to self-assemble into bundles under a stronger driving force compared with the formation of the Q phage bundles.

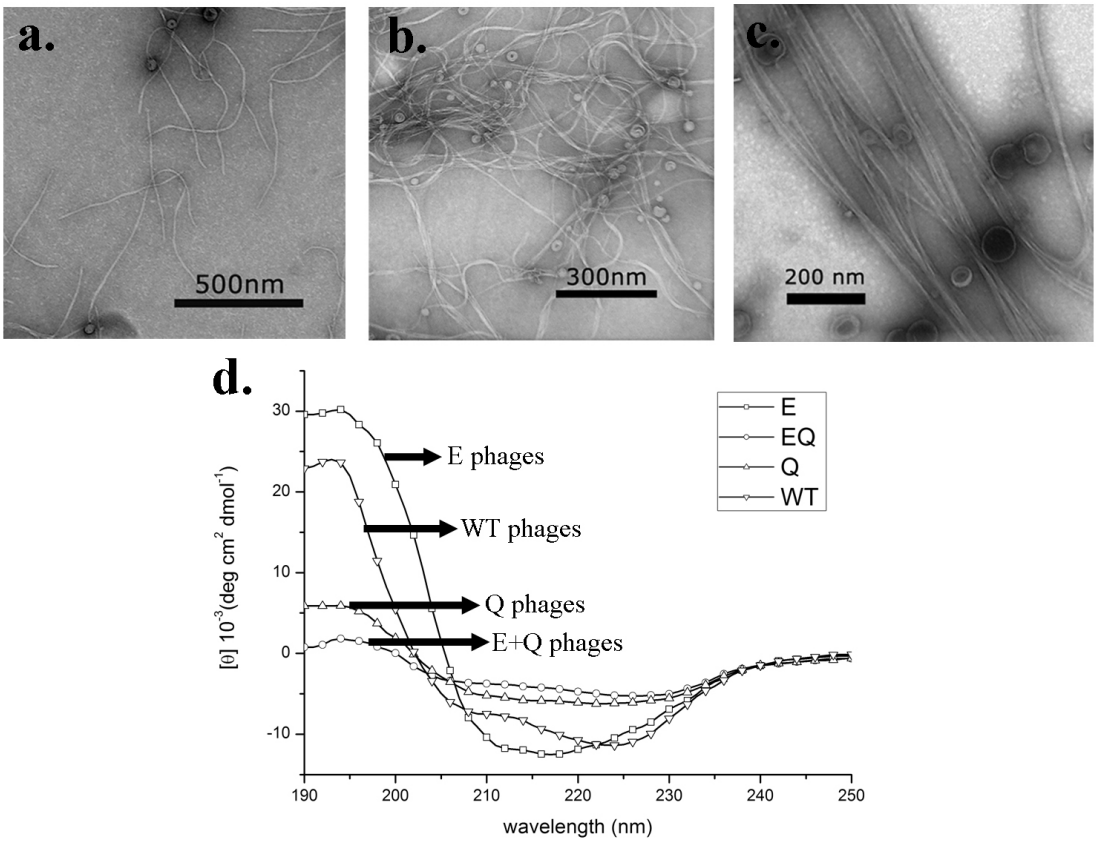



**Figure 2-2. TEM images of engineered phages. a) E phages; b) Q phage bundles; c) mixed EQ phage bundles. d) Circular dichroism spectra of wildtype, E, Q and EQ phages.**

Since pE and pQ are capable of forming intermolecular beta-sheet structures in DMP-1,[126] we expect that engineered E and Q phage bundle should also form beta-sheet structures. In order to demonstrate the secondary structure, circular dichroism (CD) measurements were performed on engineered phages while wild-type phage served as control. The CD spectrum of wild-type phages confirmed that α-helix existed as the major protein secondary structure of intact M13 phage (Figure 2-2d). Its spectrum had one positive band at 192 nm and two negative bands at 208 nm and 222 nm, corresponding to the parallel $\pi \rightarrow \pi^*$, perpendicular $\pi \rightarrow \pi^*$, and well-known $n \rightarrow \pi^*$ transitions of α-helix, respectively.[129] It has been well documented that α-helix is the

major structure of pVIII coat protein and each phage has ~3000 copies of pVIII protein, so the presence of α-helix in the spectrum is anticipated. Using the method from Whitmore,[130] the α-helical and β-sheet contents of wild type phage were estimated to be 74% and 1%, respectively. The CD spectrum of E phages (Figure 2-2d) shows a combination of α-helical and β-sheet structures, which were estimated to be 63% and 16%, respectively. Since no obvious interactions between individual E phages could be observed from the TEM, we believed that the increased β-sheet contents of E phages were due to the hydrogen bonding between displayed pE peptides and neighboring pVIII protein on the surface of an individual phage. Q phages have a similar CD spectrum demonstrating a combination of α-helix and β-sheet structures, but its β-sheet contents were higher (22%) than those in wild type and E phages. In our opinion, the driving force of Q phage bundles is possibly the hydrogen bonding in β-sheet structure formed between displayed pQ peptides on neighboring Q phages. The CD spectrum of mixed E and Q phages (Figure 1d) shows a highest content of β-sheet (29%) and lowest content of α-helix (43%) among all samples. Considering the large bundles formed between E and Q phages (Figure 2-2c), we conclude that the potential driven force was the hydrogen bonding in β-sheet structure formed between pE and pQ peptides displayed on pE and pQ phages, respectively. In addition, increased β-sheet structures were formed between E and Q phages than between Q phages only. These results are consistent with the earlier finding that pE and pQ from DMP1 can form an intermolecular beta-sheet structure.[126]

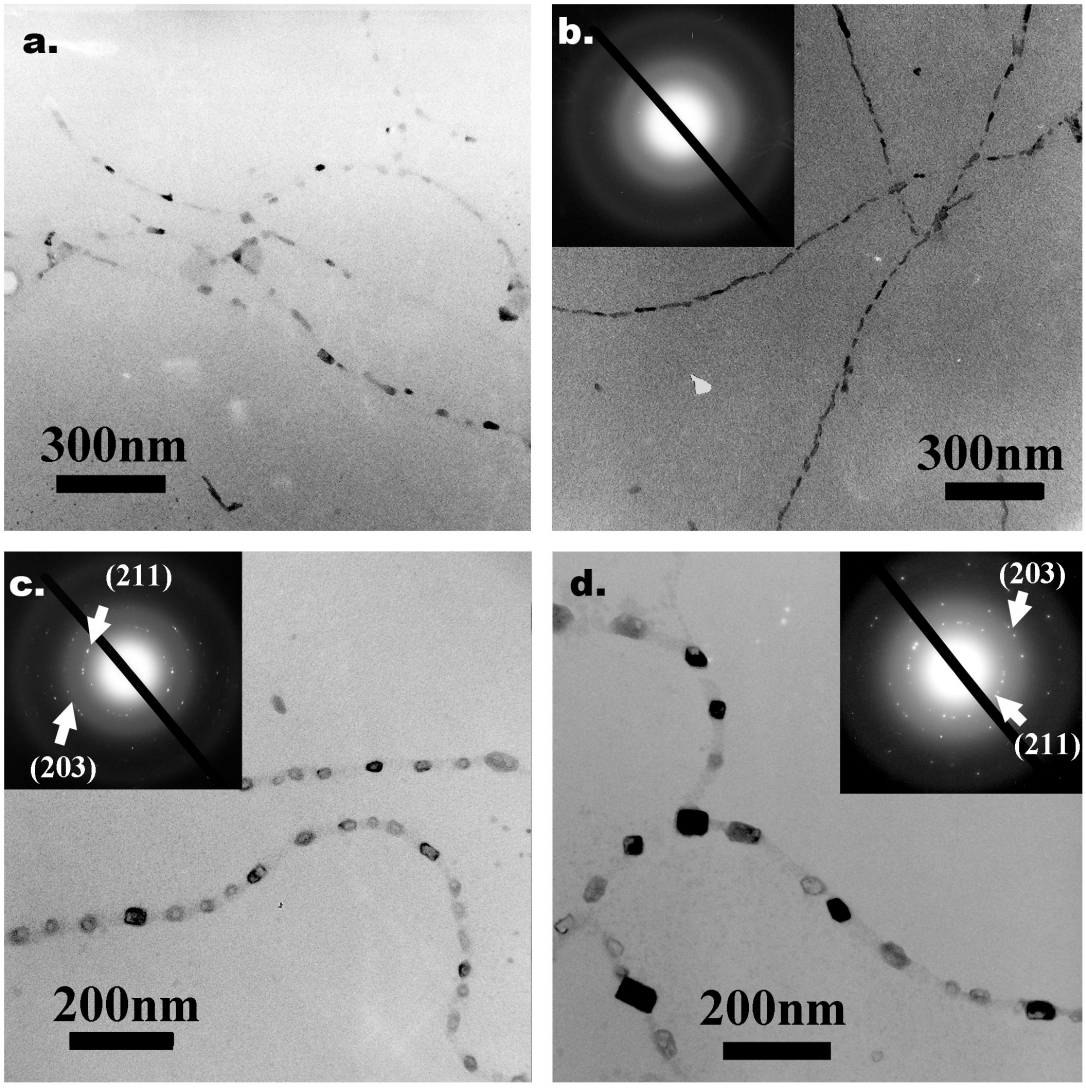



**Figure 2-3 TEM images of nucleation of HAP on E and Q phages after incubation in supersaturated HAP solution for 10 days and 20 days. a) HAP nucleation on E phages for 10 days. b) HAP nucleation on E phages for 20 days. c) HAP nucleation on Q phages for 10 days. d) HAP nucleation on Q phages for 20 days.**

Subsequently, we did a series of in vitro HAP nucleation tests on E and Q phages. Specifically, 20 μl of E and Q phages were separately incubated in 1 ml supersaturated HAP (pH=7.01) solution[131] at room temperature. Mineral deposited samples were rinsed and characterized under TEM without any staining after 5 days as

interval. On E phages, only some amorphous calcium phosphate phase could be observed after incubation for 10 days (Figure 2-3a). But on day 20, almost all E phage fibers were coated by amorphous calcium phosphate, resulting in a necklace structure (Figure 2-3b). The amorphous phase of nucleated minerals was confirmed by the electron diffraction (ED) pattern (Figure 2-3b). While on Q phage bundles, small minerals could be found after incubation for 10 days (Figure 2-3c). The diffraction spots from the (211) and (203) planes of HAP in ED pattern of Q phage samples indicated that the minerals were HAP poly-crystals. At 20 days, those HAP crystals had grown into larger crystals but no preferred orientation was observed from the ED pattern (Figure 2-3d). In addition, Figure 2-3c and Figure 2-3d suggest that the nucleation sites on Q phage bundles were not distributed uniformly. Similarly, we mixed 10 μl of E phages and 10 μl of Q phages with equal concentrations into 1 ml of HAP supersaturated solution. On day 5 and 10, small HAP crystals appeared on EQ phage bundles. The crystalline structures were verified by the ED patterns. But no obvious preferred orientations of the crystals were found (Figure 2-4a and b). On day 15 and 20, more and larger HAP crystals appeared along EQ phage bundles (Figure 2-4c and d). The ED patterns of the bundles show arcs corresponding to (00l) planes of HAP, indicating that HAP crystals on bundles are oriented with their c-axis preferentially parallel to the phage bundles.[125] These results show that E and Q phages could co-self-assemble to induce oriented HAP nucleation while individual E phages or Q phages by themselves could not.

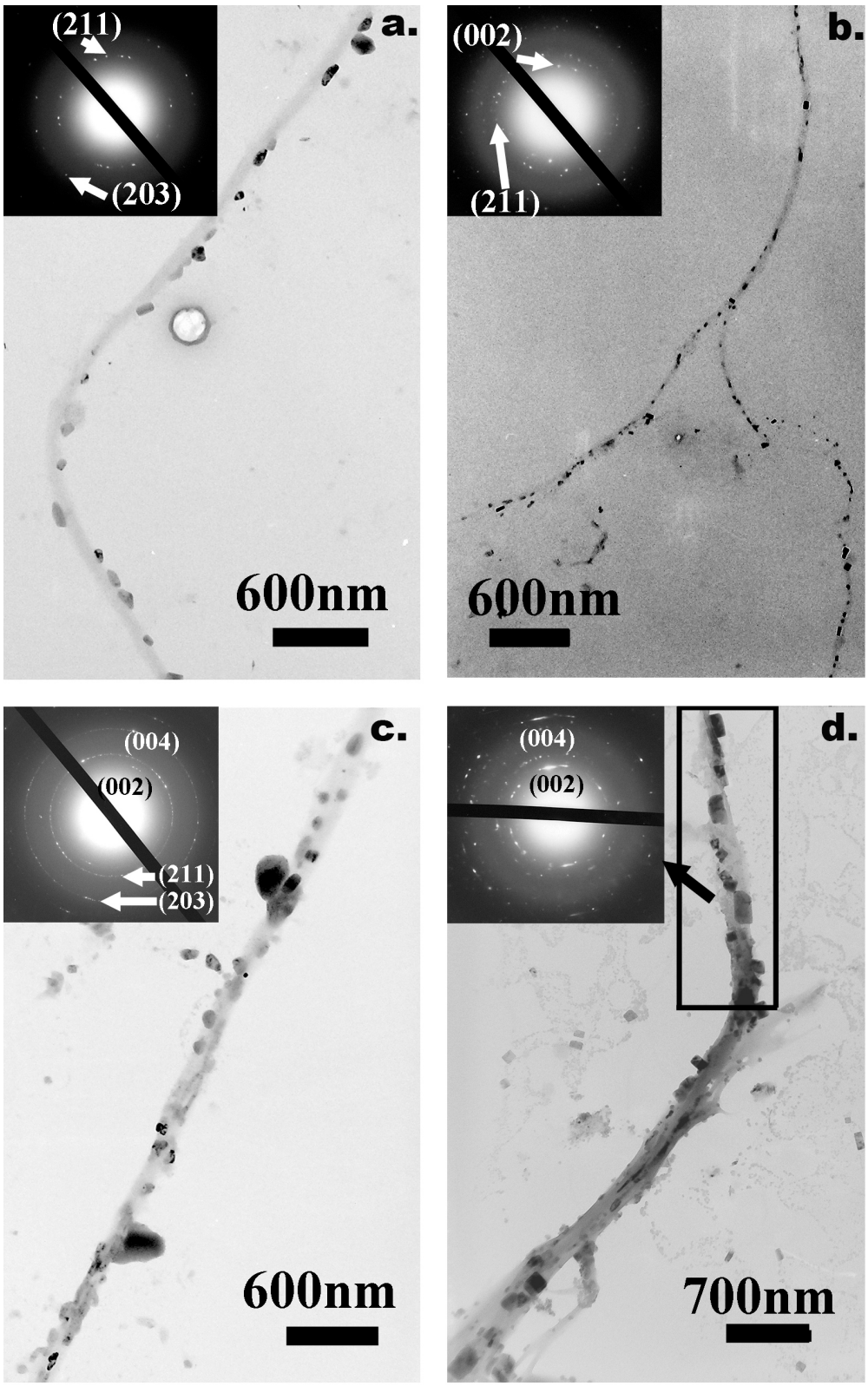



**Figure 2-4 TEM images of the HAP nucleation on EQ phage bundles after incubation for: a) 5 days, b) 10 days, c) 15 days and d) 20 days.**

The mechanism of bone biomineralization has been controversial. [120, 132-134] Most recently, a new mechanism was proposed,[135] where an amorphous calcium phosphate phase forms "liquid-droplets" that can interact with the non-collagenous proteins and then bind to the preformed collagen matrix. However, we did not find the evidence of converting amorphous calcium phosphate phase into crystalline one in our study. We believe that the orientation control of nucleated HAP crystals on EQ phage bundles was directed by the β-sheets formed between E and Q phages (Figure 2-5). It is known that pE and pQ could self-assemble into microfibrils by forming intermolecular β-sheets.[126] When displayed on phage, pE and pQ peptides are fully exposed and free to interact with other molecules. Therefore, when E and Q phages were mixed, displayed pE and pQ could form β-sheets between neighboring phages which induced the formation of EQ phage bundles (Figure 2-2a). This was also confirmed by the relatively high content of β-sheet in the CD spectrum of EQ phage bundles (Figure 2-2d). The possible β-sheet formed was simulated in Figure 4b. Aspartic acid (Asp, D) is the following amino acid of inserted foreign peptides in pVIII proteins of M13 phages. We believe that it is also important for inducing HAP crystals so that it was included in our models. Previous studies found that negatively charged amino acids (D, E or phospho S) had the trend to induce the nucleation of HAP crystals.[136, 137] From Figure 2-5b, we can see that $E_4$, $D_6$ from $E_1S_2Q_3E_4S_5D_6$ and $D_1$, $D_3$, $E_5$, $E_9$ from $D_1S_2D_3Q_4E_5S_6Q_7S_8E_9Q_{10}$ are on the same side of β-sheet which could create an attracting center for calcium ions and thus initiate the nucleation of HAP crystal.

In our experiments, HAP crystals nucleated on EQ bundles were oriented with their c-axis preferentially parallel to the phage bundles (Figure 2-4c and d). Previous

work has demonstrated that β-sheets formed from pE and pQ could nucleate HAP crystals on them. [126] We further made a model to illustrate how the β-sheets within phage bundles facilitated the oriented nucleation and growth of HAP crystals. Figure 2-5c, d, and e demonstrate glutamic acids and aspartic acids from both pE and pQ can attract calcium ions and trigger the nucleation process. Specifically, $E_4$ and $D_6$ from pE as well as $E_5$ and $E_9$ from pQ are able to attract 4 calcium ions and those attracted 4 calcium ions on the β-sheet can perfectly match 4 calcium ions in the (001) plane of HAP crystals (Figure 2-5c and d). As we know, mostly, HAP crystal tends to grow along its [001] direction. Therefore, the electrostatic interaction and stereochemical match will further encourage the nucleation of HAP crystals on the β-sheet with their c-axis parallel to the phage bundles. The nucleated HAP will grow along its c-axis, that is, perpendicular to the plane where the nucleating β-sheet is lying in between neighboring phages. Since the long axis of phage is also perpendicular with the β-sheet, the c-axis of HAP crystals should be parallel to phage bundles (Figure 2-5f). This structure greatly mimicked the lowest level of hierarchical structure of natural bone in which HAP crystal are nucleated and grown with their c-axis preferentially parallel to the collagen fibrils.[136]

Our results supported the previous findings that pE and pQ can form β-sheet and nucleate HAP crystals. [126] Moreover, this work suggests the feasibility in the field of bone regeneration of using genetically modifiable biomaterials (e.g. bacteriophage) displaying pE and pQ and inducing HAP deposits by forming β-sheets. Scientists are always looking for a new method to achieve self-assembly. In this study we demonstrate the feasibility by taking advantage of forming β-sheet intermolecular

bridge without any artificial inductive or additive reagents. β-sheet structure is a common type of secondary structures of peptides or protein formed via hydrogen bonding. It is a spontaneous and naturally evolved process. If fused on specific positions of genetically engineerable biomaterials, pE and pQ are able to act like leucine zipper peptides[138] to assemble biomaterials into hierarchical structures with a precise control by forming β-sheets. We previously found that $Ca^{2+}$ ions could induce the bundling of negatively charged phages.[124, 125] However, the mineralization of such electrostatically bound bundles is faster than that of beta-structure-stabilized bundles although both bundles induce the formation of oriented HAP along the bundles. This fact may reflect the different mechanisms involved in the mineralization in this work and suggest that beta-structure driven nucleation may be slower.

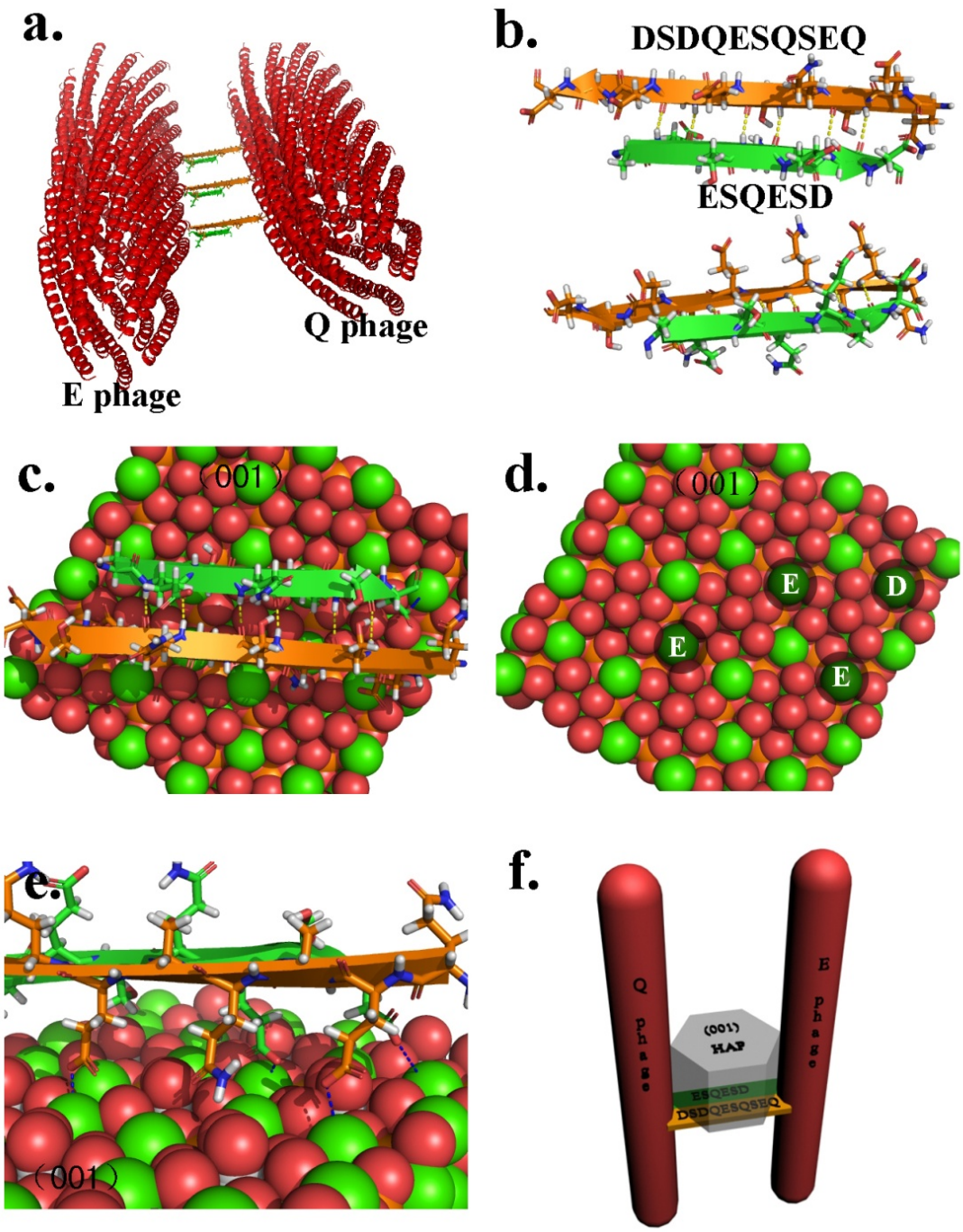



**Figure 2-5 The three dimensional simulation of possible HAP nucleation mechanism. a) 3D model of possible EQ phage bundles. b) The simulation of intermolecular beta sheet formed by two HAP nucleating peptides displayed on phage pVIII. This model includes the aspartic acid (D) which is the following amino acid right after the inserted foreign peptides in pVIII due to its possible contribution to the beta sheet formation. c) describes the possible mechanism of the HAP nucleation and growth along c-axis due to the specific match between the**

**negatively charged amino acid in HAP nucleating peptides forming intermolecular beta sheet and the (001) plane of HAP crystals. d) shows the four calcium ions on HAP (001) plane that can perfectly match four negatively charged amino acids. e) is a closer look of electrostatic attraction between matched negatively charged amino acids and calcium ions. f) is the 3D model which schematically illustrates the possible mechanism of HAP crystal nucleation and oriented growth triggered by EQ phage bundles.**

## 2.4 Conclusions

In summary, we have used M13 bacteriophage with pE and pQ derived from DMP1 protein genetically displayed on the surface to form self-assembled bundles with c-axis oriented HAP crystals decorated along the bundles. Displayed pE and pQ formed a β-sheet structure, inducing the self-assembly of E and Q phages into EQ phage bundles. This formation of β-sheet can be applied as a general method to induce precise assemblies between engineerable biomaterials. We also found HAP crystals could be nucleated on EQ bundles with their c-axis preferentially parallel to the phage bundles. This structure greatly mimicked the lowest level of hierarchical structure of natural bone in which HAP crystal are nucleated and grown with their c-axis preferentially parallel to the collagen fibrils. The oriented nucleation and growth arose from the fact that glutamic acids and aspartic acids from pE and pQ attracted calcium ions with a pattern matching with calcium ions in the (001) plane of HAP crystals. Such specific match further induced the nucleation of HAP crystals on the β-sheet and directed the nucleated HAP crystal to grow along their c axis. Our work demonstrated a new route for fabricating bone repair materials through biomimicking and bioinspiration.

# Chapter 3: Bacteriophage-Gold Nanocomposites As a Model to Study Transmission Electron Microscopy of bioinorganic nanohybrids

## 3.1 INTRODUCTION

This work has been published as reference [139]. In recent years, bioinorganic nanohybrids composed of biological macromolecules and functional inorganic nanomaterials have revealed many unique properties that show promise for the future. Transmission electron microscopy (TEM) is a popular and relatively simple tool that can offer a direct visualization of the nanomaterials with high resolutions. When TEM is applied to visualize bioinorganic nanohybrids, a treatment of negative staining is necessary due to the pres- ence of biological molecules in the nanohybrids except for those with densely packed inorganic materials. However, the conventional negative-staining procedure for regular biological samples cannot be directly applied to such bioinorganic nanohybrids. To image a specific bioinorganic nano- hybrid, negative-staining factors such as negative stain type, working pH, staining time, and dry- ing method, should be identified. Currently, no detailed studies have been done to investigate how to adjust negative-staining factors based on specific bioinorganic nanohybrids. In this study, bacte- riophage-gold nanoparticle hybrids were chosen as a model to systematically study the effects of each factor on the negative staining of the nanohybrids. The best staining conditions for gold nano- particle-phage nanohybrids were obtained and the effects of each factor on the negative staining of general nanohybrids were discussed. This work indicates that with proper staining it is possible

to use TEM to visualize directly both biological and inorganic components without introducing any artifact.

Nano-scale inorganic materials exhibit unique properties and show great promise for the future [140-143]. One particular challenge with nano-scale inorganic materials has been in assembling them into well-defined structures or integrating them into large-scale devices. One strategy incorporates the use of self-ordered biomolecules, which are directly obtained from Nature such as nucleic acids, proteins and viruses, to organize nanomaterials into pre-designed patterns. The combination of these biological molecules with functional inorganic nano-materials have led to many hierarchical nanostructure organizations with controlled shape, size, alignment and orientation [111, 144-148]. The characterization of the designed bio-inorganic nano-hybrids is a crucial step in the development of novel nanomaterials. A variety of imaging techniques have been applied in this field such as transmission electron microscopy (TEM), atomic force microscopy (AFM), scanning electron microscopy (SEM) and fluorescence microscopy. Among them, TEM is a relatively simple technique that can offer a direct visualization of the individual nano-hybrids with high resolutions. Therefore, it has become one of the most commonly used techniques for the characterization of nanomaterials.

It is easy to visualize inorganic nanomaterials such as gold nanoparticles under TEM without any staining due to the high contrast between the inorganic materials and the underlying supporting film such as carbon. Biological molecules are mainly composed of carbon, hydrogen, and nitrogen atoms, and thus are only recognized under TEM with heavy metal ion staining. Bio-inorganic nano-hybrids are composites of biological molecules with functional inorganic nanomaterials. If biological molecules

are densely packed by inorganic materials, the structures of the hybrids can be observed without staining. Our previous results have shown that in a nano-composite of silica-coated bacterial flagella, both silica and flagella could be recognized without staining [149]. However, if inorganic materials are loosely arranged around biological molecules, only inorganic materials having higher molecular weights can be visualized. In such characterization, direct evidence showing the close proximity between inorganic and biological components, which can help us understand the interactions between both components, is missing. Therefore, negative staining is needed to visualize the biological components in such nano-hybrids so that both components can be observed under TEM.

Negative staining is based on the principle that heavy staining ions are repelled by the charged groups of the specimen and sit along biological molecules [150]. However, the conventional negative-staining procedure for regular biological samples cannot be directly applied to such bio-inorganic nanohybrids. For a specific bio-inorganic nanohybrid, some negative-staining factors should be modified, such as the type of negative stain, working pH, staining time, and drying method. In this work, bacteriophage-gold nanoparticle nanohybrid was used as a model to systematically study the effects of each factor on the negative staining of the nanohybrids (Figure 3-1 b). The optimum negative-staining condition for bacteriophage-gold nanoparticle hybrid was obtained and the effects of each factor on the negative staining of the nanohybrids are discussed.

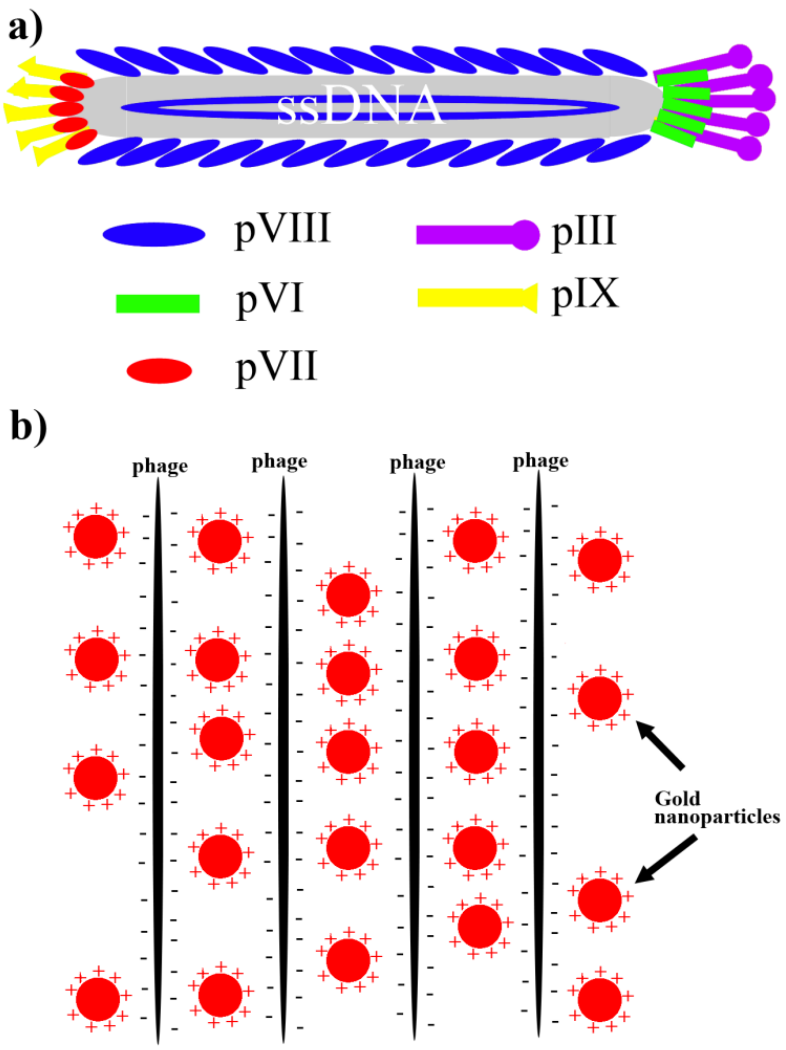



**Figure 3-1 a) M13 wild type phage particles composed of ~2700 copies of major coat proteins (pVIII) and 5 copies of each minor coat protein (including pIII, pVI, pVII, and pIX); b) Positively charged Au-NPs interacted with anionic phage particles into bundle structures.**

## 3.2 Materials and Methods

### *3.2.1 Materials*

Uranyl acetate (UA) powder was purchased from Ted Pella Inc. Phosphotungstic acid (PTA) was purchased from Ted Pella Inc. Trehalose was

purchased from Sigma Inc. Gold chloride solution was purchased from Sigma Inc. Polyethylenimine (branched, average MW=~25000) was purchased from Sigma Inc. Sodium borohydride powder was purchased from Sigma Inc. TEM grids were purchased from Ted Pella Inc. M13 wild type bacteriophage was purchased from New England Biolabs Inc.

### *3.2.2 M13 Amplification*

200 µL overnight ER2738 *E.coli* culture and 1 µL phage suspension were added into a 20 mL LB culture in a 250 ml flask. The flask was incubated at 37 °C with shaking for 4-5 h. After incubation, the culture was centrifuged at 4500 g for 20 min to remove *E. coli* cells. Then the top 16 mL of the supernatant was transferred into a new tube and 4 mL of 2.5 M NaCl/20% PEG-8000(w/v) was added to precipitate the phage. After 4 hours of precipitation at 4 °C, the phage was pelleted by centrifugation at 12000 g for 15 min. Supernatant was discarded and the phage pellet was re-suspended in 1 mL TBS buffer. 200 µL 2.5 M NaCl/20% PEG-8000 was added into the re-suspended phage solution and the mixed solution was allowed to incubate on ice for 1 h. The phage was pelleted again by centrifugation at 14000 g for 10 min. Supernatant was discarded and the phage pellet was re-suspended in 200 µL TBS buffer. The quantification of phage was achieved by monitoring its $OD_{269nm}$. Concentrations of phage solutions were determined from absorbance measurements and using published extinction coefficients in unit of $mg^{-1}cm^2$ of 3.84 at 269 nm for M13 phages [128]. Roughly, an $OD_{269nm}$ of 1 means the concentration of the phage in solution is about $1\times10^{13}$ pfu/mL .

### *3.2.3 Synthesis of Gold Nanoparticles*

AuNPs were synthesized by using a reported method [151]. Specifically, 15 μL 5% (w/w) polyethylenimine (PEI) (branched, average MW=~25000) was added into 1 mL 0.2% gold chloride ($HAuCl_4$) solution with stirring. The color of the solution changed from yellow to orange. Then 20 μL of 5M $NaBH_4$ solution was added into the PEI/$HAuCl_4$ solution with violent stirring. Immediately, the solution color turned from orange to dark red, the color of nano-sized gold particles.

### *3.2.4 Preparation of Phage-Gold Nanoparticle Hybrid*

100 μL phage solution ($1.5\times10^{13}$ pfu/ml) was added into 1 mL gold nanoparticle solution and mixed well. The mixture was incubated at room temperature for 4 hours. Gold-phage hybrids were formed and slowly precipitated to the bottom of the tube. Hybrids were pelleted by centrifugation at 10000 g for 1 min and re-suspended in 1 mL water.

### *3.2.5 Negative Staining*

In a typical UA staining, 10 μL Au-NPs-phage hybrid solution was applied onto a formvar-coated TEM grid for 3 min During this process, the Au-NPs-phage nanohybrids was absorbed to the supporting film. The rest of the solution was wicked from the edge of the grid by the wedge of the filter paper. Immediately, 10 μL 0.5% UA solution (pH=4.5) was applied to the specimen for 10 s. Then, the stain solution was wicked from the edge of the grid by the wedge of the filter paper. Lastly, the TEM grid was dried by a hair drier and characterized under TEM (Zeiss 10). In this way the effects of each factor on the negative staining of the nanohybrids could be analyzed.

### *3.2.6 Pre-fixation with 1% Glutaraldehyde (GA)*

10 μL Au-NPs-phage solution was applied onto a formvar-coated TEM grid for 3 min while the specimen was absorbed to the supporting film. The rest of the solution was wicked from the edge of the grid by the wedge of the filter paper. 20 μL 1% GA solution was applied onto the specimen for 20 min. After the incubation, the GA solution was wicked from the edge of the grid by the wedge of the filter paper and the specimen was washed 3 times by water. Then 10 μL 0.5% UA solution (pH=4.5) was applied on the specimen for 10 s. Then, the stain solution was wicked from the edge of the grid by the wedge of the filter paper. Lastly, the TEM grid was dried by a hair drier and characterized under TEM (Zeiss 10).

## 3.3 Results

### *3.3.1 Preparation of Gold Nanoparticles.*

$HAuCl_4$ was reduced by $NaBH_4$ into gold nanoparticles (Au-NPs) and stabilized by polyethylenimine (PEI) molecules. After the reaction, the Au-NP solution became transparent and its color turned to dark red. Then the solution was diluted and characterized under a TEM. Over large areas, only well-dispersed nanoparticles could be observed with a uniform size of ~5-7 nm (Figure 3-2a). In addition, a typical electron diffraction pattern corresponding to gold crystals was found from the nanoparticles, suggesting the nanoparticles in the image are gold crystals. Since the Au-NPs were stabilized by highly-branched PEI molecules, the synthesized Au-NPs should be positively-charged due to the presence of the amino groups from the surrounding PEI molecules.

### *3.3.2 Wild-Type M13 Bacteriophage.*

Wild-type M13 phage is a flexible nanofiber with its single stranded DNA (ssDNA) genome packed into a protein coat which is composed of 2700 copies of major coat proteins (pVIII) and 5 copies of each minor coat protein (including pIII, pVI, pVII, and pIX) [10]. 2700 copies of pVIII proteins form its side wall while 5 copies of pIII and pVI are located at one tip and 5 copies of pIX and pVII at the other tip (Figure 3-1 a). The ssDNA genome encodes a total of 11 proteins including 5 structural coat proteins. From its surface chemistry, the amino terminus of each pVIII protein is exposed to the surface with the first five residues (AEGDD) extending away from the phage. So it can be easily figured out that on the phage surface there are 2700 copies of Glu and 5400 copies of Asp both of which have carboxyl groups, leading to a negatively charged surface. The experimental isoelectric point (pI) value of 4.2 also confirmed the negative phage surface charge [152]. With a high concentration, phage particles tend to form bundle structures if polycationic molecules are added [125]. It was believed that the addition of polycationic molecules can trigger the assembly of neighboring phage particles via electrostatic interactions. In this work, the wild type M13 phages after the amplification were quantified by monitoring its $OD_{269nm}$. Roughly, 1 $OD_{269nm}$ means the concentration of the phage in solution is about $1\times10^{13}$ pfu/mL. The detailed calculation could be found in supporting information. The phage was stocked and used at a concentration of $1.5\times10^{13}$ pfu/mL ($OD_{269nm}$=1.5). Usually, up to $1\times10^{14}$ phages could be harvested from 1 liter of LB culture. In order to know the morphology of the wild type M13 phage, the viruses were stained with 0.5% UA and observed under a TEM (Figure 3-2b). Every single M13 phage particle has a flexible rod-like shape

with a diameter of ~6.5 nm and a length of ~930 nm (Figure 3-2b), which is consistent with previous literatures [10].

### *3.3.3 Gold Nanoparticle-Phage Hybrids.*

After a phage solution was injected into the Au-NP solution, immediately, Au-NP-phage hybrids were formed and slowly precipitated to the bottom of the tube. Free Au-NPs were then removed by centrifugation and the hybrids were re-suspended in water. Again, the gold-phage hybrids slowly precipitated to the bottom of the tube, leaving the supernatant clear and colorless (Figure 3-2c). A small quantity of the hybrids was characterized under TEM without staining. Most Au-NPs were aligned into large belts, forming a net-like structure (Figure 3-2d). Only a few free Au-NPs were observed away from the belts, indicating almost all of the free Au-NPs were removed during washing. We believe positively-charged Au-NPs electrostatically interacted with M13 phages to induce the formation of bundle-like Au-NP-phage hybrids. However, without any staining (Figure 3-2d), this hypothesis cannot be experimentally verified because we could not see any phage particle or any phage-Au-NP connections directly. In order to visualize the structural details of such hybrids, a negative staining was applied to the hybrid specimen.

### *3.3.4 Best Negative Staining Conditions.*

In order to obtain the best staining condition to image the phage-gold nanohybrids, the effects of each factor on the negative staining of the nanohybrids were systemically studied. Specifically, 10 μL hybrid solution was applied onto a formvar-coated TEM grid for 3 min. During this time, the specimen was absorbed to the supporting film. The rest of the solution was wicked from the edge of the grid by the

wedge of the filter paper. Immediately, 10 μL 0.5% UA solution (pH=4.5) was applied on the specimen for 10 s. Then, the stain solution was wicked from the edge of the grid by the wedge of the filter paper. Finally, the TEM grid was dried by a hair drier and characterized under TEM. With the help of UA, phage particles were negatively-stained so that both Au-NPs and phage particles could be observed under TEM (Figure 3-3a, b). As a result, it is clearly seen that the M13 phage particles are interacted with positively-charged Au-NPs, which could be a direct evidence to prove our initial hypothesis.

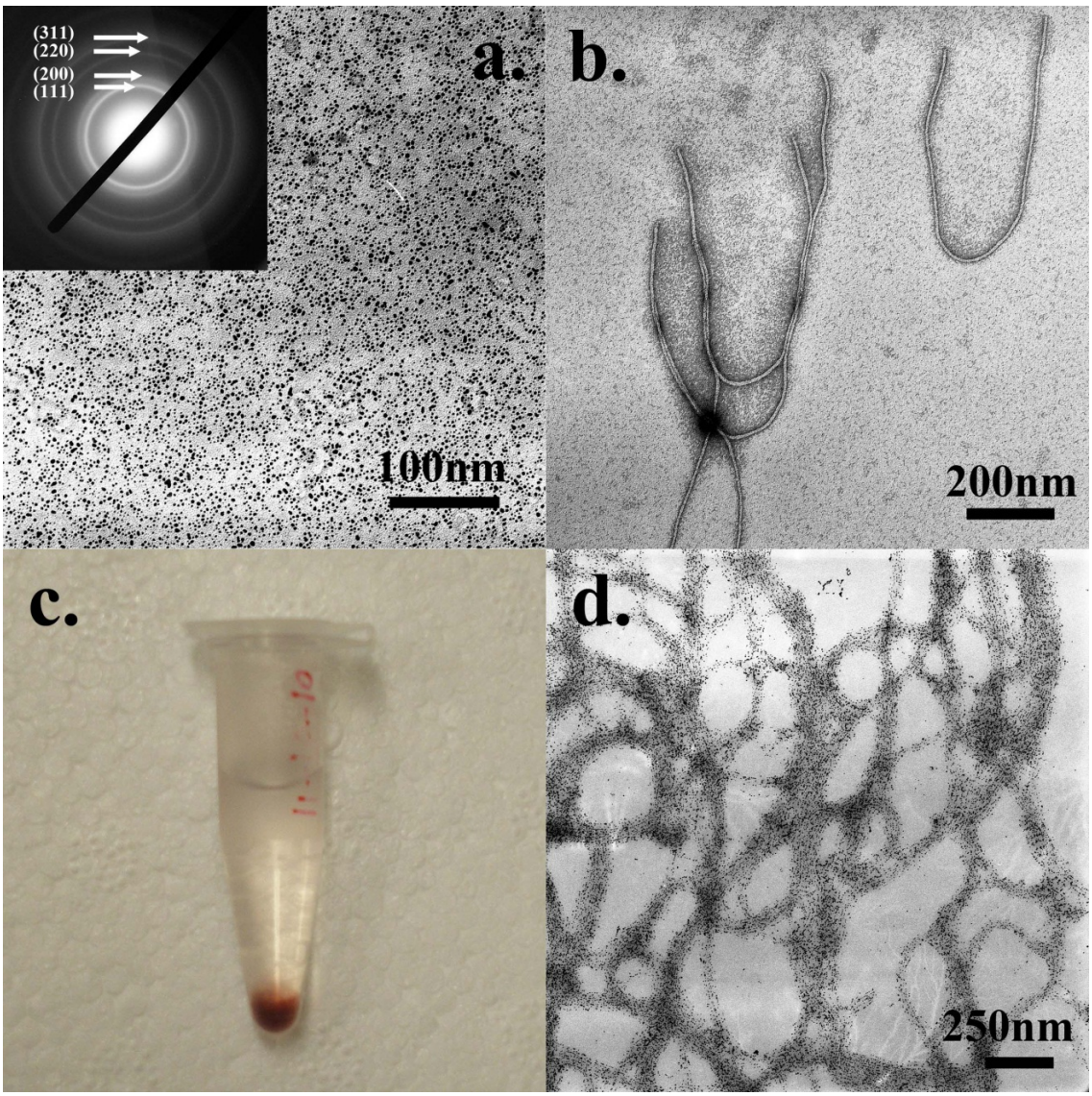



**Figure 3-2 a) Synthesized gold nanoparticles and the electron diffraction pattern; b) wild type M13 phages stained with 1% UA; c) gold-nanoparticle-phage hybrids precipitation; d) TEM image of the hybrid precipitation from c.**

One problem was in some areas the Au-NPs were covered by the heavy stain-salts so that some of the nanoparticles were not easily recognized. This situation resulted from the pH of the staining solution. As previously mentioned, the isoelectric point of M13 phages is about 4.2 which is lower than the pH value of the staining solution (4.5). Hence, the staining may contain some positive-staining effects which

darkened the biological structures in certain areas. Decreasing the pH of the stain solution could solve this problem. However, a stain solution with a low pH will cause other problems to the nanohybrids which will be mentioned later in more detail. In fact, the synthesized Au-NPs have an excellent contrast and could still be recognizable in a light staining. Therefore, when we reduced the concentration of the stain to 0.5%, this problem was reduced (Figure 3-4b). We carefully highlighted the Au-NPs in the negatively-stained sample (Figure 3-4b) and compared it with the non-stained sample (Figure 3-2d). The results clearly showed that the nanohybrids were nicely stained and most Au-NPs were still on the hybrids after negative staining (Figure 3-3).

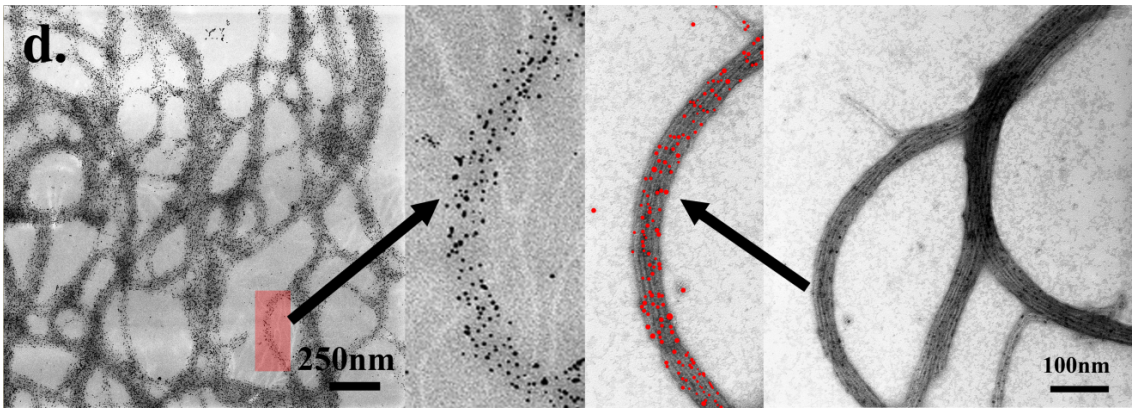



**Figure 3-3 Comparison of Figure 3-2d and Figure 3-4b. Au-NPs in Figure 3-4b are highlighted by red circles. The density of Au-NPs on the hybrids after negative staining is almost the same as without staining.**

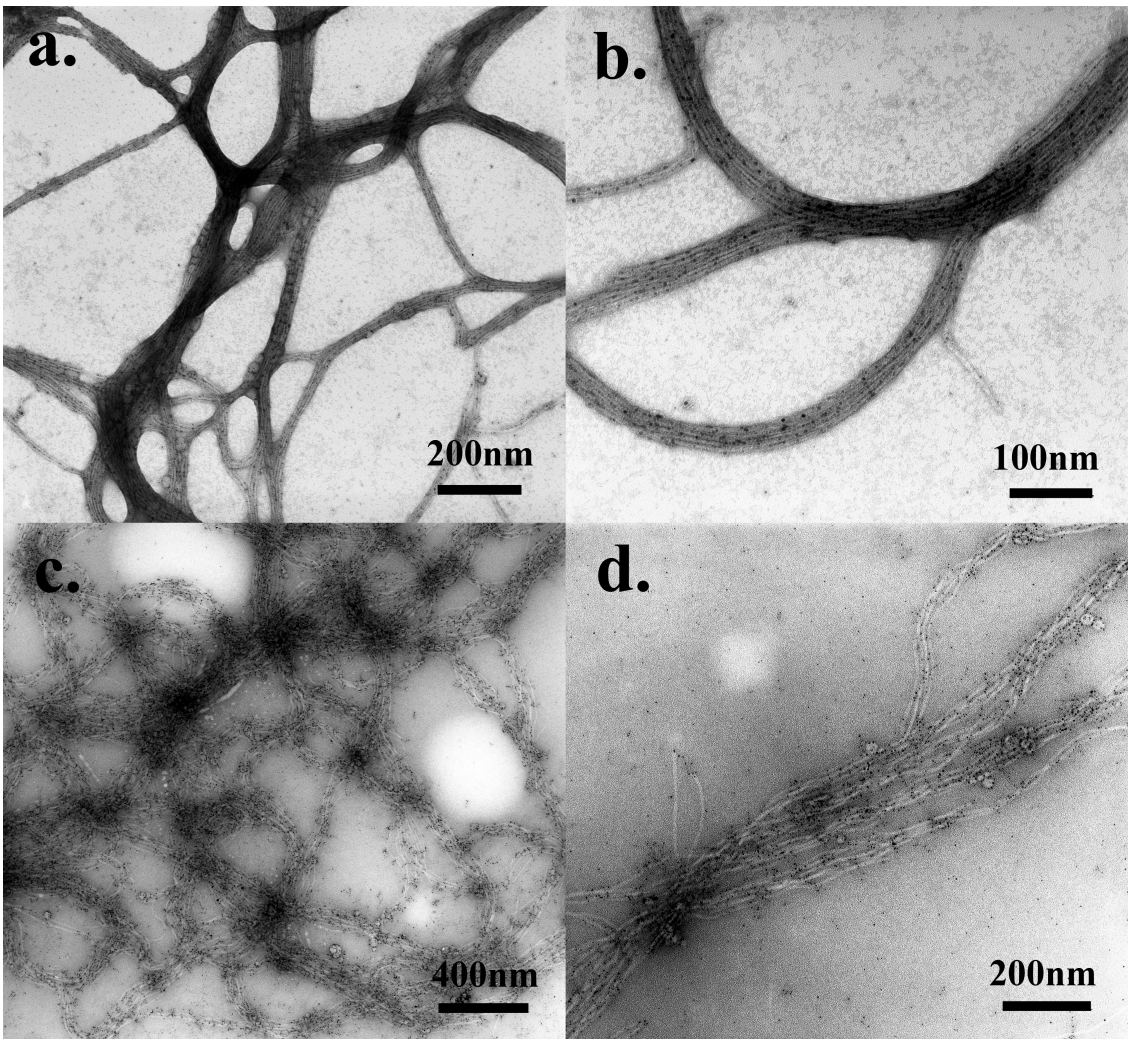



**Figure 3-4 a) Au-NP-phage hybrids were stained with 0.5% UA solution (pH=4.5, 10 s of staining, rapid drying); b) high resolution image of a); c) Au-NP-phage hybrids were stained with 0.5% PTA solution (pH=7, 10s of staining, rapid drying); d) high resolution image of c).**

### *3.3.5 Choice of Stains.*

Besides UA, phosphotungstic acid (PTA) is another popular stain for negative staining. Usually, the working concentration is about 0.5%-2% at a neutral pH. Here, we tried to use 0.5% PTA solution (pH=7.0) for the staining to check if PTA is better than UA for this system. Under similar condition using 10s of the staining solution and rapid drying, the structure of Au-NP-phage hybrid was greatly changed as a result of the

staining process. Specifically, individual phage particles within bundles were detached from each other and there was no dense packing of the Au-NPs with phage particles could be found (Figure 3-4c&d). Moreover, a lot of Au-NPs were detached from phage bodies during the process of staining (Figure 3-4d). Such detachment could not be found from the non-stained specimen (Figure 3-2d). These results suggest that the staining ions from the PTA solution interrupted the interactions between Au-NPs and phage particles, resulting in the detachment of Au-NPs from phage particles. Without the help of positively charged Au-NPs, phage particles could not be attracted any further so they repelled each other and finally broke the densely packed bundle structures. Therefore, PTA is not a suitable stain for this nanohybrid because it interrupts the interactions between the two components and greatly changes the hybrid structures. From this PTA-stained sample only inaccurate structural details were obtained.

### *3.3.6 Choice of the Concentrations of the Stain.*

In order to test if a higher concentration of the stain is better in this system, we increased the concentration of the UA solution from 0.5% up to 2% and kept other factors the same as in the optimal condition (10s of staining, rapid drying, pH=4.5). When stained with 2% UA, the Au-NP-phage hybrids were heavily darkened (Figure 3-5a). Densely packed phage bundles were still recognizable with careful identification, but the Au-NPs within Au-NP-phage hybrids were totally covered by the heavy stain and became unrecognizable (Figure 3-5a). As previously mentioned, the isoelectric point of M13 phages is about 4.2 which is lower than the pH of the staining solution (pH=4.5). So such staining by the 2% UA solution caused an obvious positive-staining

effect which heavily darkened the Au-NP-phage hybrids. This test suggested that a lower concentration (0.5%) of UA solution brought fewer positive-staining effects to the specimen and worked better on the Au-NP-phage nanohybrids than a concentrated UA solution (2%).

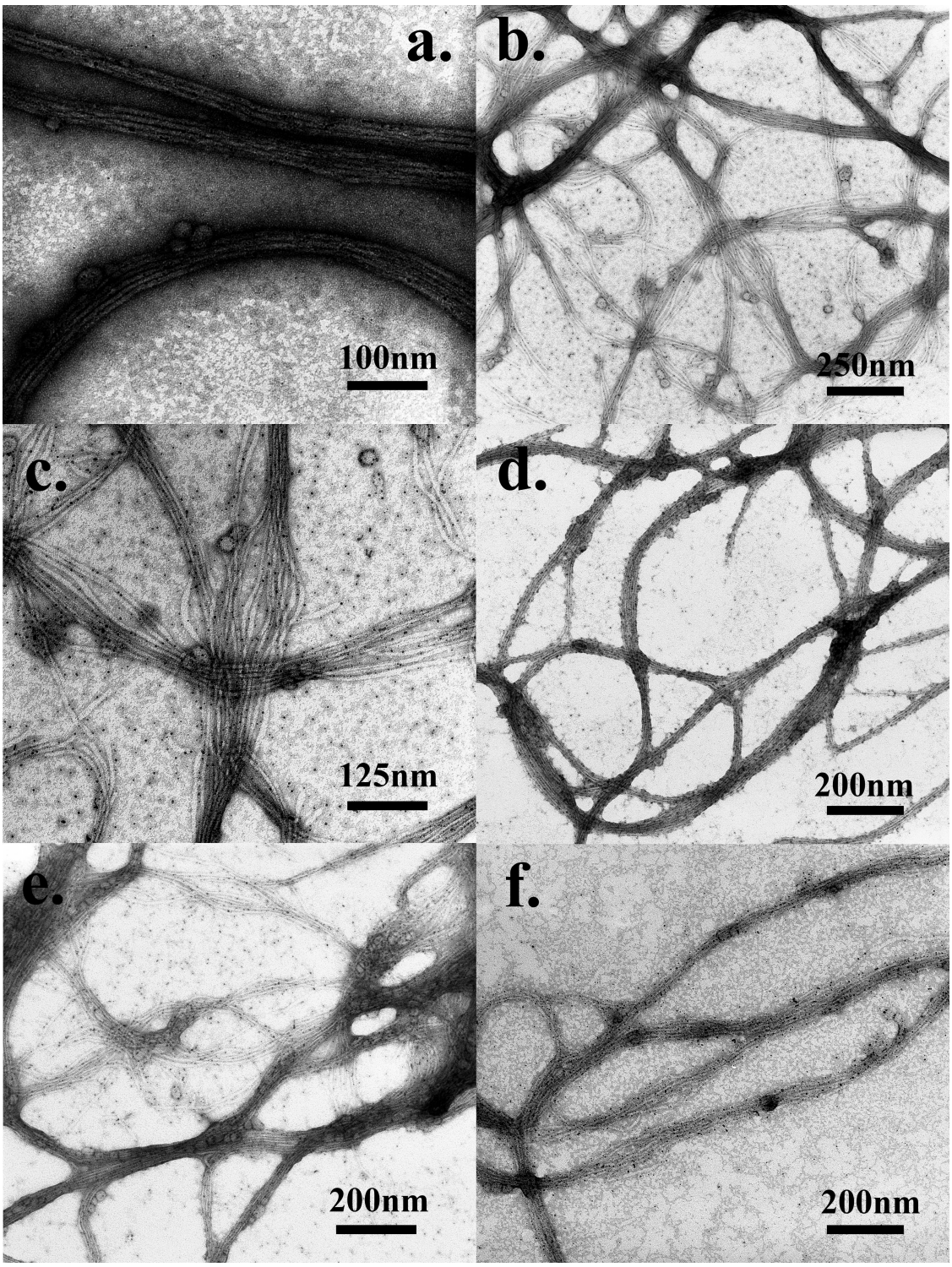



**Figure 3-5 a) Au-NP-phage hybrids were stained with 2% UA solution (pH=4.5, 10s of staining, rapid drying); b) Au-NP-phage hybrids were stained with 0.5% UA solution (pH=4.5, 1 minute of staining, rapid drying); c) high resolution image of b); d) Au-NP-phage hybrids were stained with 0.5% UA solution (pH=3.5, 10s of staining, rapid drying); e) Au-NP-phage hybrids were stained with 0.5% UA**

**solution (pH=4.5, 10s of staining, slow drying); f) Au-NP-phage hybrids were pre-fixed by 1% GA solution and stained with 0.5% UA solution (pH=3.5, 1 minute of staining, slow drying).**

### *3.3.7 Staining Time.*

Staining time is another factor that may affect the negative staining. We increased the staining time from 10 s up to 1 min and kept all other factors the same as the optimal condition (0.5% UA, rapid drying, pH=4.5). Again, the structure of Au-NP-phage hybrid was greatly changed during the staining. Phage particles were separated from each other and most of the Au-NPs were detached from the phage bodies (Figure 3-5b&c). These results suggest that the staining ions from the UA solution are more electrostatically attracted to phage particles than Au-NPs and therefore slowly replaced Au-NPs. This replacement needs a longer time to occur (1 min). Consequently, after a longer time of staining, the densely packed bundle structures were broken. Unlike the stain PTA, UA molecules needed a longer time to break up the Au-NP-phage hybrids. Therefore, we believe staining with 0.5% UA for a short time (10 s) is a better choice for this model system.

### *3.3.8 pH of the Stain.*

The pH of the stain solution plays a crucial role in most staining processes. It is known that in negative staining heavy staining ions are repelled by the charged groups of the specimen and sit along biological molecules whereas in positive staining heavy metals react with and attach to biological molecules. The charges on the surface of the biological molecules are mainly dependent on its isoelectric point and local pH value. Since the isoelectric point is constant for a specific biological molecule, the surface chemistry of the molecules is dependent on the local conditions.

In the Au-NP-phage hybrid system, the isoelectric point of M13 phages is about 4.2, so in theory, a lower pH of the UA solution should not cause positive staining effects and will have a better performance in staining. Therefore, we decreased the pH of the UA solution from 4.5 to 3.5 while keeping all other factors the same as the optimal condition (0.5% UA, rapid drying, 10s of staining). Densely packed phage bundles were nicely stained by the staining ions and Au-NPs could also be observed clearly (Figure 3-5d). However, most Au-NPs were detached from the phage bundles, which were not found in the non-stained specimen (Figure 3-2d). The possible reason for this phenomenon is the low pH of the UA solution made the M13 phage particles positively charged. Under this condition, the positive charges on phage particles made a perfect negative staining by UA, but at the same time, the positive charges also repelled positively charged Au-NPs from phage particles. Captured TEM images should ideally reflect the real structures of nanohybrids. Therefore, any stain solution with a pH lower than 4.2 is not a good choice for the visualization of Au-NP-phage hybrid.

### *3.3.9 Drying Method.*

Drying is also a factor that may affect the appearance of specimens. We tried a slow air-drying of the UA stain and kept all other factors the same as the optimal condition (0.5% UA, pH=4.5, 10s of staining). We found a lot of small stain crystals appearing on the TEM grid. Besides, most Au-NPs were found detached from the phage bodies and some phage bundles were broken (Figure 3-5e). Obviously, compared to fast drying achieved by using a hair dryer (Figure 3-4 a-b), the slow air-drying of the stain encouraged the formation of stain crystals and also interrupted the electrostatic interactions between Au-NPs and phage particles.

### *3.3.10 Choice of Pre-fixation.*

We performed a pre-fixation with 1% glutaraldehyde (GA) for 20 min before negative staining and then stained the specimen with 0.5% UA solution (pH=3.5, 1 minute of staining, slow drying). As previously mentioned, under these staining conditions without pre-fixation, phage bundles should be disassembled and Au-NPs should be detached from the phage particles. However, none of the expected phenomena happened. Instead, phage bundles were nicely stained and most Au-NPs were still attached to phage particles (Figure 3-5f). The good attachment results from the fact that phage particles and Au-NPs were covalently cross-linked by GA molecules within the hybrids. Therefore, in the process of staining, either low pH or long staining time could not break any of these covalent bonds, leaving the integrated structures of the Au-NP-phage hybrids.

## 3.4 Discussion

### *3.4.1 Mechanism of Negative Staining with UA and PTA.*

Negative staining is achieved when heavy staining ions are repelled by the charged groups of the specimen and tracking the trace of the biological molecules. These heavy atoms increase electron scattering and improve the amplitude contrast of biological molecules. Uranyl acetate (UA, $C_4H_6O_6U$) is a popular negative stain that has been most widely used since 1960. It is used at a pH ranging from 3.5 to 5.5 (the usual pH is 4.5) due to its instability at pH higher than 6.0. A molecule of uranyl acetate in water is in form of uranyl cation ($UO_2^{2+}$). At a pH of approximately 4.5, which is below the isoelectric point of most proteins, proteins are positively charged and the charged protein residues repel positively charged $UO_2^{2+}$, resulting in negative staining [150].

Phosphotungstic acid (PTA, $H_3PW_{12}O_{40}$) is another typical negative stain that usually works at a neutral pH. This stain can be employed at a pH range of 5.0 to 8.0, though its optimum pH of 6.9. A molecule of PTA in water is in form of ionic $PW_{12}O_{40}^{3-}$. At a pH of approximately 7.0, which is above the isoelectric point of most proteins, proteins are negatively charged and the charged protein residues repel negatively charged $PW_{12}O_{40}^{3-}$. This condition also results in negative staining [150]. However, a certain degree of interactions between charged groups of biological molecule and stain ions, especially $UO_2^{2+}$, may occur, producing positive staining. The main reason for the occurrence of positive staining with UA is the small difference between the pI of the protein (approximately 5.0) and the pH of the staining solution (usually 4.5).

### *3.4.2 Bio-Inorganic Nanohybrids and Negative Staining.*

The conventional negative-staining procedure for regular biological samples cannot be applied to bio-inorganic nanohybrids directly. More factors should be customized according to each specific hybrid, such as the choice of pH value, staining reagent, staining time, and drying method. First, most stain solutions contain divalent or trivalent stain ions and some of them have low pH values (e.g., for UA). These stain ions and low pH values both contribute to the interruptions of the interactions between biological molecules and inorganic nanomaterials. If biological molecules and inorganic nanomaterials are covalently linked through a chemical reaction, either low pH or stain ions can't break the covalent bonds [153]. However, if they are linked through electrostatic interactions, pH values and stain ions may greatly influence the interactions (as shown in the Au-NP-phage system). Therefore, the choices of stains, pH values, working concentrations and staining time should be selected carefully. Second, some

inorganic nanomaterials and biological molecules are not stable at low pH values. For example, hydroxyapatite nanocrystals will be dissolved at a pH lower than 4.0 [154, 155] and bacterial flagella are not stable at an acidic pH (low than 5.0). For these materials, UA solution is not a good choice due to its acidic working pH (3.5-5.5). Third, biological molecules have different isoelectric points, the pH of stain solutions should be chosen according to the specific pI of the biological molecules of interest. Fourth, some biological molecules only have one type of charged group so not all negative stains can be applied to these samples. For example, DNA assemblies only have negative charges on their surfaces. In this case, only PTA or neutral stains can be used to negatively stain DNA assemblies. Lastly, some inorganic nanomaterials also have low contrasts (such as $Al_2O_3$ or small nanoparticles) so that they cannot be identified when covered by heavy layers of stains. Under this condition, a light staining is expected to work better.

For our Au-NP-phage model system, the formation of the hybrids is based on the electrostatic interactions between positively charged Au-NPs and negatively charged phage particles. Therefore, the hybrids may not be stable when exposed in stain solutions. After the systematic studies of the effects of each factor on the negative staining of the hybrids, we found the electrostatic interactions between Au-NPs and phage particles could be greatly interrupted when the hybrids were exposed to one of the following staining conditions: (1) PTA stain solution (Figure 3-4 c&d); (2) UA stain solution for a long time (>1 min) (Figure 3-5 b&c); (3) UA stain solution with a pH lower than the pI of phage particles which is ~4.2 (Figure 3-5d); (4) UA stain solution with a slow air-drying (Figure 3-5e). The respective reasons are outlined in Table 3-1.

| Conditions interrupting the association of Au-NPs and phage | Reasons |
|---|---|
| PTA stain solution | $PW_{12}O_{40}^{3-}$ competed with the $-COO^-$ on phage particles to bind with positively charged Au-NPs |
| UA stain solution for a long time (>1 min) | $UO_2^{2+}$ competed with the positively charged amine groups on Au-NPs for the binding with negatively charged phage particles. So the staining time should be as short as possible. |
| pH lower than the pI of phage particles (~4.2) | A low pH value of UA solution (<4.2) will make the M13 phage particles have a net positive charge and thus repel positively charged Au-NPs. |
| Slow air-drying | In a process of air-drying, UA concentration will increase and the local pH will decrease. A slow air-drying sets the Au-NP-phage hybrids into the harsh local environments for a longer time and thus interrupts the electrostatic interactions between Au-NPs and phage particles. |

**Table 3-1 A summary of conditions interrupting the association of Au-NPs and phage with justification.**

### *3.4.3 Choice of Stain and Working pH Based on Specific Bio-Inorganic Nanohybrids.*

Choosing the type of stain and its working pH value according to specific bio-inorganic nanohybrids is the most important step in the negative staining. The choice of

the stain and its working pH value should be based on specific bio-inorganic hybrids. Specifically, if inorganic nanomaterials or biological molecules are not stable in acidic solutions, PTA or other neutral stains will be better for the hybrids. If both materials are not pH-sensitive, the driving forces for holding together the biological molecules and inorganic nanomaterials should be checked. If both materials are linked by covalent bonds through a chemical reaction, both UA and PTA can be used as the negative stain. But if the electrostatic interaction is the driving force to hold the biological and inorganic components, more factors should be paid attention to during the staining. PTA stain is preferred if $PW_{12}O_{40}^{3-}$ ions do not greatly interrupt the electrostatic interactions between the two components. Otherwise, UA stain will be tested to see if $UO_2^{2+}$ ions will interrupt the interactions. If yes, it means both PTA and UA stains are not suitable for the staining. If no, UA will be selected as the main negative stain for the hybrids.

Once the negative stain is selected, its working pH value needs to be determined next. For PTA, the working pH value should be within the range from 5.0 to 8.0 and also higher than the pI value of the biological molecules [150]. For UA, the situation is more complicated: first, the specific working pH value should be within the range from 3.5 to 5.5 [150]; second, if positively charged biological molecules (usually pI>7.0) are interacted with negatively charged inorganic nanomaterials through an electrostatic interaction, a regular pH of 4.5 will be good for the staining; third, if negatively charged biological molecules (usually pI<7.0) are interacted with positively charged nanomaterials through an electrostatic interaction, pH=pI+0.3<5.5 (when pI<5.2) is the best working pH value. In this case, the slightly negatively charged biological molecules and positively charged $UO_2^{2+}$ may interact with each other and cause some

positive-stain effects to specimens, but the effects are not significant. However if 5.2<pI<7.0, UA stain with any pH within 3.5 to 5.5 will change the initially anionic biological molecules to cationic, resulting in the detachment of positively charged inorganic nanomaterials from biological molecules. In this work, positively charged Au-NPs and negatively charged phage particles (pI=4.2) are stable in acidic solution, and they interact with each other through an electrostatic interaction which could be greatly interrupted by $PW_{12}O_{40}^{3-}$ ions but not $UO_2^{2+}$ ions.

With the above information, if pH < pI, the interactions between biological and inorganic components will be interrupted. If pH>pI+0.3, the pH will cause severe positive-staining effects to the sample which may darken the biological structures in certain areas. If pI<pH<pI+0.3, the biological sample may not have enough charges on their surfaces for electrostatic interactions and negative staining. Thus we can easily get the conclusion that UA solution with a pH=pI+0.3=4.5 is the optimal condition for staining Au-NP-Phage hybrids (Figure 3-4a&b). A best pH value of 4.5 is reasonable because it could not only favor the electrostatic interaction and but also reduce the positive-staining problems.

### *3.4.4 Choice of Stain Concentration Based on Specific Bio-Inorganic Nanohybrids.*

The concentration of the stain is another important factor that may affect the appearance of the specimens. A high concentration of stain solution (>1%) is not recommended for two reasons. First, highly concentrated stain ions may accelerate the departure of inorganic nanomaterials from biological molecules. Second, heavy layers of stain may cover most inorganic nanomaterials so they will be unrecognizable under

TEM (Figure 3-5a). Therefore, a low concentration (0.5%) of the stain will produce a better staining for bio-inorganic nanohybrids.

### *3.4.5 Choice of Fixation Based on Specific Bio-Inorganic Nanohybrids*

Pre-fixation has been used in negative staining in some cases. Its function is to covalently cross-link intra- and inter-molecules to prevent drastic alterations or damages in negative staining. However, the fixation should not form inter-particle cross-links, otherwise, artificial structures may appear. The most useful fixative in biological electron microscopy is glutaraldehyde (GA) which covalently cross-links nucleophilic -$NH_2$ groups. For the bio-inorganic nanohybrids, fixation should not be performed if either biological molecules or inorganic nanomaterials are covered by -$NH_2$ groups. Otherwise, inter-particle cross-linking will occur and the initial appearance of the hybrids may be changed. In our Au-NP-phage system, both phage particles and Au-NPs are covered by -$NH_2$ groups, so GA is not suitable as a fixative for the negative staining. GA molecules may cross-link neighboring phage particles so that phage bundles can be observed after fixation even without Au-NPs. They may also cross-link $NH_2$-covered Au-NPs with phage particles. It would be difficult for us to figure out whether the cross-linking between Au-NPs and phage particles were due to electrostatic interactions or fixations.

### *3.4.6 Why Rapid Drying is better*

Slow air-drying is a popular and simple strategy for the drying of stains, but it also has two main limitations. First, since hydrated crystals tend to grow by slow evaporation, slow drying of the stain after negative staining can only encourage the formation of stain crystals instead of amorphous stain deposit which is required for the

desired resolution. Second, in the process of drying, salt concentration will increase and the local pH will also decrease (e.g., for UA) or increase (e.g., for PTA). Such changes can influence the final appearance of the specimen. A slow drying will put the specimen into a harsh local environment for a longer time and has greater chances to influence the appearance of the specimen. Therefore, a rapid drying by a hair drier may improve the negative staining.

## 3.5 Conclusion

TEM characterization of negatively stained bio-inorganic nanohybrids is a popular and simple technology for viewing such nanostructures. We chose bacteriophage-gold nanoparticle hybrid as a model to systematically study the effects of each factor on the negative staining of the nanohybrids. The best staining conditions for this hybrid system include the use of 0.5% UA solution (pH=4.5), a staining time of 10 s, and a rapid drying of the stains. The experimental results suggested that each factor could influence the final appearance of the stained specimens and the best choice of each staining factor should be customized to the specific bio-inorganic nanohybrids. The effects of each factor on the negative staining of the nanohybrids were discussed and a general method about how to select each staining factor was summarized. This work provides useful information for the negative staining of bio-inorganic nanomaterials, which will greatly help research in the fields of bionanotechnology and nanomaterials.

# Chapter 4: A novel stem cell binding motif identified by phage display promotes non-viral gene delivery to stem cells

## 4.1 Introduction

Gene delivery is a promising and mostly studied method for treating traditionally incurable diseases. Although virus based delivery strategies have shown high delivery efficiency, moral controversies and potential problems of using viral gene vectors have led to a dramatic development of non-viral gene delivery[156]. Recently, mesenchymal stem cell (MSC) has become an excellent target candidate for gene therapy due to its multipotency, self-renewing ability and ease of preparation[157]. MSCs with delivered gene inside can be injected to the damaged tissue or organ and express specific functional proteins for tissue or organ recovery. However, a relatively low delivery efficiency of non-viral vectors has become a major obstacle for applying the strategy into practical use. Recently, it has been found that conjugating target-binding peptide onto the delivery system can greatly improve the delivery efficiency[158]. Therefore, to find a reliable technique that can identify MSC-targeting peptides has become a promising solution to increase the gene delivery efficiency for the MSC based gene therapy.

Phage display technology has matured to be a powerful tool to identify target-binding peptide through a process of affinity selection[10, 11, 159]. Various target-binding peptides have already been identified, including peptides that can specifically bind to proteins, inorganic materials, and living mammalian cells[159-164]. The principles of phage display technique have been reviewed elsewhere[23, 165-167].

Briefly, a phage-displayed random peptide library (also called phage library) is allowed to interact with a target (e.g., a protein or a cell), and then the nonbinding phages are washed away from the target, leaving the binding phages bound to the target. The binding phages are then eluted from the target and amplified by infecting bacteria to form an enriched phage-displayed peptide population, which can be treated as a new library to interact with the target again. This process is called biopanning and usually repeated for several rounds to identify the peptides with binding affinity against the target. We employed this matured phage display technique to identify MSC-targeting peptide for increasing the gene delivery efficiency towards MSCs. A possible scheme of applying the work in this research is shown in Figure 4-1. Efficiently recognizing MSCs by random phage library mostly depends on the distribution of cell surface receptors. A variety of nanoparticles and nanovehicles that are non-viral vector candidates have been reported to be uptaken by cells via receptor mediated endocytosis. Therefore, an understanding which type of cell surface receptors interacts with MSC binding peptide would provide hints for studying the ligand-receptor interactions of MSC and improve the transfection efficiency of non-viral gene delivery to MSCs. It may also help the study of proteomics.

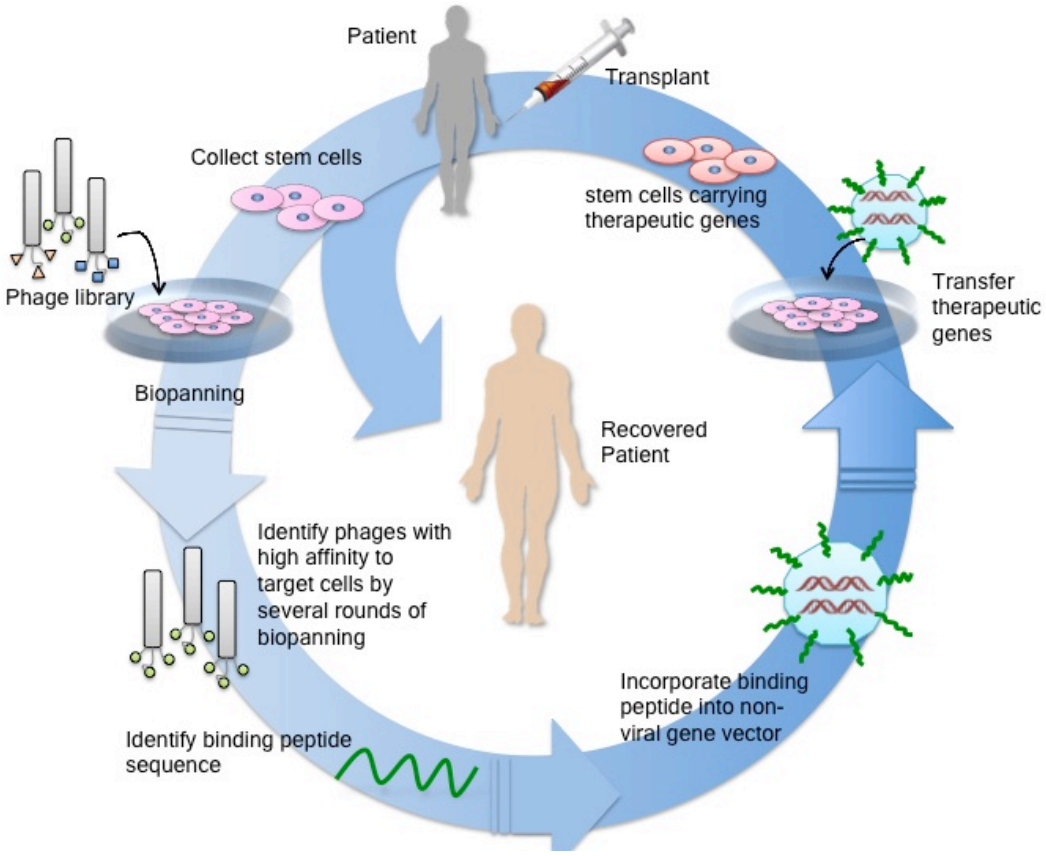



**Figure 4-1** Scheme of applying phage display and mesenchymal stem cells to customized therapy.

In this work, we conducted affinity selection based on phage display on primary rat MSCs. The phage library we used is Ph.D.-12 phage library from New England Biolabs. The specific binding peptide HMGMTK was identified from phage display based cell panning and further bioinformatics analysis. It was confirmed by immunological fluorescence imaging. We further analyzed the selected peptide under bioinformatics and found that the peptide HMGMTK shows a high similarity to the previously proposed signaling region of a chemokine CX3CL1, the ligand of CX3CR1.[168, 169] For testing the effect and future uses of selected MSCs binding peptide in non-viral gene delivery, we built up a multifunctional nanoparticle that is a

complex of the EGFP report gene, Liposome/Protamine/DNA complex (LPD), specific binding peptide HMGMTK (named PA). Nuclear localized signal (NLS) motif (DPKKKRKVDPKKKRKVDPKKKRKV) [170] was also introduced to facilities the transgenic DNA to penetrate the nuclear membrane and enter cell nucleus. The resultant complex vector (termed as LPD+PA+NLS in this article) showed highest transfection efficiency among commercial vector Lipofectamine$^{TM}$ 2000 (Invitrogen, USA), LPD without any peptides and LPD with control peptide having no affinity to MSCs as well as LPD with PA. Meanwhile, cytotoxicity evaluation result showed that LPD+PA+NLS complex did not show obvious cell toxicity and influence on the differentiation potential of rMSCs while increasing gene transfection efficiency to MSCs.

## 4.2 Experimental Procedure

### *4.2.1 Materials*

All the cell culture reagents were obtained from Gibco BRL unless otherwise stated. All chemicals were obtained from Sigma Chemical Co. unless otherwise stated. The Ph.D.-12 Phage Library, where there are billions of M13 phage particles with each particle displaying a random linear 12-mer peptide on the C-terminus of minor coat protein (pIII), was a product of New England Biolabs. Plasmids pT2 and pSB are kindly provided by Dr. Perry Hackett, University of Minnesota.

### *4.2.2 Primary rat mesenchymal stem cell isolation and culture*

The primary rat mesenchymal stem cells (rMSCs) were prepared by following previous literatures [171]. The complete culture medium was Dulbecco's modified

eagle medium (DMEM low glucose) supplemented with 100 IU/ml penicillin and 100 g/ml streptomycin, and 2 mM L-glutamine, and 10% v/v fetal bovine serum (FBS). NIH guidelines for the care and use of laboratory animals have been observed. Briefly, male Sprague-Dawley rats weighing 70-150g were killed by $CO_2$ asphyxia and the bone marrow was harvested from the hind limbs. Then marrow cells were flushed out strongly by a 27-gauge needle attached to a 10 ml syringe containing complete media and collected in a 10 ml tube on ice. After filtering the cell suspension through a 70 mm mesh to remove any bone debris, bone marrow cells were cultured in a culture dishes and incubated at 37°C with 5% $CO_2$ for 3 hours. The non-adherent cells, which are not mesenchymal stem cells, were removed by changing the medium and replaced with fresh complete medium. The medium was re-changed after an additional 8 hour of culture. The typical adherent spindle-shaped cells appeared on the third day and reached 65-70% confluence within 2 weeks. Then the cells were washed by phosphate-buffered saline and treated with 0.5ml 0.25% trypsin/1mM EDTA for 2 min at room temperature to further remove loosely bound non-MSCs. The culture medium was changed every 3 days regularly and cells typically reached confluence and sub-cultured in 7 days.

### *4.2.3 Selection of rMSC-binding peptide from a phage-displayed random peptide library: Biopanning*

Biopanning against primary rat MSCs was carried out according to manufacturer's protocols and previous literatures [172]. Primary rMSCs within 3 passages were seeded on 6-well plates in the density of $1\sim1.5\times10^5$ cells/well 1-2 days before panning and used for experiments when reaching ~90% confluence. Before the panning procedure, the complete cell culture media was replaced by serum free media

and cells were incubated for 2 hours at 37°C to clear cell surface receptors. The phage panning solution was prepared by diluting the original phage library to the final concentration of $1\times10^9$ pfu/ml with PBS and 0.1% w/v BSA and supplementing with 10µl 10mM chloroquine and 40µl protease inhibitor without EDTA (25×, Roche) and making the final volume to 1ml. The phage panning solution was applied on empty 6-well cell culture plate to eliminate any plastic-bound phages before it was allowed to interact with MSCs. The serum free media was removed and the cells were washed by PBS with 0.1% BSA once. $1\times10^9$ pfu/ml of pre-cleared phage panning solution was incubated with cells in the 6 well plate (1ml panning solution per well) for 1 hour at 37°C. After incubation, the supernatant was aspirated and the cells were washed four times at room temperature by PBS with 0.1% BSA for 5 min per wash to remove any unbound phages. Cell surface binding phages that were weakly associated to the cells were eluted by 1ml 0.1M HCl-glycine + 0.9% NaCl (PH 2.2) for 5 min, followed by neutralizing with 1.5M Tris-HCl (PH 8.8). Then cells were scraped off the plate and lysated by free-thaw disruption in order to release any tightly bound phages or phages that may internalize into the cells. The output phages were amplified by infecting the host *Escherichia coli* ER2738 and titered each round to ensure that the equal amount of input phages ($1\times10^9$ pfu) were used in each round. This panning procedure was repeated four times. The output phages of the final fourth round were sequenced to get the high-affinity peptide sequences to primary rMSCs. The output to input ratio (O/I) was calculated as the index for the recovery of phages from each round of panning on rMSCs.

### *4.2.4 Phage titering, amplification and purification*

The phage amplification and purification was done by following manufacturer's manual. Briefly, 20 ml of *E. coli* host ER2738 prepared from the overnight culture was infected by the output phage of each round and incubated with vigorous shaking for 4.5 hours at 37°C. Then the infected culture was centrifuged twice at 12000 g for 10 min at 4 °C. The top 80% of the supernatant was transferred to a fresh tube and 1/6 volume of 20% PEG/2.5M NaCl was added to allow the phage to precipitate at 4°C overnight. The PEG precipitate was centrifuged at 12000g for 15 min at 4°C twice. The white phage pellet was suspended in 1 ml of TBS and transferred to a micro-centrifuge tube to spin at 14000 rpm for 5 min at 4°C to pellet residual cells. The supernatant was transferred to a fresh tube and re-precipitated by adding 1/6 volume of 20% PEG/2.5M NaCl for 1 hour or overnight. The further purified phage pellet was obtained by centrifuging at 14000 rpm for 10 min at 4°C and suspended in 200 µl of TBS. This suspension included the amplified phages, which would be used as input phages for successive panning round after proper dilution. The input, output, and amplified phages were titered as described in the manufacturer's protocol. The E. coli host ER2738 was cultured to reach mid-log phase, $OD_{600}$ ~ 0.5 and 200µl of the culture was dispensed into microfuge tubes for phage infection. A series of dilutions of phages was prepared in LB to 1ml final volume. 10 µl of each phage dilution was added to each tube of host cells in mid-log phase with vigorous vortex and incubated at room temperature for 5 min. The infected cells were plated on pre-warmed LB/IPTG/Xgal with top agar assistance and incubated overnight at 37°C. The number of blue plaques on plates was counted next day and multiplied by the dilution factor to get phage titer in plaque forming units (pfu) per 10µl.

The titering plate of the unamplified output phage from the final round of panning that have approximately 100 plaques was used to pick individual plaques for sequencing.

### *4.2.5 Statistical Analysis*

All the biopanning data were analyzed by the bioinformatics tool — RELIC program [173]. The probability of each selected sequence was calculated by INFO program in RELIC server and compared with that of random phage library. Only the sequences having higher probability to original phage library were used for comparing with several known ligands for MSCs. The similarity scores of selected sequences to known ligands that bind to various cell surface receptors present or absent on rMSCs were obtained by using RELIC-MATCH program and plotted over the amino acid position of known ligands to find the best match.

### *4.2.6 Fluorescence imaging using synthetic peptide*

Peptide HMGMTK was chemically synthesized and conjugated with fluorescein isothiocyanate (FITC). A FITC-conjugated scramble peptide GTMHKM was also synthesized as control. FITC molecules were conjugated to the peptides during synthesis through Ahx as spacer to minimize any possible steric hindrance. Primary rMSCs were plated on the glass coverslips in a 6 well plate (Falcon). Same as in the phage screening, the cell surface receptors were pre-cleared by incubating the cells with serum-free media for 2 hours. The precleared cells were incubated with FITC-conjugated peptide diluted by PBS/0.1% BSA in a proper concentration for 1 hour at 37°C. Then the cells were washed three to five times with PBS, fixed with 4% paraformaldehyde for 15 minutes at room temperature. The cell nuclei were

counterstained with DAPI. The cells were observed under fluorescence microscopy (Nikon). The assay was performed independently for three times.

### *4.2.7 The construction of Liposome/Protamine/DNA complex (LPD)*

To construct the LPD, we used a two-step packaging technology employing a multi-layering method (13, 14). First, the DNA was packaged into a condensed core via electrostatic interactions with protamine. The targeting peptide with slightly positive potential was also added and interacted with the plasmid to form a negative charged particle. Second, liposome protamine/DNA lipoplexes (LPD) were prepared through membrane fusion of neighboring phospholipid bilayer of liposome, triggered by the assembly of positively charged DOTAP/DOPE/Chol liposome around the negatively charged core. The morphology of LPD was observed using TEM (Carl Zeiss, Germany). One drop of polyplex was placed on a copper grid and stained with 2% uranyl acetate for 3 minutes. The grid was allowed to dry further for 20 min and was then examined with the electron microscope.

### *4.2.8 Conjugation of targeting peptide to LPD*

The reduction of cysteine residues in the targeting peptide was first performed. Briefly, 5 mL peptide (100 μM, PBS, pH7.5) was first mixed with tris(2-carboxyethyl) phosphine (TCEP; 2 mM) with a 1:2 ratio of peptide/TCEP. The reaction was allowed to proceed at 37 °C for 2 h. A 10 μL DSPE-PEG2000-MAL (10 mM) stock solution was reacted with 5 mL (100 μM) of the reduced peptide in PBS buffer (pH 7.5), corresponding to 5:1 molar ratio of reduced peptide to maleimide groups. The conjugation reaction was carried out for 3 h at room temperature. Conjugated peptide-PEG-DSPE was purified by dialysis (500 Da membrane).

### *4.2.9 Preparation of Targeting LBNs*

To obtain targeting liposomes, the insertion of the peptide-conjugated lipid (peptide-PEG-DSPE) into liposomes was performed by employing a post-insertion technique. For this purpose, liposome (20 mM, as denoted by DOTAP in liposome) in water solution was incubated with a various amount of peptide-PEG-DSPE for 1 h with vortexing. The resultant solution was kept at 60 °C for 1 h. As a result, the conjugates became attached to the outer lipid layer of the vesicles via hydrophobic DSPE domain.

### *4.2.10 Transfection Efficiency*

For the transfection experiments, rMSC cells were seeded in the 24-well plate at a density of $1\times10^5$ cells/well and incubated overnight. The mass ratio of pT2/EGFP and pSB11 was 2:1 as in the earlier report.[174] The LPDs with various peptides in low glucose DMEM were added, and Lipofectamine$^{TM}$ 2000 (Invitrogen, USA) was used as a control. The cells were incubated for 4 h at 37˚C. Then, the transfection medium was replaced with fresh culture medium and the cells were further incubated for 72 hrs. Inverted fluorescent microscope was also used to observe the GFP expression. The transfected cells was digested by trypsin and fixed in a 4% paraformaldehyde for 30 min at 4˚C to prepare single-cell suspensions. The percentage of cells positive for GFP was determined by flow cytometry (Becton-Dickinson Biosciences, Franklin Lakes, NJ, USA) by setting a gate according to the control and 10,000 cells were evaluated in each experiment.

### *4.2.11 Cytotoxicity Assay*

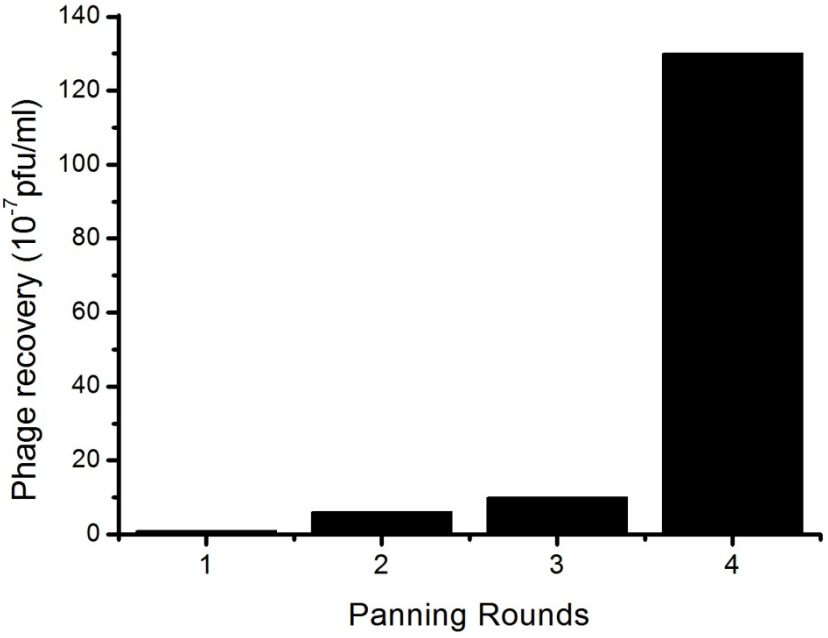
Cytotoxicity of LPD was assayed using MTT assay. Briefly, rMSC cells were seeded at 10,000 cells per well in 96-well plates. One day later, the cells were

transfected by LPD with various peptides at different liposome concentration. The Lipofectamine$^{TM}$ 2000 was used as the control. The cells were incubated for another 12 h at 37˚C. Then, the medium was replaced with 80 μl of fresh medium without serum and 20 μl of MTT (5 mg/ml) (Sigma-Aldrich Co. LLC, USA) solution, and incubated for an additional 4 h. Subsequently, the medium was removed and 100 μl of DMSO was added. The absorbance at 570 nm was measured by using a microplate reader.

## 4.3 Results

### *4.3.1 Identification of peptides that can specifically bind with primary rMSCs by phage display*

Primary rat MSCs-targeting peptides were identified by applying PhD-12 phage library to primary rMSCs for 4 rounds of panning. All the input and output phages were titered to monitor the panning procedure. The ratio of the titer of output/input (O/I) was calculated to estimate the recovery rate of phages from each panning round. A significant increase in the titer number was observed (Figure 4-2), suggesting an enrichment of phages that can bind to the primary rat MSCs with high affinity.




| Rounds | phage recovery (O/I ratio) |
|---|---|
| 1 | $1.0 \times 10^{-7}$ |
| 2 | $6.1 \times 10^{-7}$ |
| 3 | $1.0 \times 10^{-6}$ |
| 4 | $1.3 \times 10^{-5}$ |

**Figure 4-2** Recovery of phages after affinity selection on primary rat MSCs (O/I ratio)

After 4 rounds of panning, we picked total 82 individual clones with 78 sequences identified (shown in Table 4-1). The decreasing of the diversity of the sequences obtained from several rounds of selection is an important indicator of affinity selection. Here, RELIC/POPVID program was applied to estimate the sequence diversity of a combinatorial peptide library. Selected peptides with the binding affinity against rMSCs should have a diversity value lower than randomly selected peptides

from the initial library. We calculated the diversities of both affinity-selected peptides and random peptides selected from the initial parent library by using the RELIC/POPVID program. Our affinity selected peptides yielded a diversity value of 0.005191 ± std.0.005141 (for the output phages of the 4th round of affinity screening) whereas the 78 randomly selected peptides from the initial parent library yielded a diversity value of 0.036576 ± std. 0.018990. Compared to randomly selected peptides, affinity selected peptides have a significantly less diversified population. This fact is an evidence for the successful selection of peptides with binding affinity against immobilized rMSCs during the biopanning process according to the principle of RELIC/POPVID program.

Although the drop of sequence diversity is an indication of successful phage panning, it is not a characteristic of individual peptides or peptide distribution. The biological steps of phage amplification may introduce unexpected distortion and result in counterfeit drop of sequence diversity. This is because that some sequences may be more favorable and thus corresponding phages will grow faster than other members in the phage pool. In order to evaluate whether the distribution of the sequences from affinity selection (signal) is distorted by the noise introduced by the biological steps of phage amplification, RELIC-INFO program was used to measure the probability of a peptide sequence and their occurrence after phage screening process. In this program, the probability of any one peptide in the library is defined by a parameter called Information Content = - ln(P) where P is the product of the probability of each amino acid at each position, a.k.a. $P = P_1P_2P_3 \bullet\bullet\bullet P_{12}$. A peptide with smaller information content would be more possible to be observed because of amplification process but not

affinity binding. The principle of phage screening is enriching the phage displaying targeting peptide while decreasing the peptide diversity due to the affinity binding. Therefore, an enrichment of peptides with higher information content is expected for phage screening. In other words, if we plot the information content versus their occurrence in the pool, a result of phage screening is trustable when a positive shift towards higher information content is observed comparing with that of parent random phage library in the normalized plot (Figure 4-3). As expected, an obvious shift of the information content plot towards the higher information content was observed, suggesting the high reliability of the selection result of phage screening against rMSCs. Moreover, more reliable peptides can be picked out based on the information of Figure 1B. A cutoff value can be defined as 34.3 indicating significant improvement of the reliability of selected sequences compared to random library sequence, represented by dash lines on Figure 4-3. The peptides with information content higher than the cutoff value would show up on the right side of dash line. These peptides are more reliable that those lower than the cutoff values because their occurrence in library were high even they are more improbable to survive through amplification process (high information content). Their occurrences are more possible due to affinity binding rather than natural amplification, in other words, more reliable. Thus, we will only use these more reliable sequences for proteomic analysis to ensure its validity.

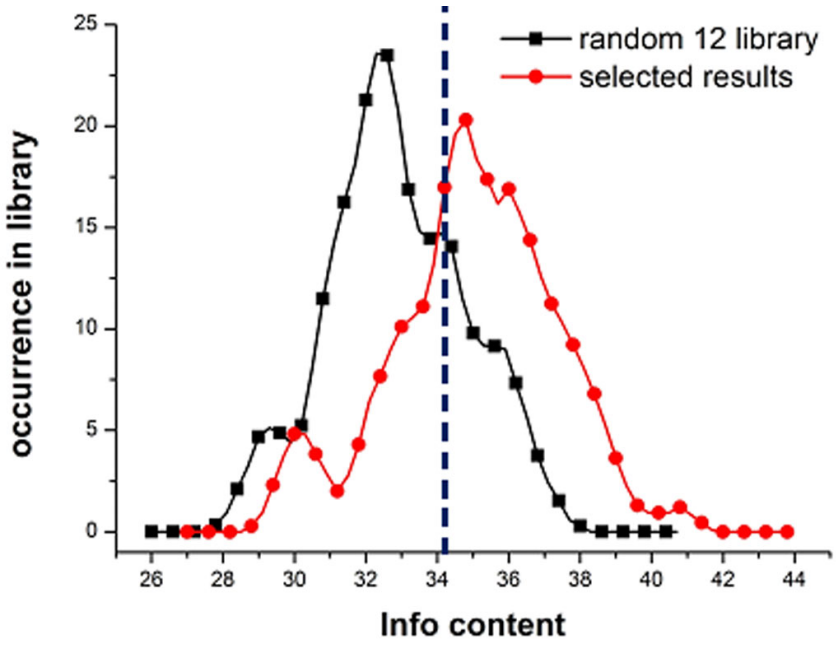



**Figure 4-3** Plot of the information content of peptide sequences calculated by RELIC-INFO program. RELIC-INFO program was used to measure the probability of a peptide sequence by random selection or by affinity selection. In this program, the probability of any one peptide in the library is defined by a parameter called Information content= - ln (P) where P is the product of the probability of each amino acid at each position, a.k.a. $P = P_1P_2P_3 \bullet\bullet\bullet P_{12}$. The red curve with round dots is the information content of selected sequences from affinity selection on rMSC. The black curve with square dots is the information content of originally random Ph.D.-12 library sequences used as control. The dark blue dash line shows the cutoff indicating significant improvement of the reliability of selected sequences compared to random library sequences.

In summary, the validity of affinity selection against primary rMSCs by phage display is supported by the results shown above: (1) the phage recovery rate was increasing as phage panning was going on. This indicated that the phage pool was enriched with sequences exhibiting strong affinity binding to the target and thus could survive from the vigorous washing in the panning step; (2) the sequence diversity of phage pool was decreased because the non-specific sequences were eliminated by subsequent phage panning process; (3) the affinity selected sequences were the peptides which are less likely to survive from natural selection.

After ensuring the reliability of phage panning results, several homological peptides were identified and underlined in Table 4-1 after careful analysis. For example, PSL (P/T/K), T(L/V)P, LGL were showed several times in the selected sequences, but the most frequent one among them is (A/H)MG(M/L)(T/L/S/R)(K/T/S) which is marked in bold in Table 4-1. Moreover, the HMGMTK peptides showed twice with the exact same sequence, which suggested that it might be the most possible binding peptide to rMSCs. In addition, the two peptides HMGMTKIKYFPL and HMGMTKGNYSAL that have the most possible binding peptide are both having information content higher than the cutoff value, further supporting the reliability of HMGMTK peptide. Therefore, we successfully identified one possible and reliable binding peptide HMGMTK after bioinformatics analysis.

| | | | |
|---|---|---|---|
| YVLLPFPVMEPN | VNTGMGSRLTYM | HSNEAAPRYLMI | NALMAVKVVSPL |
| HNPIGFDLNNPE | DSPN**MRS**WQKSE | NHIPSLPKHQSL | ITPDHRLLGLLY |
| YTYP**LSK**MKNVV | WSTQVPIRISPA | SSHEVLGLPKIR | FQSYNQARNPTI |
| NWQDLRNMNAPH | ILAGQMAYRQTH | SFFNIYEPTGLT | KTSAAMMHSMSL |
| GDNQKTDYSPKP | NTVDTHRHQGSK | GHTHEAPRVMRL | HTLPPL**MTG**LRT |
| KIEEATHRQVRE | NRPDSAQFWLHH | GAMHLPW**HMG**PL | SAGAN**LTK**TAYL |
| HAVATLKETAKV | SHDNHGTAYNPG | NIPKSDLAAYNA | VYQTGTATNDPP |
| **HMGMTK**IKYFPL | SHNSTFGQLTAR | VDKTTDSFRSVM | ANSHGLRANPTP |
| QALLEGNAKGGN | SSYYPQLTAHRF | DAISLPMPSKRS | NPSSSQSLWAHR |
| SWIPHPRWSPHH | VTWQKGLNSQVG | IVRPNAHNLPVR | DSPS**MKS**YAWFS |
| TDNPEW**MRT**HNT | **HMGMTK**GNYSAL | AINGLSSLNTRP | NAASTVHSPDRL |
| CEFPRSWDMESN | SNAYSGPAGAPL | TPSLKHH**MKT**QN | APFAQLPSVARS |
| AHKYAIHYAFPW | SWMPHPRWSPQH | YTFPARPHLDLH | TDLARETSNNSP |
| IPTKHWIQTKLD | DGQEKGHQVLNR | GPMHLPW**HMG**TL | LESHYTQASYTQ |
| TETYQPIFR**MKT** | ISAPYAKQH**LSK** | KLHISKDHIYPT | WPHPSLTVPWLP |
| STSSYSEPIWMK | GGNTEWGNNTRH | APFRTTQLPNGM | YGPPAPMTLLTV |
| ATADPGTYNSEA | DHHTRPDNIRIR | TPQFFKSLGSPM | NTWMTEKILSPQ |
| NDG**MTG**GWNVRQ | FVSTTQTHYRGE | TTSLYLKKAFAA | SPLTIPSMAYGQ |
| WQGGSQNSTHQR | TEASS**MLK**NPHA | TTIADSHRGLRQ | RVPAVQPGPPPY |
| D**AMT**TYKSLQRI | | NASMAVKVFSPL | |

**Table 4-1 Peptide sequences identified by phage display. Homological motifs were underlined and the most frequent one (A/H)MG(M/L)(T/L/S/R)(K/T/S) were also highlighted in bold.**

### *4.3.2 Bioinformatics analysis suggests that CX3CL1-CX3CR1 axis may mediate binding between the identified peptide, HMGMTK, and rMSCs.*

We further dig into the possible mechanism that is responsible for high affinity of identified peptides from phage display. Although no surface antigen has been clearly reported as a characteristic MSC marker, many cell surface receptors are expressed by MSCs including phenotypic receptors, growth factor receptors, chemokine and cytokine receptors, cell-matrix receptors, etc. (Table 4-2) [175-178]. We selected several cell surface receptors that are present (MSC+) and absent (MSC-) on the surface of MSCs and their corresponding ligands to do the proteomics analysis of our selected sequences. For example, stro-1 antibody was shown to recognize the cell surface antigen present only on MSCs. SB-10 is an antibody of CD166. So we used stro-1 and SB-10 to compare with our selected sequences. Similar treatment was applied to SDF-1 (a ligand of CXCR4, also called CXCL12), CXCL6 (a ligand of CXCR6) and CX3CL1 (a ligand of CX3CR1). We also compare our sequences with some cell adhesion molecules such as ICAM-1 and VCAM-1. Fibronectin as the most common binder of integrin was also tested in this alignment. As comparison, two ligands that bind to receptors absent on the surface of MSCs were also aligned with our sequences. One is LYN, which is a ligand of CD45, and the other one is CCL11, a ligand of CCR3.

| Molecules present (MSC+) | Molecules absent (MSC-) |
|---|---|
| *Phenotypic receptors* | |
| Stro-1 antibody | CD 34 |
| CD 73 | CD 45 |
| CD 90 | CD 25 |
| CD 105 (Endoglin) | CD 14 |
| CD 166 (ALCAM) | CD 4 |
| *Chemokine receptors* | |
| CCR1, 2, 4, 6, 7, 9, 10 | CCR3 |
| CXCR1, 2, 4, 5, 6 | |
| CX3CR1 | |
| *Cell adhesion molecules* | |
| ICAM-1, VCAM-1 | |

**Table 4-2 The cell surface molecular profile of mesenchymal stem cells**

RELIC-MATCH program was used to align our reliable affinity-selected sequences with many known ligands binding to cell surface receptors that MSCs could or could not express. As stated previously, the sequences having higher information content than the cutoff value 34.3 would be more reliable than those lower than cutoff value. So in order to obtain convincing peptide alignment results, we only use more reliable sequences (information content higher than 34.3) to the proteomics analysis. Then we plotted the similarity score of each amino acid versus amino acid position to find potential MSC binding peptide independently by RELIC-MATCH (Figure 4-4). A cutoff value of similarity score 10 was set and the area exhibiting higher similarity score than cutoff value was marked by arrows in Figure 4-4. Higher average similarity score of ligands binding to MSC positive receptors could be noticed compared to that of MSC negative receptors. And most areas with scores higher than the cutoff value were in

MSC positive category. It is also noteworthy that the highest similarity score reaching nearly 37.5 belonged to the alignment between reliable selected sequences and CX3CL1, a chemokine that binds to CX3CR1. Moreover, further investigation found that this high similarity score is caused by the best match between the putative binding site of CX3CL1 and HMGMTK peptide which has been believed to be the most possible MSC binding peptide based on other analysis (Figure 4-5). This finding further solidified our belief that HMGMTK is the MSC binding peptide and its binding may be mediated by CX3CL1-CX3CR1 axis.

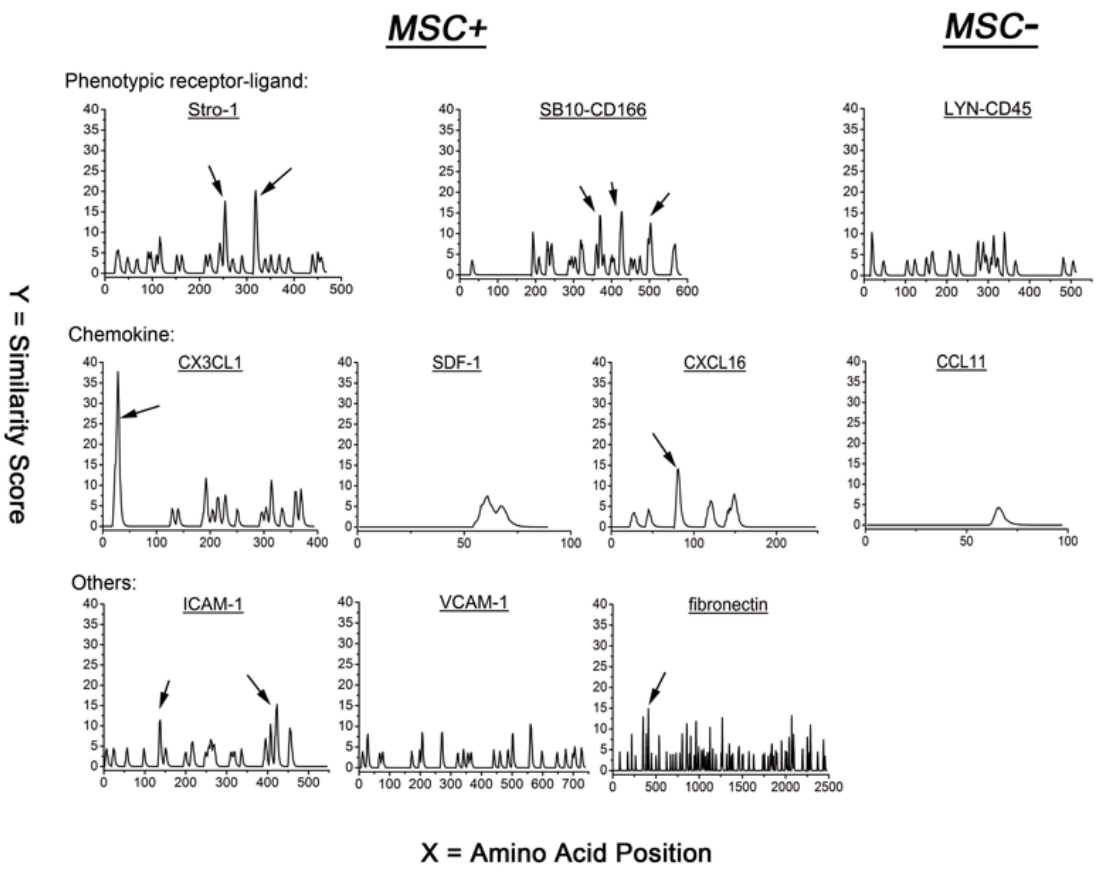



**Figure 4-4 The similarity score of reliable selected sequences and several known ligands that interact with both MSC positive and negative surface receptor. Stro-1, SB10, CX3CL1, SDF-1, CXCL16, ICAM-1, VCAM-1, fibronectin are the known ligands that could bind to the MSC expressed cell surface receptors (MSC+). LYN and CCL11 are two examples of known ligands binding the receptors that MSCs could not express (MSC-). A cutoff value 10 was set for indicating the significant similarity by arrows.**

mapsqlawllrlaaffhlctllagqhlgmtkcnilchkmtspipvtllih 50
HMGMTKIKYFPL
ILAGQMAYRQTH
HMGMTKGNYSAL
ISAPYAKQHLSK

**Figure 4-5 Best match position in the full length CX3CL1 with reliable selected sequences aligned by RELIC-MATCH program. This match position in CX3CL1 is localized in its N-terminal chemokine domain (CX3CL1-CD) which may suggests the exact binding site of CX3CL1.**

### *4.3.3 Synthetic peptide HMGMTK showed higher binding affinity to primary rMSCs compared to scrambled peptide as control and its affinity binding could be competitively inhibited by engineered phages displaying HMGMTK peptide*

To experimentally prove that HMGMTK is the MSC binding peptide, we conducted the fluorescence imaging by fluorescein-conjugated synthetic HMGMTK peptide. We treated the peptides with rMSCs in the same condition as during phage screening process to keep the cell condition consistent. And a scrambled peptide GTMHKM with the same types of amino acid but different sequences comparing to HMGMTK was also chemically synthesized and conjugated with fluorescein as control. Fibroblast cells and cancer cells MCF-7 were cultured and treated as control cells for testing peptide specificity. As expected, rMSC incubated with HMGMTK peptide showed stronger fluorescence intensity than that with scrambled peptides, indicating stronger affinity binding of HMGMTK (Figure 4-6A, B). Meanwhile, no fluorescence was observed in Fibroblasts and MCF-7 cell samples (Figure 4-6E, F), which confirms the specificity of peptide HMGMTK. To further confirm this result, we amplified the phage clone displaying HMGMTK as the competitor of synthetic HMGMTK peptide. If the stronger fluorescence intensity observed in cells treated with HMGMTK peptides was indeed induced by the strong affinity binding between the peptide and cell, the phage displaying HMGMTK should be able to bind to the cells preferentially and then block the cell surface for subsequent binding with synthetic HMGMTK peptide like competition inhibition. We observed that the fluorescence intensity was dramatically decreased in the samples treated with phage first and then synthetic peptide next (Figure

4-6C, D). This is consistent with our expectation and further confirms that HMGMTK is a MSC specific binding peptide.

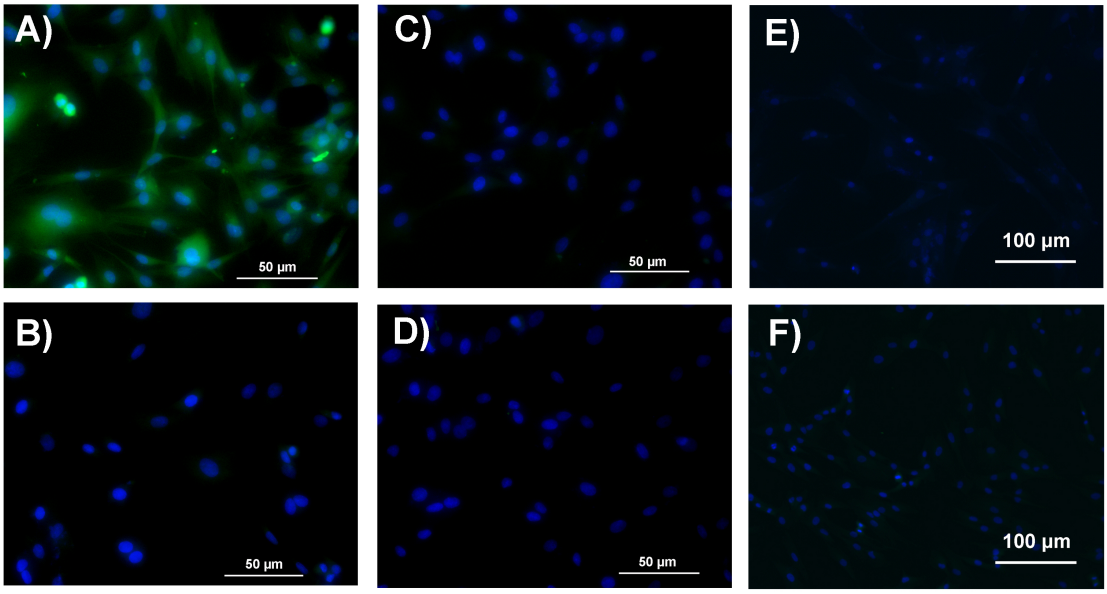



**Figure 4-6 The fluorescence imaging showing the higher affinity of peptide HMGMTK compared to scrambled peptide as control. A) rMSCs after interacted with FITC-HMGMTK peptide; B) rMSCs after interacted with FITC-scrambled control peptide; C) rMSCs after treated with phage displaying HMGMTK first and then interacted with FITC-HMGMTK peptide; D) rMSCs after treated with phage displaying HMGMTK first and then interacted with FITC-scrambled peptide. E) fibroblasts incubated with FITC-HMGMTK peptide; F) MCF-7 cells incubated with FITC-scrambled peptide. Cell nucleus was stained by DAPI. Scale bars in A, B, C, and D are 50µm and in E and F are 100µm.**

### *4.3.4 Integrating MSC-binding peptide HMGMTK and NLS peptide into Liposome/Protamine/DNA (LPD) nanocomplex showed increased transfection Efficiency but remain low cytotoxicity*

To investigate the targeted delivery efficiency of the peptide HMGMTK, we performed the transfection efficiency study using LPD system bearing the synthetic

targeting peptide HMGMTK. EGFP reporter gene was used as the transgene model. To construct the LPD, we used a two-step packaging technology based on a multi-layering method [179, 180]. The constructed LPD particles were evaluated under TEM (Figure 4-7). To further enhance the nuclear translocation efficiency of transgene, three-fold reiterated nuclear localization signal (NLS) motif of SV40 T large antigen with a sequence of DPKKKRKVDPKKKRKVDPKKKRKV was introduced to promote the gene expression of LPD [170]. We integrated both the selected peptide HMGMTK (named PA) and previously reported NLS peptide into LPD systems to build an effective gene delivery carrier (we labeled it as LPD+PA+NLS).

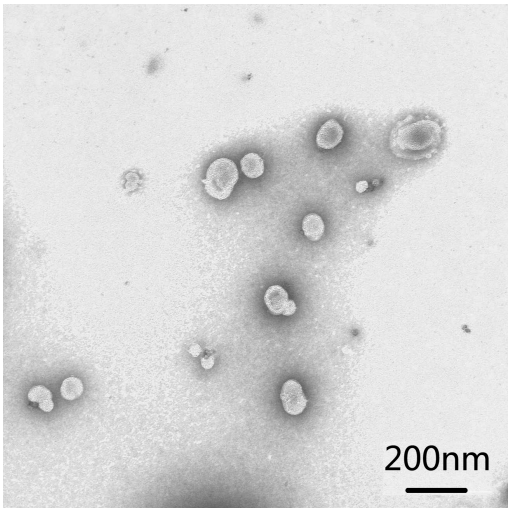



**Figure 4-7 TEM image of LPD particles.**

EGFP expression after transfection via LPD+PA, and LPD+PA+NLS at different pDNA-peptide mass ratio was examined, while LPD only (i.e., the LPD with no peptide conjugated), and LPD+control peptide were served as control. We used fluorescence microscopy, by which the intensity of fluorescence could be used to represent EGFP expression level, to determine the transfection efficiency. The result

showed that (1) LPD incorporating targeting peptide only (LPD+PA) showed greatly enhanced transfection efficiency compared to commercial vector Lipofectamine, LPD without peptide and LPD with control peptide, which means selected rMSCs binding peptide HMGMTK could facilitate gene transfer to rMSCs; (2) LPD+PA+NLS further increases efficiency compared to LPD+PA, which suggests that integrating NLS into the system would help LPD+PA bring target gene to cell nucleus and thus further increase gene-of-interest expression. We could draw the conclusions from the result that the binding ability to rMSCs of identified peptide HMGMTK was confirmed; On the other hand, involving rMSC-binding peptide HMGMTK into LPD system could enhance the efficiency of non-viral gene delivery.

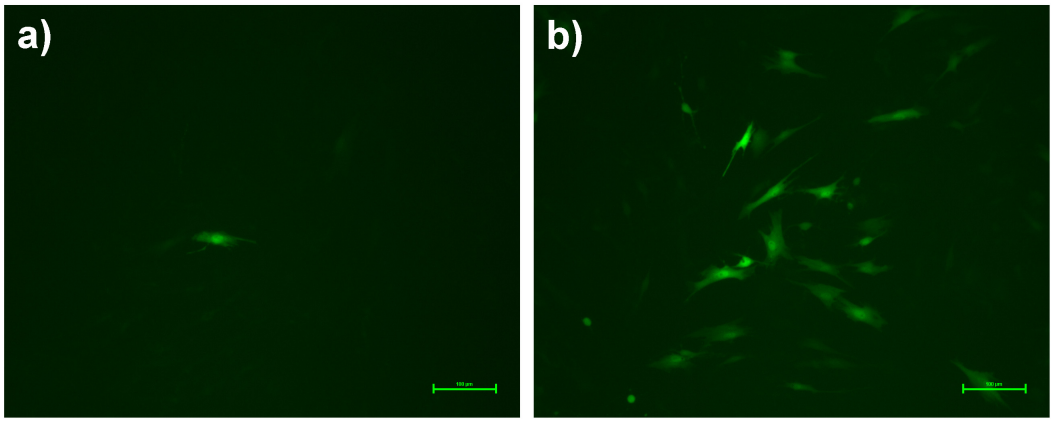



**Figure 4-8 Transfection efficiency of LPD with peptide HMGMTK and NLS peptide in rMSC. GFP expression level in rMSCs due to the delivery of EGFP reporter gene by LPD only (a) and LPD+PA+NLS (b) was visualized by fluorescence imaging. Scale bar: 100 µm.**

To further verify the feasibility of using the novel LPD-peptide complex as a gene delivery vector, we conducted MTT assay to test its *in vitro* cytotoxicity. We set the threshold to judge cytotoxicity at 60% viability, which means when cell viability

below 60% after a trial we will consider the amount of substance used in the trial as cell toxic. Various concentrations of LPD+PA+NLS, LPD and Lipofectamine™ 2000 after 12 h incubation with rMSCs at 37˚C were parallel tested in this experiment (Figure 4-9). We found that Lipofectamine™ 2000 would be considered as cell non-toxic (cell viability higher than 60%) only at relatively low dosage, 20mM. Nevertheless, both LPD and LPD+PA+NLS can reach 60 and 50 mM when they can still be judged as safe to cells. This fact demonstrates that LPD-peptide/NLS show low cytotoxicity similar to LPD only and it is even safer than the popular commercial transfection reagent Lipofectamine™ 2000.

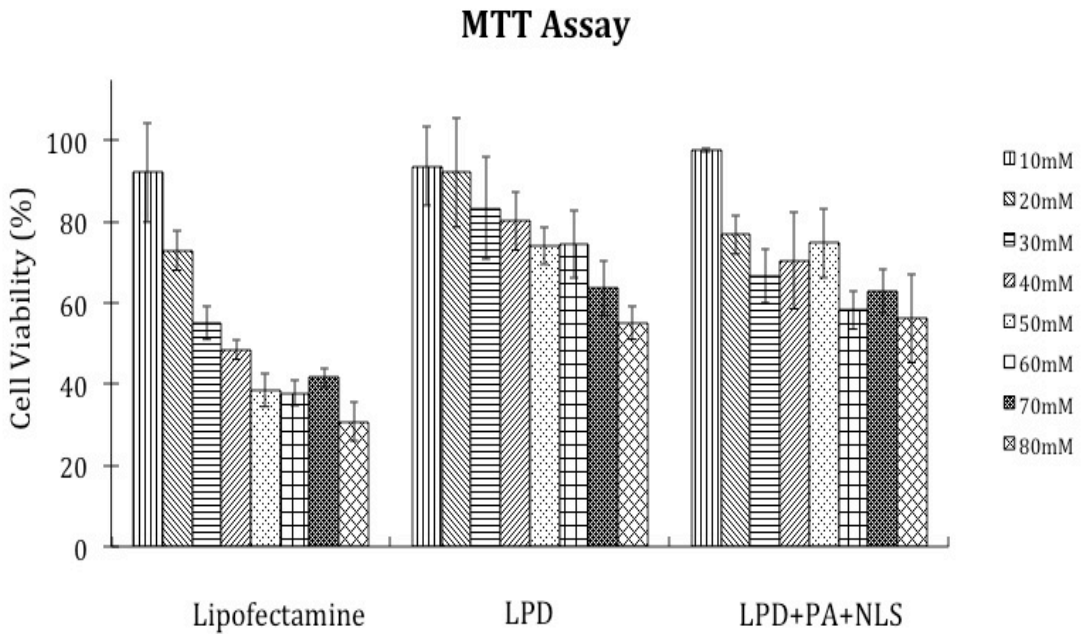



**Figure 4-9 MTT assay for evaluating cytotoxicity of LPD+PA+NLS at different liposome concentrations. Lipofectamine™ 2000 and LPD without peptide were used as a control. The cell viability of samples with LPD with PA and NLS above**

**liposome concentrations 50mM was higher than 60%. Lipofectamine™ 2000 had obvious toxicity as concentrations over 20 mM. The data points represent the mean ±SD of three trials.**

## 4.4 Discussion

The self-renewing and differentiation ability of stem cells has drawn increasing attention of researchers in the field of stem cell therapy and regenerative medicine as next-generation therapeutic method. Although embryonic stem cell is one of the best types of stem cells for this purpose, the legal and moral controversies have hindered the clinical use of embryonic stem cells and thus promoted the discovery and use of adult stem cells. MSCs are adult stem cells that could be isolated from various sources, mostly bone marrow. Compared to embryonic stem cells, the advantages of using MSCs for cell therapy and regenerative medicine include: (1) they could be isolated from the patients themselves to avoid the possible immunological rejections induced by stem cell implantation; (2) they tend to differentiate into various types of cells, such as osteoblasts, adipocytes, and chondroblasts, which could be used for fabricating biomaterials or artificial organs; (3) they are easy to culture and expand *in vitro* thus mass production for clinical uses could be easily reached in very low cost and effort. Transplanting MSCs harboring therapeutic gene or drug into the injured area has been a promising novel therapeutic method for various traditionally incurable degenerative diseases by utilizing the self-renewing ability and multiple differentiating potencies of MSCs. This has become a basic principle of applying MSCs in the field of regenerative cell therapy. Moreover, the use of non-viral carrier or nanomaterial to deliver therapeutic molecules would circumvent the moral and controversial issues associated with viral carriers. However, relatively low delivery efficiency of non-viral carrier for

therapeutic substances into MSCs has limited this practical application of MSCs [157]. This quests the multifunctional carrier with high affinity to MSCs by conjugating with a binding agent of MSCs. Therefore, it is necessary to identify the binding motif with high affinity binding to MSCs in order to facilitate the systemic delivery of therapeutic substances into MSCs.

Phage display is the high throughout selection technique applied in this work to identify specific rat mesenchymal stem cell binding peptides. Usually, a randomly phage-displayed peptide library (up to $10^9$ diversity) is panned against targets for several rounds. By washing out non-bound phages and amplifying eluted bound phages as a new library for subsequent rounds, peptide sequences with higher binding affinity than others can be picked out. In this work, 78 sequences were selected and analyzed after 4 rounds of phage selection against rat MSCs by a bioinformatics tool RELIC. It resulted in peptide HMGMTK defined as rMSCs-binding peptide, which is further confirmed by fluorescent imaging. The peptide HMGMTK showed higher binding affinity to MSCs compared to that of scrambled peptide, and phage harboring the same sequences could competitively inhibit this favorable binding. These results suggested that HMGMTK is a MSC binding motif with higher affinity, by which we may be able to increase the non-viral gene delivery efficiency to MSCs.

In order to prove our hypothesis, we integrate MSC-binding peptide HMGMTK into a non-viral gene vector, LPD system, to deliver a model EGFP gene and then evaluated the transfection efficiency as well as the cytotoxicity. The percentage of cells that express GFP genes obtained from FACS technique is our criteria for evaluating the gene transfection efficiency of vectors. The results proved that peptide HMGMTK

could enhance the liposome-mediated gene delivery to rMSCs. Transfection efficiency of LPD+PA complex to rat mesenchymal stem cells was ~13%, a more than doubling that of LPD particles only without any peptides (~4%), and widely used commercial liposome vector Lipofectamine$^{TM}$ (~6%). (Figure 4-8A) LPD+PA complex has even twice transfection level comparing to LPD+control peptide complex that does not recognize rMSCs. These above suggested that peptide HMGMTK could benefit liposome-mediated gene delivery into rMSCs, specifically. This is consistent to our expectation, as the rMSCs-recognizing property of peptide HMGMTK would make gene vector bearing them bind to rMSCs more favorably and thus increase gene transfection level.

For doubling the enhancement of gene transfer efficiency, we involved the nuclear localizing signal (NLS) motif into the liposome complex. Nuclear localization signal is the peptide DPKKKRKV derived from the simian virus 40 large tumor antigen, a binding mediator of the karyophilic protein and importin α[181]. The NLS peptide was found to play a vital role in achieving the high levels of gene expression and is sufficient to carry exogenous DNA through the nuclear membrane to the cell nucleus which is a major concern of gene delivery technologies[182]. Recent gene therapy research showed that three-fold reiterated NLS peptide (sequence DPKKKRKVDPKKKRKVDPKKKRKV) has the capability of enhancing non-viral gene delivery to MSCs[170]. Thus, we expect that involving this sequence into the system could further increase the transfection efficiency of LPD+PA vector. Our result confirmed this expectation. Integrating NLS motif into liposome complex together with rMSCs-binding peptide has highest transfection efficiency among all the liposome-

based vectors that we have tested. The optimum mass ratio of plasmid to peptide in LPD+PA+NLS is 1:6 at which the maximum transgenic level 19.43% was obtained. Its capability of enhancing gene delivery is also comparable to other common non-viral gene vectors such as polymer[183-186], inorganic nanoparticles[187, 188].

The cytotoxicity of targeting peptide-combined LPD complex remains low compared to Lipofectamine$^{TM}$ (Figure 4-9) and other common non-viral carriers[183, 184, 187]. The result proved that identified MSC-binding peptide HMGMTK is able to serve as a high-affinity binding motif of MSCs to improve the efficiency of systemic delivery of therapeutic gene or drug to MSCs. This finding pointed out that improving delivery efficiency of stem cell based systemic therapy could be one of the possible applications of rMSC binding peptide and also advanced the research of non-viral gene delivery to rMSCs.

Moreover, deeper research found the selected peptides showed higher similarity to the known ligands whose receptors are present on the rMSC surface than those absent ones, while peptide HMGMTK showed significantly high similarity to the N-terminal signaling region of CX3CL1, the ligand of CX3CR1 receptor present on rMSC. We believe that in addition to the higher binding affinity of the peptide HMGMTK, this peptide can benefit the systemic gene or drug delivery by acting as an agonist of CX3CR1 and activating the receptor mediated endocytosis. It has been believed that, in the normal physiological condition, a G-protein coupled receptor (GPCR) which normally has 7-transmembrane domains typically undergoes endocytosis after being activated by an agonist or ligand and initiating a signaling cascade[189]. This receptor-mediated endocytosis is responsible for regulating the density of a cell surface receptor

staying within a proper range. Two cell uptake pathways are involved in this ligand-induced receptor internalization: clathrin-mediated endocytosis[189] and cavelae-mediated endocytosis[190]. The cell uptake of various particles could be also mediated by this mechanism, such as virus, toxins, drugs, etc. A variety of nanoparticles and nanovehicles were reported to be uptaken by cells via receptor-mediated endocytosis [191-194].

### *4.4.1 Peptide HMGMTK may serve as CX3CL1-like ligand and bind to CX3CR1 which may narrow the putative binding site region of CX3CL1*

CX3CR1 is one of the GPCRs. The protein structure of chemokine domain of CX3CL1 has been solved by NMR and X-ray crystallography (Figure 4-10) [195, 196]. Further investigations have also been conducted to explore the detailed mechanism of binding interaction [195, 197-199], yet it is still not fully understood to date. The protein structure is different from common chemokines. It consists of a N-terminal chemokine domain whose structure is similar to common chemokine structure, a mucin-like stalk, a hydrophobic transmembrane domain and a cytoplasmic tail. It is well believed that the N-terminal region of chemokine is crucial for ligand-receptor binding by acting as a key signaling domain. Deletion and mutation in this region has been proved to result in interfering the signaling induction and sometimes the affinity interactions with their receptors [169, 200].

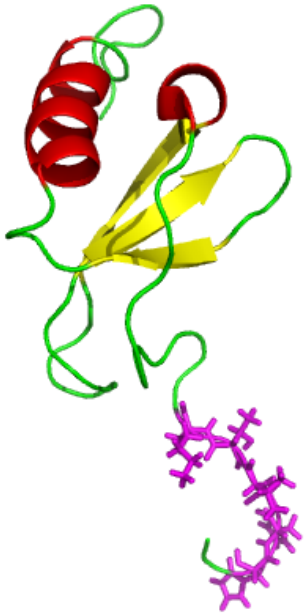


**Figure 4-10 The tertiary structure of chemokine domain of CX3CL1. It consists of a flexible N-terminal region three beta strands (in yellow), and a C-terminal helix (in red). The six amino acids showing highest similarity to peptide HMGMTK are marked in magenta.**

Although the distinctive mechanism of agonist-induced endocytosis for CX3CR1 is still unknown, unlike that for CCR5 and CXCR4[202], the fact that CX3CR1 may also mediate endocytosis is acceptable. Therefore, considering the analysis that the HMGMTK peptide showed the greatest similarity to the chemokine domain of CX3CL1, the unique ligand of CX3CR1, peptide HMGMTK may also be able to serve as an agonist of CX3CR1 to activate the receptor-mediated endocytosis. Therefore, we proposed that the higher affinity of identified peptide HMGMTK may be achieved via CX3CL1-CX3CR1 axis. Further experiments are undergoing to prove this hypothesis. On the other hand, this identification and matching result may also define the exact binding site of CX3CL1. It is possible that HLGMTK motif in the N-terminus contribute most to the binding affinity of CX3CL1, similar to RFFRESH motif in

CXCL12 [203]. This 6 amino acid sequence may be also responsible for the chemokine functions, such as cell migration and adhesion. H(L/M)GMTK may be another global cell adhesion motif next to RGD motif found in fibronectin [204]. It may be the key region for the potential functions of CX3CL1 including cell proliferation, differentiation and bone formation of MSCs.

### *4.4.2 MSC binding peptide HMGMTK may serve as a binding motif and agonist of CX3CR1 for facilitating the systemic delivery of gene or drug to MSCs via receptor mediated endocytosis and improving the use of MSCs in the field of cell therapy and regenerative medicine*

Besides the potential contribution to proteomics and cell studies, peptide HMGMTK may be able to serve as a high-affinity binding motif of MSCs to improve the efficiency of systemic delivery of therapeutic gene or drug to MSCs. Transplanting MSCs harboring therapeutic gene or drug into the injured area has been a promising novel therapeutic method for various traditionally incurable degenerative diseases by utilizing the self-renewing ability and multiple differentiating potency of MSCs. This has become a basic principle of using MSCs in the field of regenerative cell therapy. Moreover, the use of non-viral carrier or nanomaterial to deliver therapeutic molecules would circumvent the moral and controversial issues associated with viral carriers. However, relatively low delivery efficiency of non-viral carrier for therapeutic substances into MSCs has limited this practical application of MSCs [157]. This quests the multifunctional carrier with high affinity to MSCs by conjugating with a binding agent of MSCs. Therefore, it is necessary to identify the binding motif with high affinity

binding to MSCs in order to facilitate the systemic delivery of therapeutic substances into MSCs. The peptide HMGMTK identified in this work showed higher binding affinity to MSCs than that of scrambled peptide, and phage harboring the same sequences could competitively inhibit this favorable binding. These results suggested that HMGMTK is one of the MSC binding motifs, which could increase the delivery efficiency contributed by higher binding affinity.

However, there is another scenario besides higher binding affinity that may benefit the systemic gene or drug delivery: peptide HMGMTK may act as an agonist of CX3CR1 and activate the receptor mediated endocytosis. It has been believed that, in the normal physiological condition a G-protein coupled receptor (GPCR) which normally has 7-transmembrane domains typically undergoes endocytosis after being activated by an agonist or ligand and initiatings a signaling cascade[189]. This receptor endocytosis is responsible for regulating the density of a cell surface receptor staying within a proper range. Two cell uptake pathways are involved in this ligand-induced receptor internalization: clathrin-mediated endocytosis[189] and cavelae-mediated endocytosis[190]. The cell uptake of various particles could be also mediated by this mechanism, such as virus, toxins, drugs, etc. A variety of nanoparticles and nanovehicles were reported to be uptake by cells via receptor mediated endocytosis [191-194]. CX3CR1 is one of the GPCRs. Although the distinctive mechanism of agonist-induced endocytosis for CX3CR1 is still unknown, unlike that for CCR5 and CXCR4[202], the fact that CX3CR1 may also mediate endocytosis is acceptable. Therefore, considering the analysis result that the HMGMTK peptide showed the greatest similarity to the chemokine domain of CX3CL1, the unique ligand of CX3CR1,

and thus may possibly associate with CX3CR1, peptide HMGMTK may also be able to serve as an agonist of CX3CR1 to activate the receptor-mediated endocytosis. This potential property of peptide HMGMTK may facilitate the cell entry of a particle having this peptide to deliver the therapeutic gene or drug.

## 4.5 Conclusion

Peptide HMGMTK was identified as MSC binding peptide through phage display-based affinity selection. A LPD complex was constructed with this peptide and NLS peptide as an effective MSC gene delivery vector. Fluorescence imaging results proved the MSC targeting property of selected peptide. High similarity between peptide HMGMTK and signaling region of CX3CL1 was found by bioinformatics analysis. CX3CL1 is one of a chemokine whose receptor CX3CR1 existed on MSC surface. This may suggest a possible mechanism that could explain the MSC homing effect of the selected peptide. Later on, we built up a multifunctional complex as an effective MSC gene delivery vector by combining LPD, selected MSC peptide and NLS peptide. The transfection mediated by the resultant complex LPD+PA+NLS showed higher efficiency and specificity compared to those achieved by LPD only, LPD with control peptide, or LPD with PA only. Meanwhile, MTT results supported the low cytotoxicity of LPD+PA+NLS complex. All together, a conclusion could be draw that a novel rMSC binding peptide with sequence HMGTMK was identified and could be used to build up a promising gene carrier for facilitating liposome-mediated MSC gene delivery as shown in Figure 4-1.

# Chapter 5: Summary of Results and Future Directions

## 5.1 Summary of results

The filamentous shape of bacteriophages in nanorange and its programmable surface chemistry make it a great template for phage-based material synthesis and assembly. These phage-based materials have many applications including tissue engineering, drug and/or gene delivery, cancer treatment, bioimaging, etc. In previous chapters, the use of bacteriophage as template for nanosynthesis and the applications of tissue engineering and drug/gene delivery are discussed.

Chapter 2 demonstrates the hydroxyapatite crystals can be nucleated on self-assembled bacteriophages in a preferred c-axis orientation. The resultant bacteriophage may serve as the building block to substitute collagen and form bone implant. It has a great potential in the field of tissue engineering. This work also proved that the driving force of phage self-assembly is beta sheet secondary structure and beta sheet between phage bundles can induce the orientated nucleation of hydroxyapatite crystals. The beta sheet formation can be used as a general method to precisely control assemblies between engineerable biomaterials. In natural bone, HAP crystals are nucleated and grown with their c-axis preferentially parallel to collagen fibrils. In the work of Chapter 2, we also found that HAP crystals were also nucleated on EQ bundles with their c-axis preferentially parallel to phage bundles, which greatly mimicked the base level of hierarchical structure of natural bone. We further found that calcium ions were attracted to the glutamic acids and aspartic acids of peptide E and Q with a pattern matching with calcium ions on the (001) plane of HAP crystals. This specific matching then induced the HAP nucleation on the beta sheet and the growth along the c-axis. This work

provided the proof for a new way of fabricating bone biomaterials by biomimicking and bioinspiration.

Bacteriophage-gold nanocomposite was constructed in the work of Chapter 3 to use as a model to study the optimum condition for best TEM imaging of bioinorganic nanohybrids. In this work, wild type M13 phage was combined with gold nanoparticles to form phage-gold nanocomposite. Most Au-NPs were aligned into large belts, forming a net-like structure. TEM imaging of negatively stained bioinorganic nanohybrids is a simple way to characterize these nanostructures that may have biomedical functions. By studying the effects of different factors on the negative staining of phage-gold nanocomposites, we found that the optimum staining conditions for these bioinorganic nanohybrids are using 0.5% UA solution with pH 4.5, staining for 10 seconds, and rapidly drying the stains. This work demonstrates that each staining factor has an influence to the final appearance of stained specimens and optimum staining condition needs to be customized to the individual type of bioinorganic nanohybrids. The effects of each staining factor and a general guideline for selecting staining condition were provided in this work. Therefore, this research provides useful information for the characterization of bioinorganic nanomaterials by TEM imaging. It will help the research in the field of nanomaterials and bionanotechnology.

Different from Chapter 2 and Chapter 3, Chapter 4 is about identifying target-specific motif by affinity selection based on phage display technique to improve transfection efficiency and specificity of gene or drug delivery. In this work, we did cell panning on primary mesenchymal stem cells and identified peptide HMGMTK as MSC binding peptide. Further bioinformatics analysis suggests that peptide HMGMTK has

high similarity to the signaling regions of chemokine CX3CL1. This may suggest a possible mechanism that could explain the MSC homing effect of the selected peptide. We then constructed a novel and effective mesenchymal stem cell gene delivery vector by liposome/protamine/DNA complex incorporating with identified MSC-targeting motif and Nuclear localized signal (NLS) motif. Through several evaluations, we proved that this resultant complex is multifunctional, effective, but low-cytotoxic MSC gene delivery vector. The transfection mediated by the resultant complex LPD+PA+NLS showed higher efficiency and specificity compared to those achieved by LPD only, LPD with control peptide, or LPD with PA only. Meanwhile, MTT results supported the low cytotoxicity of LPD+PA+NLS complex. Based on all the results, we can conclude that a novel rMSC binding peptide HMGMTK was identified and could be used to build up a promising gene carrier for facilitating liposome-mediated MSC gene delivery.

## 5.2 Outlook and future directions

### *5.2.1 Tissue engineering for bone regeneration*

An ideal bone material should have osteoconductivity, osteogenity, and osteoinductivity. It should have great mechanical properties to serve as a scaffold of resultant bone material. It should have appropriate surface to promote cell attachment, differentiation, and proliferation. It should also be able to stimulate HAP nucleation and oriented growht. Hydroxyapaptite by itself is a great bioceramic for fabricating bone materials due to its excellent biocompartibility and the ability to enhance cell adhesion and proliferation. However, it lacks osteoinductivity to initiate crystal nucleation.

Introducing HAP nucleating peptides by phage display is the key I used in the work of Chapter 2 to fix this problem. Chapter 2 describe genetically engineered phages with HAP nucleating peptides displayed on the surface can form bundles as a bone scaffold and nucleate hydroxyapatite to form bioactive composite materials for cell adhesion and proliferation. The following work can be done to further dig the findings: (1) Cell culture test and characterization to examine the ability of the genetically engineered phage scaffold to enhance cell adhesion and proliferation. I may coat a film of genetically engineered phage scaffold onto the cell culture plate and culture mesenchymal stem cell to see how the cells response to the phage scaffolds. In vivo animal test can be expected if ex vivo cell culture test is successful. (2) One of the advantages of phage as bone scaffold is their tunable surface chemistry by genetic modifications. This may offer more promising directions of using phages in the study of tissue engineering.

### *5.2.2 Proteomic analysis (Ligand-receptor/Antibody-antigen interaction)*

Chapter 4 describes how to take advantage of phage display technique to identify a targeting motif that can specifically bind to live cells and give a promising method for proteomic studies on cells. Phage display has many advantages for studying proteomics: (1) no pre-knowledge of the target is needed to study the binding proteins to the target. This is a great way to predict new interacting proteins since other common methods can only confirm the proposed interaction. (2) The identified binding peptides can provide insight of the precise binding site to the targets due to the much smaller size of identified peptides selected by phage display than other traditional affinity selection

methods. (3) Phage display biopanning is time and cost-effective. The experimental procedure of affinity selection by phage display just needs several weeks to finish and the results can be analyzed by bioinformatics software such as RELIC.

In the work stated in Chapter 4, the identified MSC-binding motif HMGMTK was found to have great similarity to the chemokine domain of CX3CL1, the unique binding ligand of CX3CR1. This matching result may define the exact binding site of CX3CL1. It is possible that HLGMTK motif in the N-terminus contribute most to the binding affinity of CX3CL1, similar to RFFRESH motif in CXCL12 [203]. Therefore, we proposed that the higher affinity of identified peptide HMGMTK may be achieved via CX3CL1-CX3CR1 axis. Further experiments need to do to prove this hypothesis. The work in Chapter 4 describes a reasonable way for studying protein-protein interactions is to use the potential binding sites identified from biopanning process to narrow the target binding domains and direct practical experiments.

### *5.2.3 Customized diagnosis and targeted therapy*

Biomedical researchers are continuously pursuing a more efficient and reliable therapeutic delivery. An ideal carrier (1) should be able to efficiently deliver the therapeutic materials (genes or drugs) into the target cell, (2) should be protective to the gene inside and biocompatible so that it will not cause cytotoxicity, or most importantly, (3) should be target-specific like a “magic bullet” that will only transfect into specific target cells without harming neighbouring healthy areas. It is noteworthy that the targeting ability is a requirement for these applications since human disease is often

associated with protein expression profile abnormalities. Currently, it has been commonly accepted that the efficiency and specificity of delivery vehicles can be increased by coupling specific targeting ligands with them. Therefore, as an efficient target-binder identification system, phage display can facilitate the systematic delivery by identifying novel targeting motifs which can incorporate into the delivery vehicles.

Chapter 4 shows an example of incorporating a novel targeting motif into delivery vectors to improve gene delivery efficiency and specificity. The multifunctional gene vector built in this work has been proved to have higher efficiency and specificity than regular vectors such as commercially available lipofectomine. This provides a promising vector for customized therapy by mesenchymal stem cell. Future works that can be done to prove it include: (1) In vivo animal test can be expected to check the transfection efficiency of the vector to the target organ or tissue. (2) I will then obtain human mesenchymal stem cells and use the method in the work of Chapter 4 to identify a targeting motif to human mesenchymal stem cells which can be incorporate into the delivery system to build an efficient and specific vector of human MSCs.

# Chapter 6: References


1. Smith, G., *Filamentous fusion phage: novel expression vectors that display cloned antigens on the virion surface.* Science, 1985. **228**(4705): p. 1315-1317.

2. Marvin, D.A., et al., *Molecular-Models and Structural Comparisons of Native and Mutant Class-I Filamentous Bacteriophages Ff (Fd, F1, M13), If1 and Ike.* Journal of Molecular Biology, 1994. **235**(1): p. 260-286.

3. Riechmann, L. and P. Holliger, *The C-Terminal Domain of TolA Is the Coreceptor for Filamentous Phage Infection of E. coli.* Cell, 1997. **90**(2): p. 351-360.

4. Hufton, S.E., et al., *Phage display of cDNA repertoires: the pVI display system and its applications for the selection of immunogenic ligands.* Journal of Immunological Methods, 1999. **231**(1-2): p. 39-51.

5. Gao, C., et al., *Making artificial antibodies: A format for phage display of combinatorial heterodimeric arrays.* Proceedings of the National Academy of Sciences of the United States of America, 1999. **96**(11): p. 6025-6030.

6. Gao, C., et al., *A method for the generation of combinatorial antibody libraries using pIX phage display.* Proceedings of the National Academy of Sciences of the United States of America, 2002. **99**(20): p. 12612-12616.

7. Fuh, G. and S.S. Sidhu, *Efficient phage display of polypeptides fused to the carboxy-terminus of the M13 gene-3 minor coat protein.* FEBS Letters, 2000. **480**(2-3): p. 231-234.

8. Weiss, G.A. and S.S. Sidhu, *Design and evolution of artificial M13 coat proteins.* Journal of Molecular Biology, 2000. **300**(1): p. 213-219.

9. Mao, C., A. Liu, and B. Cao, *Virus-Based Chemical and Biological Sensing.* Angewandte Chemie (International ed. in English), 2009. **48**(37): p. 6790-6810.

10. Smith, G.P. and V.A. Petrenko, *Phage display.* Chemical Reviews, 1997. **97**(2): p. 391-410.

11. Kehoe, J.W. and B.K. Kay, *Filamentous Phage Display in the New Millennium.* Chemical Reviews, 2005. **105**(11): p. 4056-4072.

12. McCafferty, J., et al., *Phage antibodies: filamentous phage displaying antibody variable domains.* Nature, 1990. **348**(6301): p. 552-554.

13. Smith, G.P., *Surface presentation of protein epitopes using bacteriophage expression systems.* Current Opinion in Biotechnology, 1991. **2**(5): p. 668-673.

14. Smith, G.P. and J.K. Scott, *Libraries of peptides and proteins displayed on filamentous phage.* Methods Enzymol., 1993. **217**: p. 228-257.

15. Chu, C.-T., et al., *Hydroxylamine mutagenesis of HSV DNA and DNA fragments: Introduction of mutations into selected regions of the viral genome.* Virology, 1979. **98**(1): p. 168-181.

16. Kadonaga, J.T. and J.R. Knowles, *A simple and efficient method for chemical mutagenesis of DNA.* Nucleic Acids Research, 1985. **13**(5): p. 1733-1745.

17. Zakour, R.A. and L.A. Loeb, *Site-specific mutagenesis by error-directed DNA synthesis.* Nature, 1982. **295**(5851): p. 708-710.

18. Cadwell, R.C. and G.F. Joyce, *Randomization of genes by PCR mutagenesis.* Genome Research, 1992. **2**(1): p. 28-33.

19. Waterhouse, P., et al., *Combinatorial infection and in vivo recombination: a strategy for making large phage antibody repertoires.* Nucleic Acids Research, 1993. **21**(9): p. 2265-2266.

20. Sblattero, D. and A. Bradbury, *Exploiting recombination in single bacteria to make large phage antibody libraries.* Nat Biotech, 2000. **18**(1): p. 75-80.

21. Pasqualini, R. and E. Ruoslahti, *Organ targeting In vivo using phage display peptide libraries.* Nature, 1996. **380**(6572): p. 364-366.

22. Kay, B.K., J. Winter, and J. McCafferty, *Phage Display of Peptides and Proteins: a laboratory manual.* 1996.

23. Clackson, T. and H. Lowman, *Phage display: a practical approach*. 2004: Oxford University Press, USA.

24. Brigati, J.R., et al., *Phage Display for Generating Peptide Reagents*. Current Protocols in Protein Science. 2001: John Wiley & Sons, Inc.

25. Shadidi, M. and M. Sioud, *Selection of Peptides for Specific Delivery of Oligonucleotides Into Cancer Cells*, in *Ribozymes and siRNA Protocols*, M. Sioud, Editor. 2004, Humana Press. p. 569-580.

26. Tonikian, R., et al., *Identifying specificity profiles for peptide recognition modules from phage-displayed peptide libraries.* Nat. Protocols, 2007. **2**(6): p. 1368-1386.

27. McGuire, M.J., S. Li, and K.C. Brown, *Biopanning of Phage Displayed Peptide Libraries for the Isolation of Cell-Specific Ligands*, in *Biosensors and Biodetection*, A. Rasooly and K.E. Herold, Editors. 2009, Humana Press. p. 291-321.

28. Shadidi, M. and M. Sioud, *Selective targeting of cancer cells using synthetic peptides.* Drug Resistance Updates, 2003. **6**(6): p. 363-371.

29. Craig, R. and S. Li, *Function and Molecular Mechanism of Tumor-Targeted Peptides for Delivering Therapeutic Genes and Chemical Drugs.* Mini Reviews in Medicinal Chemistry, 2006. **6**: p. 757-764.

30. Krumpe, L. and T. Mori, *The Use of Phage-Displayed Peptide Libraries to Develop Tumor-Targeting Drugs.* International Journal of Peptide Research and Therapeutics, 2006. **12**(1): p. 79-91.

31. Rezler, E.M., et al., *Peptide-Mediated Targeting of Liposomes to Tumor Cells*, in *Peptide Characterization and Application Protocols*, G.B. Fields, Editor. 2007, Humana Press. p. 269-298.

32. Krag, D.N., et al., *Selection of Tumor-binding Ligands in Cancer Patients with Phage Display Libraries.* Cancer Research, 2006. **66**(15): p. 7724-7733.

33. Staquicini, F.I., et al., *Discovery of a functional protein complex of netrin-4, laminin γ1 chain, and integrin α6β1 in mouse neural stem cells.* Proceedings of the National Academy of Sciences, 2009. **106**(8): p. 2903-2908.

34. Wu, X., et al., *Identification and characterization of a novel peptide ligand of Tie2 for targeting gene therapy.* Acta Biochimica et Biophysica Sinica, 2008. **40**(3): p. 217-225.

35. SHADIDI, M. and M. SIOUD, *Identification of novel carrier peptides for the specific delivery of therapeutics into cancer cells.* The FASEB Journal, 2003. **17**(2): p. 256-258.

36. Abbineni, G., et al., *Evolutionary Selection of New Breast Cancer Cell-Targeting Peptides and Phages with the Cell-Targeting Peptides Fully Displayed on the Major*

*Coat and Their Effects on Actin Dynamics during Cell Internalization.* Molecular Pharmaceutics, 2010. **7**(5): p. 1629-1642.

37. Wang, T., et al., *Enhanced binding and killing of target tumor cells by drug-loaded liposomes modified with tumor-specific phage fusion coat protein.* Nanomedicine, 2010. **5**(4): p. 563-574.

38. Zhang, J., H. Spring, and M. Schwab, *Neuroblastoma tumor cell-binding peptides identified through random peptide phage display.* Cancer Letters, 2001. **171**(2): p. 153-164.

39. Hong, F.D. and G.L. Clayman, *Isolation of a Peptide for Targeted Drug Delivery into Human Head and Neck Solid Tumors.* Cancer Research, 2000. **60**(23): p. 6551-6556.

40. Matsuo, A., et al., *A novel melanoma-targeting peptide screened by phage display exhibits antitumor activity.* Journal of Molecular Medicine, 2010. **88**(12): p. 1255-1264.

41. De Angelis, F., et al., *Water soluble nanoporous nanoparticle for in vivo targeted drug delivery and controlled release in B cells tumor context.* Nanoscale, 2010. **2**(10): p. 2230-2236.

42. Kelly, K.A., et al., *Targeted Nanoparticles for Imaging Incipient Pancreatic Ductal Adenocarcinoma.* PLoS Med, 2008. **5**(4): p. e85.

43. Li, M., et al., *Affinity Peptide for Targeted Detection of Dysplasia in Barrett's Esophagus.* Gastroenterology, 2010. **139**(5): p. 1472-1480.

44. Jayanna, P.K., et al., *Landscape phage ligands for PC3 prostate carcinoma cells.* Protein Engineering Design and Selection, 2010. **23**(6): p. 423-430.

45. Zang, L., et al., *Screening and Identification of a peptide specifically targeted to NCI-H1299 from a phage display peptide library.* Cancer Letters, 2009. **281**(1): p. 64-70.

46. Chang, D.-K., et al., *A Novel Peptide Enhances Therapeutic Efficacy of Liposomal Anti-Cancer Drugs in Mice Models of Human Lung Cancer.* PLoS ONE, 2009. **4**(1): p. e4171.

47. Ho, I.A.W., K.M. Hui, and P.Y.P. Lam, *Isolation of peptide ligands that interact specifically with human glioma cells.* Peptides, 2010. **31**(4): p. 644-650.

48. Wu, C., et al., *A peptide-based carrier for intracellular delivery of proteins into malignant glial cells in vitro.* Journal of Controlled Release, 2008. **130**(2): p. 140-145.

49. Böckmann, M., M. Drosten, and B.M. Pützer, *Discovery of targeting peptides for selective therapy of medullary thyroid carcinoma.* The Journal of Gene Medicine, 2005. **7**(2): p. 179-188.

50. Lee, T.-Y., et al., *A Novel Peptide Specifically Binding to Nasopharyngeal Carcinoma For Targeted Drug Delivery.* Cancer Research, 2004. **64**(21): p. 8002-8008.

51. Zhi, M., et al., *Characterization of a specific phage-displayed Peptide binding to vasculature of human gastric cancer.* Cancer biology & therapy, 2004. **3**(12): p. 1232.

52. Jost, P.J., et al., *A novel peptide, THALWHT, for the targeting of human airway epithelia.* FEBS Letters, 2001. **489**(2-3): p. 263-269.

53. Writer, M.J., et al., *Targeted Gene Delivery to Human Airway Epithelial Cells with Synthetic Vectors Incorporating Novel Targeting Peptides Selected by Phage Display.* Journal of Drug Targeting, 2004. **12**(4): p. 185-193.

54. Ivanenkov, V.V., F. Felici, and A.G. Menon, *Targeted delivery of multivalent phage display vectors into mammalian cells.* Biochimica et Biophysica Acta (BBA) - Molecular Cell Research, 1999. **1448**(3): p. 463-472.

55. Guo, Y., et al., *Identification of Peptides Inhibiting Adhesion of Monocytes to the Injured Vascular Endothelial Cells through Phage-displaying Screening.* Acta Biochimica et Biophysica Sinica, 2005. **37**(4): p. 227-233.

56. Giordano, R.J., et al., *Targeted Induction of Lung Endothelial Cell Apoptosis Causes Emphysema-like Changes in the Mouse.* Journal of Biological Chemistry, 2008. **283**(43): p. 29447-29460.

57. Veleva, A.N., S.L. Cooper, and C. Patterson, *Selection and initial characterization of novel peptide ligands that bind specifically to human blood outgrowth endothelial cells.* Biotechnology and Bioengineering, 2007. **98**(1): p. 306-312.

58. Nicklin, S., et al., *Efficient and selective AAV2-mediated gene transfer directed to human vascular endothelial cells.* Molecular Therapy, 2001. **4**(3): p. 174-181.

59. Michon, I.N., et al., *Targeting of peptides to restenotic vascular smooth muscle cells using phage display in vitro and in vivo.* Biochimica et Biophysica Acta (BBA) - Molecular Cell Research, 2002. **1591**(1-3): p. 87-97.

60. Work, L.M., et al., *Development of Efficient Viral Vectors Selective for Vascular Smooth Muscle Cells.* Mol Ther, 2004. **9**(2): p. 198-208.

61. Samoylov, A., et al., *Recognition of cell-specific binding of phage display derived peptides using an acoustic wave sensor.* Biomolecular Engineering, 2002. **18**(6): p. 269-272.

62. McGuire, M.J., et al., *In vitro Selection of a Peptide with High Selectivity for Cardiomyocytes In vivo.* Journal of Molecular Biology, 2004. **342**(1): p. 171-182.

63. Nicol, C.G., et al., *Use of in vivo phage display to engineer novel adenoviruses for targeted delivery to the cardiac vasculature.* FEBS Letters, 2009. **583**(12): p. 2100-2107.

64. Thapa, N., et al., *Identification of a peptide ligand recognizing dysfunctional endothelial cells for targeting atherosclerosis.* Journal of Controlled Release, 2008. **131**(1): p. 27-33.

65. Zhao, W., et al., *Isolation and Initial Application of a Novel Peptide That Specifically Recognizes the Neural Stem Cells Derived from Rhesus Monkey Embryonic Stem Cells.* Journal of Biomolecular Screening, 2010. **15**(6): p. 687-694.

66. Zhao, S., W. Zhao, and L. Ma, *Novel peptide ligands that bind specifically to mouse embryonic stem cells.* Peptides, 2010. **31**(11): p. 2027-2034.

67. Lu, S., et al., *Targeting of Embryonic Stem Cells by Peptide-Conjugated Quantum Dots.* PLoS ONE, 2010. **5**(8): p. e12075.

68. Chamarthy, S.P., et al., *Gene delivery to dendritic cells facilitated by a tumor necrosis factor alpha-competing peptide.* Molecular Immunology, 2004. **41**(8): p. 741-749.

69. Curiel, T.J., et al., *Peptides Identified through Phage Display Direct Immunogenic Antigen to Dendritic Cells.* The Journal of Immunology, 2004. **172**(12): p. 7425-7431.

70. Samoylova, T.I., et al., *Phage probes for malignant glial cells.* Molecular Cancer Therapeutics, 2003. **2**(11): p. 1129-1137.

71. Samoylova, T.I., et al., *Targeting peptides for microglia identified via phage display.* Journal of Neuroimmunology, 2002. **127**(1-2): p. 13-21.

72. Barry, M.A., W.J. Dower, and S.A. Johnston, *Toward cell-targeting gene therapy vectors: Selection of cell-binding peptides from random peptide-presenting phage libraries.* Nat Med, 1996. **2**(3): p. 299-305.

73. Klingelhöfer, J., et al., *Epidermal growth factor receptor ligands as new extracellular targets for the metastasis-promoting S100A4 protein.* FEBS Journal, 2009. **276**(20): p. 5936-5948.

74. Rasmussen, U.B., et al., *Tumor cell-targeting by phage-displayed peptides.* Cancer Gene Ther, 2002. **9**(7): p. 606-612.

75. Kim, S.-H., et al., *The M Cell-Targeting Ligand Promotes Antigen Delivery and Induces Antigen-Specific Immune Responses in Mucosal Vaccination.* The Journal of Immunology, 2010. **185**(10): p. 5787-5795.

76. Yoo, M.-K., et al., *Targeted delivery of chitosan nanoparticles to Peyer's patch using M cell-homing peptide selected by phage display technique.* Biomaterials, 2010. **31**(30): p. 7738-7747.

77. Fievez, V., et al., *In vitro identification of targeting ligands of human M cells by phage display.* International Journal of Pharmaceutics, 2010. **394**(1-2): p. 35-42.

78. EDA, K., S. EDA, and I.W. SHERMAN, *IDENTIFICATION OF PEPTIDES TARGETING THE SURFACE OF PLASMODIUM FALCIPARUM-INFECTED ERYTHROCYTES USING A PHAGE DISPLAY PEPTIDE LIBRARY.* Am J Trop Med Hyg, 2004. **71**(2): p. 190-195.

79. McGuire, M.J., et al., *A Library-Selected, Langerhans Cell-Targeting Peptide Enhances an Immune Response.* DNA & Cell Biology, 2004. **23**(11): p. 742-752.

80. Robinson, P., et al., *Identification using phage display of peptides promoting targeting and internalization into HPV-transformed cell lines.* Journal of Molecular Recognition, 2005. **18**(2): p. 175-182.

81. Eidne, K.A., C.C. Henery, and R.J. Aitken, *Selection of Peptides Targeting the Human Sperm Surface Using Random Peptide Phage Display Identify Ligands Homologous to ZP3.* Biology of Reproduction, 2000. **63**(5): p. 1396-1402.

82. Maruta*, F., et al., *Use of a Phage Display Library to Identify Oligopeptides Binding to the Lumenal Surface of Polarized Endothelium by Ex Vivo Perfusion of Human Umbilical Veins.* Journal of Drug Targeting, 2003. **11**(1): p. 53-59.

83. Mi, Z., et al., *Identification of a Synovial Fibroblast-specific Protein Transduction Domain for Delivery of Apoptotic Agents to Hyperplastic Synovium.* Mol Ther, 2003. **8**(2): p. 295-305.

84. Mummert, M.E., et al., *Development of a Peptide Inhibitor of Hyaluronan-Mediated Leukocyte Trafficking.* The Journal of Experimental Medicine, 2000. **192**(6): p. 769-780.

85. Böckmann, M., et al., *Novel SRESPHP Peptide Mediates Specific Binding to Primary Medullary Thyroid Carcinoma After Systemic Injection.* Human Gene Therapy, 2005. **16**(11): p. 1267-1275.

86. Whitney, M., et al., *Parallel in Vivo and in Vitro Selection Using Phage Display Identifies Protease-dependent Tumor-targeting Peptides.* Journal of Biological Chemistry, 2010. **285**(29): p. 22532-22541.

87. Samli, K.N., et al., *Peptide-Mediated Targeting of the Islets of Langerhans.* Diabetes, 2005. **54**(7): p. 2103-2108.

88. Teesalu, T., et al., *C-end rule peptides mediate neuropilin-1-dependent cell, vascular, and tissue penetration.* Proceedings of the National Academy of Sciences, 2009. **106**(38): p. 16157-16162.

89. Hong, H.-Y., et al., *Detection of apoptosis in a rat model of focal cerebral ischemia using a homing peptide selected from in vivo phage display.* Journal of Controlled Release, 2008. **131**(3): p. 167-172.

90. Chang, D.-K., et al., *Antiangiogenic Targeting Liposomes Increase Therapeutic Efficacy for Solid Tumors.* Journal of Biological Chemistry, 2009. **284**(19): p. 12905-12916.

91. Joyce, J.A., et al., *Stage-specific vascular markers revealed by phage display in a mouse model of pancreatic islet tumorigenesis.* Cancer Cell, 2003. **4**(5): p. 393-403.

92. Schluesener, H.J. and T. Xianglin, *Selection of recombinant phages binding to pathological endothelial and tumor cells of rat glioblastoma by in-vivo display.* Journal of the Neurological Sciences, 2004. **224**(1-2): p. 77-82.

93. Rajotte, D., et al., *Molecular heterogeneity of the vascular endothelium revealed by in vivo phage display.* Journal of Clinical Investigation, 1998. **102**(2): p. 430.

94. Kolonin, M., R. Pasqualini, and W. Arap, *Teratogenicity induced by targeting a placental immunoglobulin transporter.* Proceedings of the National Academy of Sciences of the United States of America, 2002. **99**(20): p. 13055.

95. Chen, Y., et al., *Transdermal protein delivery by a coadministered peptide identified via phage display.* Nat Biotech, 2006. **24**(4): p. 455-460.

96. Denby, L., et al., *Development of Renal-targeted Vectors Through Combined In Vivo Phage Display and Capsid Engineering of Adenoviral Fibers From Serotype 19p.* Mol Ther, 2007. **15**(9): p. 1647-1654.

97. Duerr, D.M., S.J. White, and H.J. Schluesener, *Identification of peptide sequences that induce the transport of phage across the gastrointestinal mucosal barrier.* Journal of Virological Methods, 2004. **116**(2): p. 177-180.

98. Kang, S.K., et al., *Identification of a peptide sequence that improves transport of macromolecules across the intestinal mucosal barrier targeting goblet cells.* Journal of Biotechnology, 2008. **135**(2): p. 210-216.

99. Kelly, K., et al., *In Vivo Phage Display Selection Yields Atherosclerotic Plaque Targeted Peptides for Imaging.* Molecular Imaging and Biology, 2006. **8**(4): p. 201-207.

100. Lee, L., et al., *Identification of synovium-specific homing peptides by in vivo phage display selection.* Arthritis & Rheumatism, 2002. **46**(8): p. 2109-2120.

101. Liu, C., et al., *In Vivo Interrogation of the Molecular Display of Atherosclerotic Lesion Surfaces.* Am J Pathol, 2003. **163**(5): p. 1859-1871.

102. Yao, V.J., et al., *Targeting Pancreatic Islets with Phage Display Assisted by Laser Pressure Catapult Microdissection.* Am J Pathol, 2005. **166**(2): p. 625-636.

103. Yamane, K. and S. Mizushima, *Introduction of basic amino acid residues after the signal peptide inhibits protein translocation across the cytoplasmic membrane of Escherichia coli. Relation to the orientation of membrane proteins.* Journal of Biological Chemistry, 1988. **263**(36): p. 19690-19696.

104. Andersson, H. and G. von Heijne, *A 30-residue-long "export initiation domain" adjacent to the signal sequence is critical for protein translocation across the inner membrane of Escherichia coli.* Proceedings of the National Academy of Sciences of the United States of America, 1991. **88**(21): p. 9751-9754.

105. Schuenemann, T.A., V.M. Delgado-Nixon, and R.E. Dalbey, *Direct Evidence That the Proton Motive Force Inhibits Membrane Translocation of Positively Charged Residues within Membrane Proteins.* Journal of Biological Chemistry, 1999. **274**(11): p. 6855-6864.

106. Rodi, D.J., A.S. Soares, and L. Makowski, *Quantitative Assessment of Peptide Sequence Diversity in M13 Combinatorial Peptide Phage Display Libraries.* Journal of Molecular Biology, 2002. **322**(5): p. 1039-1052.

107. McConnell, S., et al., *Construction and screening of M13 phage libraries displaying long random peptides.* Molecular Diversity, 1996. **1**(3): p. 165-176.

108. Varghese, R. and H.-A. Wagenknecht, *DNA as a supramolecular framework for the helical arrangements of chromophores: towards photoactive DNA-based nanomaterials.* Chemical Communications, 2009(19): p. 2615-2624.

109. Lazzari, M. and M.A. Lopez-Quintela, *Block Copolymers as a Tool for Nanomaterial Fabrication.* Advanced Materials, 2003. **15**(19): p. 1583-1594.

110. Merzlyak, A. and S.-W. Lee, *Phage as templates for hybrid materials and mediators for nanomaterial synthesis.* Current opinion in chemical biology, 2006. **10**(3): p. 246-252.

111. Mao, C.B., et al., *Virus-based toolkit for the directed synthesis of magnetic and semiconducting nanowires.* Science, 2004. **303**(5655): p. 213-217.

112. Kim, K., M. Kang, and E. Yi, *Applications of cell-based phage display panning to proteomic analysis.* Genes & Genomics, 2011. **33**(1): p. 9-15.

113. Schirrmann, T., et al., *Phage Display for the Generation of Antibodies for Proteome Research, Diagnostics and Therapy.* Molecules, 2011. **16**(1): p. 412-426.

114. Lee, S., J. Xie, and X. Chen, *Peptide-Based Probes for Targeted Molecular Imaging.* Biochemistry, 2010. **49**(7): p. 1364-1376.

115. Stefanidakis, M. and E. Koivunen, *Peptide-Mediated Delivery of Therapeutic and Imaging Agents Into Mammalian Cells.* Current Pharmaceutical Design, 2004. **10**(24): p. 3033-3044.

116. Petrenko, V., *Evolution of phage display: from bioactive peptides to bioselective nanomaterials.* Expert Opinion on Drug Delivery, 2008. **5**(8): p. 825-836.

117. Petrenko, V.A., *Landscape phage as a molecular recognition interface for detection devices.* Microelectronics Journal, 2008. **39**(2): p. 202-207.

118. Xu, H., et al., *Self-assembly and mineralization of genetically modifiable biological nanofibers driven by beta-structure formation.* Biomacromolecules, 2011. **12**(6): p. 2193-2199.

119. Cao, B., H. Xu, and C. Mao, *Phage as a Template to Grow Bone Mineral Nanocrystals.* Methods in molecular biology (Clifton, N.J.), 2014. **1108**: p. 123-135.

120. Price, P., D. Toroian, and J. Lim, *Mineralization by inhibitor exclusion: the calcification of collagen with fetuin.* J. Biol. Chem., 2009. **284**: p. 17092-17101.

121. Deshpande, A.S. and E. Beniash, *Bioinspired synthesis of mineralized collagen fibrils.* Crystal Growth & Design, 2008. **8**(8): p. 3084-3090.

122. Zhang, W., S.S. Liao, and F.Z. Cui, *Hierarchical Self-Assembly of Nano-Fibrils in Mineralized Collagen.* Chemistry of Materials, 2003. **15**(16): p. 3221-3226.

123. Nudelman, F., et al., *The role of collagen in bone apatite formation in the presence of hydroxyapatite nucleation inhibitors.* Nat Mater, 2010. **9**(12): p. 1004-1009.

124. He, T., et al., *Nanofibrous bio-inorganic hybrid structures formed through self-assembly and oriented mineralization of genetically engineered phage nanofibers.* Small, 2010. **6**: p. 2230-2235.

125. Wang, F.K., B.R. Cao, and C.B. Mao, *Bacteriophage Bundles with Prealigned Ca2+ Initiate the Oriented Nucleation and Growth of Hydroxylapatite.* Chemistry of Materials, 2010. **22**(12): p. 3630-3636.

126. He, G., et al., *Nucleation of apatite crystals in vitro by self-assembled dentin matrix protein, 1.* Nature Materials, 2003. **2**(8): p. 552-558.

127. George, A., et al., *Characterization of a Novel Dentin Matrix Acidic Phosphoprotein - Implications for Induction of Biomineralization.* Journal of Biological Chemistry, 1993. **268**(17): p. 12624-12630.

128. Berkowitz, S.A. and L.A. Day, *Mass, Length, Composition and Structure of Filamentous Bacterial Virus Fd.* Journal of Molecular Biology, 1976. **102**(3): p. 531-547.

129. Clack, B.A. and D.M. Gray, *A CD determination of the alpha-helix contents of the coat proteins of four filamentous bacteriophages: fd, IKe, Pf1, and Pf3.* Biopolymers, 1989. **28**(11): p. 1861-1873.

130. Whitmore, L. and B.A. Wallace, *Protein secondary structure analyses from circular dichroism spectroscopy: Methods and reference databases.* Biopolymers, 2008. **89**(5): p. 392-400.

131. Silverstone, L.M., et al., *Remineralization of Natural and Artificial Lesions in Human Dental Enamel Invitro - Effect of Calcium-Concentration of the Calcifying Fluid.* Caries Research, 1981. **15**(2): p. 138-144.

132. Nudelman, F., et al., *The role of collagen in bone apatite formation in the presence of hydroxyapatite nucleation inhibitors.* Nature Mater., 2010. **9**: p. 1004-1009.

133. Silver, F.H. and W.J. Landis, *Deposition of apatite in mineralizing vertebrate extracellular matrices: a model of possible nucleation sites on type I collagen.* Connect. Tissue Res., 2011. **52**: p. 1-13.

134. Boskey, A.L., *Matrix proteins and mineralization: an overview.* Connect. Tissue Res. , 1996. **35**: p. 357-363.

135. Cölfen, H., *Biomineralization: a crystal-clear view.* Nature Mater, 2010. **9**: p. 960-961.

136. Mann, S., *Molecular Recognition in Biomineralization.* Nature, 1988. **332**(6160): p. 119-124.

137. Hartgerink, J.D., E. Beniash, and S.I. Stupp, *Self-assembly and mineralization of peptide-amphiphile nanofibers.* Science, 2001. **294**(5547): p. 1684-1688.

138. Landschulz, W.H., P.F. Johnson, and S.L. Mcknight, *The Leucine Zipper - a Hypothetical Structure Common to a New Class of DNA-Binding Proteins.* Science, 1988. **240**(4860): p. 1759-1764.

139. Cao, B., H. Xu, and C. Mao, *Transmission electron microscopy as a tool to image bioinorganic nanohybrids: The case of phage-gold nanocomposites.* Microscopy Research and Technique, 2011. **74**(7): p. 627-635.

140. Daniel, M.C. and D. Astruc, *Gold nanoparticles: Assembly, supramolecular chemistry, quantum-size-related properties, and applications toward biology, catalysis, and nanotechnology.* Chemical Reviews, 2004. **104**(1): p. 293-346.

141. Sargent, E.H., *Infrared quantum dots.* Advanced Materials, 2005. **17**(5): p. 515-522.

142. Tasis, D., et al., *Chemistry of carbon nanotubes.* Chemical Reviews, 2006. **106**(3): p. 1105-1136.

143. Lu, A.H., E.L. Salabas, and F. Schuth, *Magnetic nanoparticles: Synthesis, protection, functionalization, and application.* Angewandte Chemie-International Edition, 2007. **46**(8): p. 1222-1244.

144. Belcher, A.M., et al., *Virus-based genetic toolkit for the directed synthesis of magnetic and semiconducting nanowires.* Abstracts of Papers of the American Chemical Society, 2004. **228**: p. U542-U542.

145. Mao, C.B., et al., *Viral assembly of oriented quantum dot nanowires.* Proceedings of the National Academy of Sciences of the United States of America, 2003. **100**(12): p. 6946-6951.

146. Sharma, J., et al., *Control of Self-Assembly of DNA Tubules Through Integration of Gold Nanoparticles.* Science, 2009. **323**(5910): p. 112-116.

147. Lin, C.X., et al., *Mirror Image DNA Nanostructures for Chiral Supramolecular Assemblies.* Nano Letters, 2009. **9**(1): p. 433-436.

148. Cao, B. and C. Mao, *Oriented nucleation of hydroxylapatite crystals on spider dragline silks.* Langmuir, 2007. **23**(21): p. 10701-10705.

149. Wang, F., et al., *Genetically Modifiable Flagella as Templates for Silica Fibers: From Hybrid Nanotubes to 1D Periodic Nanohole Arrays (vol 18, pg 4007, 2008).* Advanced Functional Materials, 2009. **19**(21): p. 3355-3355.

150. Hayat, M.A. and S.E. Miller, *Negative staining*. 1990, New York: McGraw-Hill Pub. Co. x, 253 p.

151. Note, C., S. Kosmella, and J. Koetz, *Poly(ethyleneimine) as reducing and stabilizing agent for the formation of gold nanoparticles in w/o microemulsions.* Colloids and Surfaces a-Physicochemical and Engineering Aspects, 2006. **290**(1-3): p. 150-156.

152. Monjezi, R., et al., *Purification of bacteriophage M13 by anion exchange chromatography.* Journal of Chromatography B-Analytical Technologies in the Biomedical and Life Sciences, 2010. **878**(21): p. 1855-1859.

153. Sharma, J., et al., *Toward reliable gold nanoparticle patterning on self-assembled DNA nanoscaffold.* Journal of the American Chemical Society, 2008. **130**(25): p. 7820-+.

154. Chen, Z.F., et al., *Solubility of Bovine-Derived Hydroxyapatite by Solid Titration, pH 3.5-5.* Crystal Growth & Design, 2009. **9**(6): p. 2816-2820.

155. Pan, H.B. and B.W. Darvell, *Solubility of hydroxyapatite by solid titration at pH 3-4.* Archives of Oral Biology, 2007. **52**(7): p. 618-624.

156. Gao, X., K.S. Kim, and D.X. Liu, *Nonviral gene delivery: What we know and what is next.* Aaps Journal, 2007. **9**(1): p. E92-E104.

157. Izadpanah, R. and B.A. Bunnell, *Gene Delivery to Mesenchymal Stem Cells*. 2008. p. 153-167.

158. Deshayes, S., et al., *Peptide-Mediated Delivery of Nucleic Acids into Mammalian Cells, Peptide Characterization and Application Protocols*, G.B. Fields, Editor. 2007, Humana Press. p. 299-308.

159. Vodnik, M., et al., *Phage Display: Selecting Straws Instead of a Needle from a Haystack.* Molecules, 2011. **16**(1): p. 790.

160. Staquicini, F.I., et al., *Phage display technology for stem cell delivery and systemic therapy.* Advanced Drug Delivery Reviews, 2010. **62**(12): p. 1213-1216.

161. Shao, Z., et al., *Polycaprolactone electrospun mesh conjugated with an MSC affinity peptide for MSC homing in vivo.* Biomaterials, 2012. **33**: p. 3375-3387.

162. Kean, T.J., et al., *Development of a peptide-targeted, myocardial ischemia-homing, mesenchymal stem cell.* J. Drug Targeting, 2011. **20**: p. 23-32.

163. Xitong, D. and Z. Xiaorong, *Targeted therapeutic delivery using engineered exosomes and its applications in cardiovascular diseases.* Gene, 2015. **in press**.

164. Bradbury, A.R.M., et al., *Beyond natural antibodies: the power of in vitro display technologies.* Nat Biotech, 2011. **29**(3): p. 245-254.

165. Szardenings, M., *Phage Display of Random Peptide Libraries: Applications, Limits, and Potential.* Journal of Receptors and Signal Transduction, 2003. **23**(4): p. 307-349.

166. Barbass III, C., et al., *Phage display: a laboratory manual*. 2004: Cold Spring Harbor Laboratory Press.

167. Pande, J., M.M. Szewczyk, and A.K. Grover, *Phage display: Concept, innovations, applications and future.* Biotechnology Advances, 2010. **28**(6): p. 849-858.

168. Zlotnik, A. and O. Yoshie, *Chemokines: A New Classification System and Their Role in Immunity.* Immunity, 2000. **12**(2): p. 121-127.

169. Allen, S.J., S.E. Crown, and T.M. Handel, *Chemokine:Receptor Structure, Interactions, and Antagonism.* Annual Review of Immunology, 2007. **25**(1): p. 787-820.

170. Hoare, M., et al., *Enhanced lipoplex-mediated gene expression in mesenchymal stem cells using reiterated nuclear localization sequence peptides.* The Journal of Gene Medicine, 2010. **12**(2): p. 207-218.

171. Soleimani, M. and S. Nadri, *A protocol for isolation and culture of mesenchymal stem cells from mouse bone marrow.* Nat. Protocols, 2009. **4**(1): p. 102-106.

172. McGuire, M.J., S. Li, and K.C. Brown, *Biopanning of Phage Displayed Peptide Libraries for the Isolation of Cell-Specific Ligands*. 2008. p. 291-321.

173. Mandava, S., et al., *RELIC– A bioinformatics server for combinatorial peptide analysis and identification of protein-ligand interaction sites.* Proteomics, 2004. **4**(5): p. 1439-1460.

174. Belur, L.R., et al., *Lung-directed gene therapy in mice using the nonviral Sleeping Beauty transposon system.* Nat. Protocols, 2007. **2**(12): p. 3146-3152.

175. Sordi, V., et al., *Bone marrow mesenchymal stem cells express a restricted set of functionally active chemokine receptors capable of promoting migration to pancreatic islets.* Blood, 2005. **106**(2): p. 419-427.

176. Dominici, M., et al., *Minimal criteria for defining multipotent mesenchymal stromal cells. The International Society for Cellular Therapy position statement.* Cytotherapy, 2006. **8**(4): p. 315-317.

177. Fox, J.M., et al., *Recent advances into the understanding of mesenchymal stem cell trafficking.* British Journal of Haematology, 2007. **137**(6): p. 491-502.

178. Docheva, D.H., Florian; Schieker, Matthias, *Mesenchymal Stem Cells and Their Cell Surface Receptors.* Current Rheumatology Reviews, 2008. **4**: p. 155-160.

179. Li, S.-D., S. Chono, and L. Huang, *Efficient gene silencing in metastatic tumor by siRNA formulated in surface-modified nanoparticles.* Journal of Controlled Release, 2008. **126**(1): p. 77-84.

180. Masuda, T., et al., *Envelope-type lipid nanoparticles incorporating a short PEG-lipid conjugate for improved control of intracellular trafficking and transgene transcription.* Biomaterials, 2009. **30**(27): p. 4806-4814.

181. Kalderon, D., et al., *A short amino acid sequence able to specify nuclear location.* Cell, 1984. **39**(3, Part 2): p. 499-509.

182. Zanta, M.A., P. Belguise-Valladier, and J.-P. Behr, *Gene delivery: A single nuclear localization signal peptide is sufficient to carry DNA to the cell nucleus.* Proceedings of the National Academy of Sciences, 1999. **96**(1): p. 91-96.

183. Needham, C.J., et al., *Engineering a Polymeric Gene Delivery Vector Based on Poly(ethylenimine) and Hyaluronic Acid.* Biomacromolecules, 2012. **13**(5): p. 1429-1437.

184. Park, J.S., et al., *Chondrogenesis of human mesenchymal stem cells mediated by the combination of SOX trio SOX5, 6, and 9 genes complexed with PEI-modified PLGA nanoparticles.* Biomaterials, 2011. **32**(14): p. 3679-3688.

185. Díaz, P., F. Cuevas, and O.A. Peralta, *GFP labelling and epigenetic enzyme expression of bone marrow-derived mesenchymal stem cells from bovine foetuses.* Research in Veterinary Science, 2015. **99**: p. 120-128.

186. Rey-Rico, A., et al., *PEO–PPO–PEO micelles as effective rAAV-mediated gene delivery systems to target human mesenchymal stem cells without altering their differentiation potency.* Acta Biomaterialia, 2015. **27**: p. 42-52.

187. Curtin, C.M., et al., *Innovative Collagen Nano-Hydroxyapatite Scaffolds Offer a Highly Efficient Non-Viral Gene Delivery Platform for Stem Cell-Mediated Bone Formation.* Advanced Materials, 2012. **24**(6): p. 749-754.

188. Schade, A., et al., *Innovative Strategy for MicroRNA Delivery in Human Mesenchymal Stem Cells via Magnetic Nanoparticles.* International Journal of Molecular Sciences, 2013. **14**(6): p. 10710-10726.

189. Schmid, S.L., *CLATHRIN-COATED VESICLE FORMATION AND PROTEIN SORTING:An Integrated Process.* Annual Review of Biochemistry, 1997. **66**(1): p. 511-548.

190. Anderson, R.G.W., *THE CAVEOLAE MEMBRANE SYSTEM.* Annual Review of Biochemistry, 1998. **67**(1): p. 199-225.

191. Nam, H.Y., et al., *Cellular uptake mechanism and intracellular fate of hydrophobically modified glycol chitosan nanoparticles.* Journal of Controlled Release, 2009. **135**(3): p. 259-267.

192. Oh, J.-M., et al., *Cellular Uptake Mechanism of an Inorganic Nanovehicle and Its Drug Conjugates: Enhanced Efficacy Due To Clathrin-Mediated Endocytosis.* Bioconjugate Chemistry, 2006. **17**(6): p. 1411-1417.

193. Zhang, L.W. and N.A. Monteiro-Riviere, *Mechanisms of Quantum Dot Nanoparticle Cellular Uptake.* Toxicological Sciences, 2009. **110**(1): p. 138-155.

194. Chithrani, B.D. and W.C.W. Chan, *Elucidating the Mechanism of Cellular Uptake and Removal of Protein-Coated Gold Nanoparticles of Different Sizes and Shapes.* Nano Letters, 2007. **7**(6): p. 1542-1550.

195. Mizoue, L.S., et al., *Solution Structure and Dynamics of the CX3C Chemokine Domain of Fractalkine and Its Interaction with an N-Terminal Fragment of CX3CR1†,‡.* Biochemistry, 1999. **38**(5): p. 1402-1414.

196. Kuloğlu, E.S., et al., *Monomeric Solution Structure of the Prototypical 'C' Chemokine Lymphotactin†,‡.* Biochemistry, 2001. **40**(42): p. 12486-12496.

197. Hermand, P., et al., *Functional Adhesiveness of the CX3CL1 Chemokine Requires Its Aggregation: ROLE OF THE TRANSMEMBRANE DOMAIN.* Journal of Biological Chemistry, 2008. **283**(44): p. 30225-30234.

198. Fong, A.M., *CX3CR1 Tyrosine Sulfation Enhances Fractalkine-induced Cell Adhesion.* Journal of Biological Chemistry, 2002. **277**(22): p. 19418-19423.

199. Imai, T., et al., *Identification and Molecular Characterization of Fractalkine Receptor CX3CR1, which Mediates Both Leukocyte Migration and Adhesion.* Cell, 1997. **91**(4): p. 521-530.

200. Baysal, C. and A.R. Atilgan, *Elucidating the structural mechanisms for biological activity of the chemokine family.* Proteins: Structure, Function, and Bioinformatics, 2001. **43**(2): p. 150-160.

201. Marchler-Bauer, A., et al., *CDD: specific functional annotation with the Conserved Domain Database.* Nucleic Acids Research, 2009. **37**(suppl 1): p. D205-D210.

202. Venkatesan, S., et al., *Distinct Mechanisms of Agonist-induced Endocytosis for Human Chemokine Receptors CCR5 and CXCR4.* Mol. Biol. Cell, 2003. **14**(8): p. 3305-3324.

203. Crump, M.P., et al., *Solution structure and basis for functional activity of stromal cell-derived factor-1; dissociation of CXCR4 activation from binding and inhibition of HIV-1.* EMBO J, 1997. **16**(23): p. 6996-7007.

204. D'Souza, S.E., M.H. Ginsberg, and E.F. Plow, *Arginyl-glycyl-aspartic acid (RGD): a cell adhesion motif.* Trends in biochemical sciences, 1991. **16**: p. 246-250.

# [Appendix A: Permissions and Copyrights]



**JOHN WILEY AND SONS LICENSE TERMS AND CONDITIONS**

Nov 20, 2015

This Agreement between Hong Xu ("You") and John Wiley and Sons ("John Wiley and Sons") consists of your license details and the terms and conditions provided by John Wiley and Sons and Copyright Clearance Center.

| | |
|---|---|
| License Number | 3753281134858 |
| License date | Nov 20, 2015 |
| Licensed Content Publisher | John Wiley and Sons |
| Licensed Content Publication | Angewandte Chemie International Edition |
| Licensed Content Title | Virus-Based Chemical and Biological Sensing |
| Licensed Content Author | Chuanbin Mao,Aihua Liu,Binrui Cao |
| Licensed Content Date | Aug 7, 2009 |
| Pages | 21 |
| Type of use | Dissertation/Thesis |
| Requestor type | University/Academic |
| Format | Print and electronic |
| Portion | Figure/table |
| Number of figures/tables | 1 |
| Original Wiley figure/table number(s) | Figure 1 |
| Will you be translating? | No |
| Title of your thesis / dissertation | BACTERIOPHAGE NANOFIBERS ENABLED NANOSTRUCTURES AND TARGET-RECOGNITION FOR BIO-APPLICATIONS |
| Expected completion date | Dec 2015 |
| Expected size (number of pages) | 200 |
| Requestor Location | Hong Xu<br>101 Stephenson Pkwy<br><br>NORMAN, OK 73019<br>United States<br>Attn: Hong Xu |
| Billing Type | Invoice |
| Billing Address | Hong Xu<br>101 Stephenson Pkwy |

NORMAN, OK 73019
United States
Attn: Hong Xu

Total 0.00 USD

Terms and Conditions

**TERMS AND CONDITIONS**

This copyrighted material is owned by or exclusively licensed to John Wiley & Sons, Inc. or one of its group companies (each a"Wiley Company") or handled on behalf of a society with which a Wiley Company has exclusive publishing rights in relation to a particular work (collectively "WILEY"). By clicking "accept" in connection with completing this licensing transaction, you agree that the following terms and conditions apply to this transaction (along with the billing and payment terms and conditions established by the Copyright Clearance Center Inc., ("CCC's Billing and Payment terms and conditions"), at the time that you opened your RightsLink account (these are available at any time at http://myaccount.copyright.com).

**Terms and Conditions**

- The materials you have requested permission to reproduce or reuse (the "Wiley Materials") are protected by copyright.

- You are hereby granted a personal, non-exclusive, non-sub licensable (on a stand-alone basis), non-transferable, worldwide, limited license to reproduce the Wiley Materials for the purpose specified in the licensing process. This license, **and any CONTENT (PDF or image file) purchased as part of your order,** is for a one-time use only and limited to any maximum distribution number specified in the license. The first instance of republication or reuse granted by this license must be completed within two years of the date of the grant of this license (although copies prepared before the end date may be distributed thereafter). The Wiley Materials shall not be used in any other manner or for any other purpose, beyond what is granted in the license. Permission is granted subject to an appropriate acknowledgement given to the author, title of the material/book/journal and the publisher. You shall also duplicate the copyright notice that appears in the Wiley publication in your use of the Wiley Material. Permission is also granted on the understanding that nowhere in the text is a previously published source acknowledged for all or part of this Wiley Material. Any third party content is expressly excluded from this permission.

- With respect to the Wiley Materials, all rights are reserved. Except as expressly granted by the terms of the license, no part of the Wiley Materials may be copied, modified, adapted (except for minor reformatting required by the new Publication), translated, reproduced, transferred or distributed, in any form or by any means, and no derivative works may be made based on the Wiley Materials without the prior permission of the respective copyright owner.**For STM Signatory Publishers clearing permission under the terms of the STM Permissions Guidelines only, the terms of the license are extended to include subsequent editions and for editions in other languages, provided such editions are for the work as a whole in situ and does not involve the separate exploitation of the permitted figures or extracts,**

You may not alter, remove or suppress in any manner any copyright, trademark or other notices displayed by the Wiley Materials. You may not license, rent, sell, loan, lease, pledge, offer as security, transfer or assign the Wiley Materials on a stand-alone basis, or any of the rights granted to you hereunder to any other person.

- The Wiley Materials and all of the intellectual property rights therein shall at all times remain the exclusive property of John Wiley & Sons Inc, the Wiley Companies, or their respective licensors, and your interest therein is only that of having possession of and the right to reproduce the Wiley Materials pursuant to Section 2 herein during the continuance of this Agreement. You agree that you own no right, title or interest in or to the Wiley Materials or any of the intellectual property rights therein. You shall have no rights hereunder other than the license as provided for above in Section 2. No right, license or interest to any trademark, trade name, service mark or other branding ("Marks") of WILEY or its licensors is granted hereunder, and you agree that you shall not assert any such right, license or interest with respect thereto

- NEITHER WILEY NOR ITS LICENSORS MAKES ANY WARRANTY OR REPRESENTATION OF ANY KIND TO YOU OR ANY THIRD PARTY, EXPRESS, IMPLIED OR STATUTORY, WITH RESPECT TO THE MATERIALS OR THE ACCURACY OF ANY INFORMATION CONTAINED IN THE MATERIALS, INCLUDING, WITHOUT LIMITATION, ANY IMPLIED WARRANTY OF MERCHANTABILITY, ACCURACY, SATISFACTORY QUALITY, FITNESS FOR A PARTICULAR PURPOSE, USABILITY, INTEGRATION OR NON-INFRINGEMENT AND ALL SUCH WARRANTIES ARE HEREBY EXCLUDED BY WILEY AND ITS LICENSORS AND WAIVED BY YOU.

- WILEY shall have the right to terminate this Agreement immediately upon breach of this Agreement by you.

- You shall indemnify, defend and hold harmless WILEY, its Licensors and their respective directors, officers, agents and employees, from and against any actual or threatened claims, demands, causes of action or proceedings arising from any breach of this Agreement by you.

- IN NO EVENT SHALL WILEY OR ITS LICENSORS BE LIABLE TO YOU OR ANY OTHER PARTY OR ANY OTHER PERSON OR ENTITY FOR ANY SPECIAL, CONSEQUENTIAL, INCIDENTAL, INDIRECT, EXEMPLARY OR PUNITIVE DAMAGES, HOWEVER CAUSED, ARISING OUT OF OR IN CONNECTION WITH THE DOWNLOADING, PROVISIONING, VIEWING OR USE OF THE MATERIALS REGARDLESS OF THE FORM OF ACTION, WHETHER FOR BREACH OF CONTRACT, BREACH OF WARRANTY, TORT, NEGLIGENCE, INFRINGEMENT OR OTHERWISE (INCLUDING, WITHOUT LIMITATION, DAMAGES BASED ON LOSS OF PROFITS, DATA, FILES, USE, BUSINESS OPPORTUNITY OR CLAIMS OF THIRD PARTIES), AND WHETHER OR NOT THE PARTY HAS BEEN ADVISED OF THE POSSIBILITY OF SUCH DAMAGES. THIS LIMITATION SHALL APPLY NOTWITHSTANDING ANY

FAILURE OF ESSENTIAL PURPOSE OF ANY LIMITED REMEDY PROVIDED HEREIN.

- Should any provision of this Agreement be held by a court of competent jurisdiction to be illegal, invalid, or unenforceable, that provision shall be deemed amended to achieve as nearly as possible the same economic effect as the original provision, and the legality, validity and enforceability of the remaining provisions of this Agreement shall not be affected or impaired thereby.

- The failure of either party to enforce any term or condition of this Agreement shall not constitute a waiver of either party's right to enforce each and every term and condition of this Agreement. No breach under this agreement shall be deemed waived or excused by either party unless such waiver or consent is in writing signed by the party granting such waiver or consent. The waiver by or consent of a party to a breach of any provision of this Agreement shall not operate or be construed as a waiver of or consent to any other or subsequent breach by such other party.

- This Agreement may not be assigned (including by operation of law or otherwise) by you without WILEY's prior written consent.

- Any fee required for this permission shall be non-refundable after thirty (30) days from receipt by the CCC.

- These terms and conditions together with CCC's Billing and Payment terms and conditions (which are incorporated herein) form the entire agreement between you and WILEY concerning this licensing transaction and (in the absence of fraud) supersedes all prior agreements and representations of the parties, oral or written. This Agreement may not be amended except in writing signed by both parties. This Agreement shall be binding upon and inure to the benefit of the parties' successors, legal representatives, and authorized assigns.

- In the event of any conflict between your obligations established by these terms and conditions and those established by CCC's Billing and Payment terms and conditions, these terms and conditions shall prevail.

- WILEY expressly reserves all rights not specifically granted in the combination of (i) the license details provided by you and accepted in the course of this licensing transaction, (ii) these terms and conditions and (iii) CCC's Billing and Payment terms and conditions.

- This Agreement will be void if the Type of Use, Format, Circulation, or Requestor Type was misrepresented during the licensing process.

- This Agreement shall be governed by and construed in accordance with the laws of the State of New York, USA, without regards to such state's conflict of law rules. Any legal action, suit or proceeding arising out of or relating to these Terms and Conditions or the breach thereof shall be instituted in a court of competent jurisdiction in New

York County in the State of New York in the United States of America and each party hereby consents and submits to the personal jurisdiction of such court, waives any objection to venue in such court and consents to service of process by registered or certified mail, return receipt requested, at the last known address of such party.

**WILEY OPEN ACCESS TERMS AND CONDITIONS**

Wiley Publishes Open Access Articles in fully Open Access Journals and in Subscription journals offering Online Open. Although most of the fully Open Access journals publish open access articles under the terms of the Creative Commons Attribution (CC BY) License only, the subscription journals and a few of the Open Access Journals offer a choice of Creative Commons Licenses. The license type is clearly identified on the article.

**The Creative Commons Attribution License**

The Creative Commons Attribution License (CC-BY) allows users to copy, distribute and transmit an article, adapt the article and make commercial use of the article. The CC-BY license permits commercial and non-

**Creative Commons Attribution Non-Commercial License**

The Creative Commons Attribution Non-Commercial (CC-BY-NC)License permits use, distribution and reproduction in any medium, provided the original work is properly cited and is not used for commercial purposes.(see below)

**Creative Commons Attribution-Non-Commercial-NoDerivs License**

The Creative Commons Attribution Non-Commercial-NoDerivs License (CC-BY-NC-ND) permits use, distribution and reproduction in any medium, provided the original work is properly cited, is not used for commercial purposes and no modifications or adaptations are made. (see below)

**Use by commercial "for-profit" organizations**

Use of Wiley Open Access articles for commercial, promotional, or marketing purposes requires further explicit permission from Wiley and will be subject to a fee.

Further details can be found on Wiley Online Library

http://olabout.wiley.com/WileyCDA/Section/id-410895.html

**Other Terms and Conditions:**

**v1.10 Last updated September 2015**

**Questions? customercare@copyright.com or +1-855-239-3415 (toll free in the US) or +1-978-646-2777.**

**NATURE PUBLISHING GROUP LICENSE**
**TERMS AND CONDITIONS**

Nov 20, 2015

This is a License Agreement between Hong Xu ("You") and Nature Publishing Group ("Nature Publishing Group") provided by Copyright Clearance Center ("CCC"). The license consists of your order details, the terms and conditions provided by Nature Publishing Group, and the payment terms and conditions.

**All payments must be made in full to CCC. For payment instructions, please see information listed at the bottom of this form.**

| | |
|---|---|
| License Number | 3753290424552 |
| License date | Nov 20, 2015 |
| Licensed content publisher | Nature Publishing Group |
| Licensed content publication | Nature |
| Licensed content title | Nanotechnology: Boning up on biology |
| Licensed content author | T. Andrew Taton |
| Licensed content date | Aug 2, 2001 |
| Volume number | 412 |
| Issue number | 6846 |
| Type of Use | reuse in a dissertation / thesis |
| Requestor type | academic/educational |
| Format | print and electronic |
| Portion | figures/tables/illustrations |
| Number of figures/tables/illustrations | 1 |
| Figures | figure 1 |
| Author of this NPG article | no |
| Your reference number | None |
| Title of your thesis / dissertation | BACTERIOPHAGE NANOFIBERS ENABLED NANOSTRUCTURES AND TARGET-RECOGNITION FOR BIO-APPLICATIONS |
| Expected completion date | Dec 2015 |
| Estimated size (number of pages) | 200 |
| Total | 0.00 USD |
| Terms and Conditions | |

Terms and Conditions for Permissions

Nature Publishing Group hereby grants you a non-exclusive license to reproduce this

material for this purpose, and for no other use,subject to the conditions below:

1. NPG warrants that it has, to the best of its knowledge, the rights to license reuse of this material. However, you should ensure that the material you are requesting is original to Nature Publishing Group and does not carry the copyright of another entity (as credited in the published version). If the credit line on any part of the material you have requested indicates that it was reprinted or adapted by NPG with permission from another source, then you should also seek permission from that source to reuse the material.

2. Permission granted free of charge for material in print is also usually granted for any electronic version of that work, provided that the material is incidental to the work as a whole and that the electronic version is essentially equivalent to, or substitutes for, the print version.Where print permission has been granted for a fee, separate permission must be obtained for any additional, electronic re-use (unless, as in the case of a full paper, this has already been accounted for during your initial request in the calculation of a print run).NB: In all cases, web-based use of full-text articles must be authorized separately through the 'Use on a Web Site' option when requesting permission.

3. Permission granted for a first edition does not apply to second and subsequent editions and for editions in other languages (except for signatories to the STM Permissions Guidelines, or where the first edition permission was granted for free).

4. Nature Publishing Group's permission must be acknowledged next to the figure, table or abstract in print. In electronic form, this acknowledgement must be visible at the same time as the figure/table/abstract, and must be hyperlinked to the journal's homepage.

5. The credit line should read:
   Reprinted by permission from Macmillan Publishers Ltd: [JOURNAL NAME] (reference citation), copyright (year of publication)
   For AOP papers, the credit line should read:
   Reprinted by permission from Macmillan Publishers Ltd: [JOURNAL NAME], advance online publication, day month year (doi: 10.1038/sj.[JOURNAL ACRONYM].XXXXX)

   **Note: For republication from the *British Journal of Cancer,* the following credit lines apply.**
   Reprinted by permission from Macmillan Publishers Ltd on behalf of Cancer Research UK: [JOURNAL NAME] (reference citation), copyright (year of publication)For AOP papers, the credit line should read:
   Reprinted by permission from Macmillan Publishers Ltd on behalf of Cancer Research UK: [JOURNAL NAME], advance online publication, day month year (doi: 10.1038/sj.[JOURNAL ACRONYM].XXXXX)

6. Adaptations of single figures do not require NPG approval. However, the adaptation should be credited as follows:

   Adapted by permission from Macmillan Publishers Ltd: [JOURNAL NAME] (reference citation), copyright (year of publication)

   **Note: For adaptation from the *British Journal of Cancer,* the following credit line applies.**
   Adapted by permission from Macmillan Publishers Ltd on behalf of Cancer Research UK: [JOURNAL NAME] (reference citation), copyright (year of publication)

7. Translations of 401 words up to a whole article require NPG approval. Please visit http://www.macmillanmedicalcommunications.com for more information.Translations of up

to a 400 words do not require NPG approval. The translation should be credited as follows:

Translated by permission from Macmillan Publishers Ltd: [JOURNAL NAME] (reference citation), copyright (year of publication).

**Note: For translation from the *British Journal of Cancer*, the following credit line applies.**
Translated by permission from Macmillan Publishers Ltd on behalf of Cancer Research UK: [JOURNAL NAME] (reference citation), copyright (year of publication)

We are certain that all parties will benefit from this agreement and wish you the best in the use of this material. Thank you.
Special Terms:
v1.1

**Questions? customercare@copyright.com or +1-855-239-3415 (toll free in the US) or +1-978-646-2777.**

**JOHN WILEY AND SONS LICENSE TERMS AND CONDITIONS**

Nov 20, 2015

This Agreement between Hong Xu ("You") and John Wiley and Sons ("John Wiley and Sons") consists of your license details and the terms and conditions provided by John Wiley and Sons and Copyright Clearance Center.

| | |
|---|---|
| License Number | 3753290604686 |
| License date | Nov 20, 2015 |
| Licensed Content Publisher | John Wiley and Sons |
| Licensed Content Publication | Microscopy Research and Technique |
| Licensed Content Title | Transmission electron microscopy as a tool to image bioinorganic nanohybrids: The case of phage-gold nanocomposites |
| Licensed Content Author | Binrui Cao,Hong Xu,Chuanbin Mao |
| Licensed Content Date | Jun 15, 2011 |
| Pages | 9 |
| Type of use | Dissertation/Thesis |
| Requestor type | Author of this Wiley article |
| Format | Print and electronic |
| Portion | Full article |
| Will you be translating? | No |
| Title of your thesis / dissertation | BACTERIOPHAGE NANOFIBERS ENABLED NANOSTRUCTURES AND TARGET-RECOGNITION FOR BIO-APPLICATIONS |
| Expected completion date | Dec 2015 |
| Expected size (number of pages) | 200 |
| Requestor Location | Hong Xu<br>101 Stephenson Pkwy<br><br>NORMAN, OK 73019<br>United States<br>Attn: Hong Xu |
| Billing Type | Invoice |
| Billing Address | Hong Xu<br>101 Stephenson Pkwy<br><br>NORMAN, OK 73019<br>United States<br>Attn: Hong Xu |

Total 0.00 USD

Terms and Conditions

**TERMS AND CONDITIONS**

This copyrighted material is owned by or exclusively licensed to John Wiley & Sons, Inc. or one of its group companies (each a"Wiley Company") or handled on behalf of a society with which a Wiley Company has exclusive publishing rights in relation to a particular work (collectively "WILEY"). By clicking "accept" in connection with completing this licensing transaction, you agree that the following terms and conditions apply to this transaction (along with the billing and payment terms and conditions established by the Copyright Clearance Center Inc., ("CCC's Billing and Payment terms and conditions"), at the time that you opened your RightsLink account (these are available at any time at http://myaccount.copyright.com).

**Terms and Conditions**

- The materials you have requested permission to reproduce or reuse (the "Wiley Materials") are protected by copyright.

- You are hereby granted a personal, non-exclusive, non-sub licensable (on a stand-alone basis), non-transferable, worldwide, limited license to reproduce the Wiley Materials for the purpose specified in the licensing process. This license, **and any CONTENT (PDF or image file) purchased as part of your order,** is for a one-time use only and limited to any maximum distribution number specified in the license. The first instance of republication or reuse granted by this license must be completed within two years of the date of the grant of this license (although copies prepared before the end date may be distributed thereafter). The Wiley Materials shall not be used in any other manner or for any other purpose, beyond what is granted in the license. Permission is granted subject to an appropriate acknowledgement given to the author, title of the material/book/journal and the publisher. You shall also duplicate the copyright notice that appears in the Wiley publication in your use of the Wiley Material. Permission is also granted on the understanding that nowhere in the text is a previously published source acknowledged for all or part of this Wiley Material. Any third party content is expressly excluded from this permission.

- With respect to the Wiley Materials, all rights are reserved. Except as expressly granted by the terms of the license, no part of the Wiley Materials may be copied, modified, adapted (except for minor reformatting required by the new Publication), translated, reproduced, transferred or distributed, in any form or by any means, and no derivative works may be made based on the Wiley Materials without the prior permission of the respective copyright owner.**For STM Signatory Publishers clearing permission under the terms of the STM Permissions Guidelines only, the terms of the license are extended to include subsequent editions and for editions in other languages, provided such editions are for the work as a whole in situ and does not involve the separate exploitation of the permitted figures or extracts,** You may not alter, remove or suppress in any manner any copyright, trademark or other notices displayed by the Wiley Materials. You may not license, rent, sell, loan,

lease, pledge, offer as security, transfer or assign the Wiley Materials on a stand-alone basis, or any of the rights granted to you hereunder to any other person.

- The Wiley Materials and all of the intellectual property rights therein shall at all times remain the exclusive property of John Wiley & Sons Inc, the Wiley Companies, or their respective licensors, and your interest therein is only that of having possession of and the right to reproduce the Wiley Materials pursuant to Section 2 herein during the continuance of this Agreement. You agree that you own no right, title or interest in or to the Wiley Materials or any of the intellectual property rights therein. You shall have no rights hereunder other than the license as provided for above in Section 2. No right, license or interest to any trademark, trade name, service mark or other branding ("Marks") of WILEY or its licensors is granted hereunder, and you agree that you shall not assert any such right, license or interest with respect thereto

- NEITHER WILEY NOR ITS LICENSORS MAKES ANY WARRANTY OR REPRESENTATION OF ANY KIND TO YOU OR ANY THIRD PARTY, EXPRESS, IMPLIED OR STATUTORY, WITH RESPECT TO THE MATERIALS OR THE ACCURACY OF ANY INFORMATION CONTAINED IN THE MATERIALS, INCLUDING, WITHOUT LIMITATION, ANY IMPLIED WARRANTY OF MERCHANTABILITY, ACCURACY, SATISFACTORY QUALITY, FITNESS FOR A PARTICULAR PURPOSE, USABILITY, INTEGRATION OR NON-INFRINGEMENT AND ALL SUCH WARRANTIES ARE HEREBY EXCLUDED BY WILEY AND ITS LICENSORS AND WAIVED BY YOU.

- WILEY shall have the right to terminate this Agreement immediately upon breach of this Agreement by you.

- You shall indemnify, defend and hold harmless WILEY, its Licensors and their respective directors, officers, agents and employees, from and against any actual or threatened claims, demands, causes of action or proceedings arising from any breach of this Agreement by you.

- IN NO EVENT SHALL WILEY OR ITS LICENSORS BE LIABLE TO YOU OR ANY OTHER PARTY OR ANY OTHER PERSON OR ENTITY FOR ANY SPECIAL, CONSEQUENTIAL, INCIDENTAL, INDIRECT, EXEMPLARY OR PUNITIVE DAMAGES, HOWEVER CAUSED, ARISING OUT OF OR IN CONNECTION WITH THE DOWNLOADING, PROVISIONING, VIEWING OR USE OF THE MATERIALS REGARDLESS OF THE FORM OF ACTION, WHETHER FOR BREACH OF CONTRACT, BREACH OF WARRANTY, TORT, NEGLIGENCE, INFRINGEMENT OR OTHERWISE (INCLUDING, WITHOUT LIMITATION, DAMAGES BASED ON LOSS OF PROFITS, DATA, FILES, USE, BUSINESS OPPORTUNITY OR CLAIMS OF THIRD PARTIES), AND WHETHER OR NOT THE PARTY HAS BEEN ADVISED OF THE POSSIBILITY OF SUCH DAMAGES. THIS LIMITATION SHALL APPLY NOTWITHSTANDING ANY FAILURE OF ESSENTIAL PURPOSE OF ANY LIMITED REMEDY PROVIDED HEREIN.

- Should any provision of this Agreement be held by a court of competent jurisdiction to be illegal, invalid, or unenforceable, that provision shall be deemed amended to achieve as nearly as possible the same economic effect as the original provision, and the legality, validity and enforceability of the remaining provisions of this Agreement shall not be affected or impaired thereby.

- The failure of either party to enforce any term or condition of this Agreement shall not constitute a waiver of either party's right to enforce each and every term and condition of this Agreement. No breach under this agreement shall be deemed waived or excused by either party unless such waiver or consent is in writing signed by the party granting such waiver or consent. The waiver by or consent of a party to a breach of any provision of this Agreement shall not operate or be construed as a waiver of or consent to any other or subsequent breach by such other party.

- This Agreement may not be assigned (including by operation of law or otherwise) by you without WILEY's prior written consent.

- Any fee required for this permission shall be non-refundable after thirty (30) days from receipt by the CCC.

- These terms and conditions together with CCC's Billing and Payment terms and conditions (which are incorporated herein) form the entire agreement between you and WILEY concerning this licensing transaction and (in the absence of fraud) supersedes all prior agreements and representations of the parties, oral or written. This Agreement may not be amended except in writing signed by both parties. This Agreement shall be binding upon and inure to the benefit of the parties' successors, legal representatives, and authorized assigns.

- In the event of any conflict between your obligations established by these terms and conditions and those established by CCC's Billing and Payment terms and conditions, these terms and conditions shall prevail.

- WILEY expressly reserves all rights not specifically granted in the combination of (i) the license details provided by you and accepted in the course of this licensing transaction, (ii) these terms and conditions and (iii) CCC's Billing and Payment terms and conditions.

- This Agreement will be void if the Type of Use, Format, Circulation, or Requestor Type was misrepresented during the licensing process.

- This Agreement shall be governed by and construed in accordance with the laws of the State of New York, USA, without regards to such state's conflict of law rules. Any legal action, suit or proceeding arising out of or relating to these Terms and Conditions or the breach thereof shall be instituted in a court of competent jurisdiction in New York County in the State of New York in the United States of America and each party hereby consents and submits to the personal jurisdiction of such court, waives any

objection to venue in such court and consents to service of process by registered or certified mail, return receipt requested, at the last known address of such party.

**WILEY OPEN ACCESS TERMS AND CONDITIONS**

Wiley Publishes Open Access Articles in fully Open Access Journals and in Subscription journals offering Online Open. Although most of the fully Open Access journals publish open access articles under the terms of the Creative Commons Attribution (CC BY) License only, the subscription journals and a few of the Open Access Journals offer a choice of Creative Commons Licenses. The license type is clearly identified on the article.

**The Creative Commons Attribution License**

The Creative Commons Attribution License (CC-BY) allows users to copy, distribute and transmit an article, adapt the article and make commercial use of the article. The CC-BY license permits commercial and non-

**Creative Commons Attribution Non-Commercial License**

The Creative Commons Attribution Non-Commercial (CC-BY-NC)License permits use, distribution and reproduction in any medium, provided the original work is properly cited and is not used for commercial purposes.(see below)

**Creative Commons Attribution-Non-Commercial-NoDerivs License**

The Creative Commons Attribution Non-Commercial-NoDerivs License (CC-BY-NC-ND) permits use, distribution and reproduction in any medium, provided the original work is properly cited, is not used for commercial purposes and no modifications or adaptations are made. (see below)

**Use by commercial "for-profit" organizations**

Use of Wiley Open Access articles for commercial, promotional, or marketing purposes requires further explicit permission from Wiley and will be subject to a fee.

Further details can be found on Wiley Online Library

http://olabout.wiley.com/WileyCDA/Section/id-410895.html

**Other Terms and Conditions:**

**v1.10 Last updated September 2015**

**Questions? customercare@copyright.com or +1-855-239-3415 (toll free in the US) or +1-978-646-2777.**

# [Appendix B: Copy of Approval from Institutional Animal Care and Use Committee (IACUC)]

The University of Oklahoma

LABORATORY ANIMAL RESOURCES

17 December 2010

C. Mao
Department of Biochemistry

Dear Dr. Mao:

The following AUS protocol extension was reviewed and approved by the Institutional Animal Care and Use Committee:

Title of Application: **"Bone regeneration from bone mesenchymal stem cells seeded on biomimetic scaffold constructs formed by mineralization of M13 phage with hydroxyapatite crystals"**

Institution: University of Oklahoma

The protocol for this unfunded study extends the previously approved AUS R07-003; the new institutional tracking number is **R10-013**. Key personnel for this study are Drs. Haibao Zhu and Jianglin Wang – postdocs. It will be in effect for a period of three years. If significant changes are needed and or new personnel are to be added, you will need to file an amendment. Refer to the current tracking number when communicating with this office and when ordering animals.

The University of Oklahoma has an Animal Welfare Assurance on file with the Office of Laboratory Animal Welfare (A3240-01) which is effective through June 2013 and the Institution is registered as a research facility with USDA (Certificate number 73-R-0100) which is in effect through March 2013.

Sincerely yours,

William Shelton, IACUC Chair

Cc: IO

730 Van Vleet Oval, Richards Hall 314, Norman, Oklahoma 73019-6121 PHONE: (405) 325-2609